



Durham E-Theses

Radiochemical studies of fast neutron-induced reactions

East, Brian William

How to cite:

East, Brian William (1967) *Radiochemical studies of fast neutron-induced reactions*, Durham theses, Durham University. Available at Durham E-Theses Online: <http://etheses.dur.ac.uk/8769/>

Use policy

The full-text may be used and/or reproduced, and given to third parties in any format or medium, without prior permission or charge, for personal research or study, educational, or not-for-profit purposes provided that:

- a full bibliographic reference is made to the original source
- a [link](#) is made to the metadata record in Durham E-Theses
- the full-text is not changed in any way

The full-text must not be sold in any format or medium without the formal permission of the copyright holders.

Please consult the [full Durham E-Theses policy](#) for further details.

"Radiochemical studies of fast neutron-induced reactions"

THESIS

presented in candidature for the degree

of

DOCTOR OF PHILOSOPHY

of the

University of Durham

by

BRIAN WILLIAM EAST, B.Sc. (Dunelm)



P.263

MEMORANDUM

The work described in this thesis was performed in the Londonderry Laboratory for Radiochemistry, University of Durham during the period from October 1962 to September 1964 and in the University Chemical Laboratory, University of Kent at Canterbury during the period from October 1964 to December 1965, under the supervision of Professor G.R. Martin B.Sc., A.R.C.S., F.R.I.C., professor of Chemistry in the University of Kent.

This thesis contains the results of some original research by the author, and no part of the material offered has previously been submitted by the candidate for a degree in this or any other university. Where use has been made of the results and conclusions of other authors in relevant studies, care has been taken to ensure that the source of information is always clearly indicated, unless it is of such general nature that indication is impracticable.

Brian W. East.

BRIAN W. EAST.

AN ACKNOWLEDGEMENT

The author wishes to thank:-

Professor G.R. Martin for suggesting the research topic, and for his expert advice and helpful supervision.

Mrs. E.B.M. Martin for her interest in the work and for making several of her results available.

Mr. R. Oliver for much technical assistance, for operating the accelerating machines, and for his companionship.

Mr. C.G.B. Williams for many valuable discussions during the course of the work, and for his close companionship.

The Science Research Council for the award of a Research Studentship.

The University of Kent at Canterbury for appointment to a Research Assistantship, sponsored by the Atomic Energy Research Establishment, during the tenure of which, part of this work was carried out.

SUMMARY

The cross-sections of twenty-six nuclear reactions occurring in the natural elements, copper, gallium, silver germanium, rubidium and thallium at a neutron energy of 14 MeV have been measured. Of particular importance has been the investigation of the $(n,\alpha n) + (n,n\alpha)$ reaction, and cross-sections have been obtained for the first three elements mentioned, while upper limits have been set in each of the remaining cases. The results, together with those of the (n,p) (n,α) and $(n,2n)$ cross-sections, are discussed in relation to theoretical values insofar as these may be predicted by evaporation and direct interaction theories. A comparison is also made with the general trend of results obtained by other workers over a wide mass range.

Neutrons have been generated by the (D,T) reaction using both 150 KeV Cockcroft-Walton and 400 KeV electrostatic accelerating machines.

Radiochemical techniques have been employed throughout, end-window proportional counting being used to determine absolute disintegration rates. Calibration of the counter by the method of Bayhurst and Prestwood has allowed the interpolation of β -counting efficiencies to within 3% over

the energy range 0.254-3.58 MeV. γ -spectroscopy has been used where practicable for the identification of product nuclides using NaI(Tl) crystals in conjunction with multichannel pulse amplitude analysers. Internal gas-counting techniques have also been developed to investigate the krypton (n,p) products from rubidium.

The cross-sections have been measured relative to the $^{56}\text{Fe}(n,p)^{56}\text{Mn}$ and $^{27}\text{Al}(n,\alpha)^{24}\text{Na}$ reactions for which absolute values were available. Both sandwiched-foil and homogeneous mixture techniques have been used to introduce the reference material into the sample for irradiation under conditions of poor geometry.

CONTENTS

<u>Chapter 1</u>	-	<u>Introduction</u>	<u>Page</u>
1.		<u>General</u>	
		Neutrons.	1
		Nuclear models.	3
		Neutron sources.	7
		Nuclear reactions at a neutron energy of 14 MeV.	10
2.		<u>The present studies</u>	
		The measurement of activation cross-sections.	18
		The application of chemistry to the activation method.	21
		Introduction to the present work.	23
<u>Chapter 2</u>	-	<u>A description of general experimental techniques</u>	
1.		<u>The sources of neutrons</u>	25
		1.a. The Cockroft-Walton accelerator.	26
		1.b. The electrostatic accelerator.	27
		1.c. Tritium targets.	28
		1.d. Relative flux measurements.	29
		1.e. Neutron energies.	30
2.		<u>The secondary standards</u>	30

Contents Cont'd

3.	<u>Methods of calculation</u>	<u>Page</u>
3.a.	Corrections for the variation in neutron flux.	36
3.b.	Calculation of proportional counter efficiency.	39
4.	<u>Chemical separation methods</u>	
4.a.	The choice of sample material.	41
4.b.	Chemical separation procedures.	43
4.c.	The preparation of sources for end-window counting.	44
5.	<u>Counting techniques</u>	
5.a.	<u>End-window proportional counting</u>	46
5.a. (i)	A description of the counter and its operation.	47
5.a. (ii)	The demountable counter stand.	50
5.a. (iii)	The melinex window.	52
5.a. (iv)	Calibration	54
5.b.	<u>Scintillation counting</u>	
5.b. (i)	The operation of NaI(Tl) crystals.	59
5.b. (ii)	The energy calibration of crystals.	62
5.b. (iii)	The 2" x 1 $\frac{3}{4}$ " well crystal.	63
5.b. (iv)	The 1 $\frac{1}{2}$ " x 1" and 3" x 3" flat crystals.	64

Contents Cont'd

	<u>Page</u>
5.c. <u>Geiger counting</u>	
5.c. (i) The operation of Geiger counters.	64
5.c. (ii) Calibration of the liquid counter.	65
5.c. (iii) Internal gas-counting.	69
<u>Chapter 3.</u> - <u>A description of the individual cross-section measurements and the results</u>	
1. <u>The reactions of copper</u>	72
The chemical separation procedure.	73
The preparation of carrier solutions.	75
The determination of cobalt.	75
Observations.	76
Discussion.	77
2. <u>The reactions of gallium</u>	79
The chemical separation procedure.	82
The preparation of the carrier solutions.	84
The titrimetric determination of gallium.	85
The determination of zinc.	85
Observations.	86
Discussion.	89
3. <u>The reactions of rubidium</u>	
3.a. <u>The measurement of the bromine activities</u>	91
The chemical separation procedure.	92
The preparation of bromate carrier solution.	94

Contents Cont'd

	<u>Page</u>
<u>3.a. Cont'd</u>	
The determination of the chemical yield of bromine.	94
Observations.	95
Discussion.	96
The chemical exchange of the bromine activities.	98
The reaction of product bromine activities with the iron reference material.	100
The measurement of the $^{87}\text{Rb}(n,2n)^{86}\text{Rb}$ and $^{85}\text{Rb}(n,\alpha)^{82}\text{Br}$ cross-sections without chemical separation.	101
<u>3.b. The measurement of the krypton activities</u>	104
The apparatus used for the isolation of krypton.	105
The procedure for the isolation of krypton.	107
Observations.	110
Discussion.	111
4. <u>The reactions of germanium</u>	113
The preparation and determination of the zinc carrier solution.	114
The preparation and determination of the gallium carrier solution.	115
The chemical separation procedure.	116
Observations.	120
Discussion.	125
5. <u>The reactions of silver</u>	
The preparation of rhodium carrier solution.	130
The determination of the rhodium carrier solution.	132

Contents Cont'd

	<u>Page</u>
5. <u>The reactions of silver cont'd</u>	
The preparation of the palladium carrier solution.	134
The determination of the palladium carrier.	135
The chemical separation procedure.	136
Observations.	138
Discussion.	144
6. <u>The reactions of thallium</u>	146
The preparation of mercury carrier solution.	147
The determination of the chemical yield of mercury.	148
The preparation of the gold carrier solution.	149
The chemical separation procedure.	150
Observations.	151
Discussion.	154
<u>Chapter 4</u> - <u>The Discussion</u>	
1. An assessment of the experimental techniques.	156
2. <u>The collected results and the discussion</u>	159

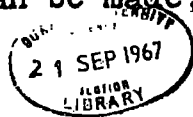
CHAPTER 1

INTRODUCTION

Neutrons

In nuclear interactions neutrons differ greatly from charged bombarding particles. With the latter there is the initial difficulty of surmounting the Coulomb barrier associated with the nucleus before strong interactions can take place. This sets a lower limit upon the energy which these particles must possess before nuclear reactions can be initiated. For example, protons will only interact strongly with the heaviest nuclei at energies of 15 MeV or above. In contrast, the lower limit for neutrons is fixed principally by the availability of workable fluxes and these can be obtained in practice at the relatively minute energies of 10^{-4} eV. It is thus in the low energy regions that neutrons are unique in providing information about nuclear structure. At the opposite extreme, neutron energies of approximately 10^4 MeV can be achieved, further emphasising the usefulness of the particles in allowing an examination of nuclear phenomena over a wide energy range.

A large variety of interactions is observed over the whole neutron spectrum and some classification of neutrons according to energy can be made, depending upon the type



of interaction taking place. At energies from 10^{-4} to 10^{-1} eV the term "thermal neutrons" is used, since fluxes of such neutrons have energy distributions comparable with those of gaseous molecules in thermal equilibrium. Predominantly optical properties are exhibited in this region, the wavelength of the neutrons being long even in comparison with interatomic distances. As the energy increases up to approximately 100 eV, resonances can be observed for the capture of neutrons, corresponding to the nuclear excitation levels. This range of neutron energies is known as the "resonance region" and results obtained in this part of the spectrum are of great importance to the understanding of nuclear structure and have immediate practical applications in the operation of reactors. Fast neutrons are those which have energies in excess of about 0.1 MeV, since for most nuclei the resonances can no longer be resolved and the measure of interaction becomes continuous. In contrast with thermal neutrons, the wavelength of fast neutrons is generally comparable with the range of nuclear binding forces and interactions are best considered to be of a particulate nature. These distinctions between various types of neutrons are however somewhat vague and an example of the ambiguity is the division between "resonance" and "fast" neutrons. In some light nuclides, resonances can still be resolved at energies of 40 MeV using what are effectively

"fast"neutrons.

A measure of the interaction of neutrons with nuclei is provided by the neutron cross-section. The probability that a neutron will collide with a target nucleus is proportional to the cross-sectional area of the latter, projected onto a plane normal to the incident neutron flux. Cross-sections are measured in units of area called barns, one barn being equal to 10^{-24} cm². This quantity is conveniently chosen because nuclei in the region of A=100 have projected areas of approximately this magnitude. For any nucleus a total cross-section can be defined which accounts for all the possible modes of interaction, including scattering. The total cross-section can be divided into partial cross-sections each proportional to the probability of a particular reaction following the collision of a neutron. While this concept of nuclear processes provides a sound quantitative basis for their study, it cannot be extended too far into the detailed discussion of nuclear structure. Thus, it is often difficult to reconcile large variations of neutron cross-sections occurring with small changes in energy, with the relatively constant dimensions of the target nucleus.

Nuclear models

Apart from being of immediate practical value, especially

in the fields of activation analysis and the production of radioactive isotopes for tracer studies, the determination of neutron cross-sections is important in the elucidation of nuclear structure. By constructing plausible nuclear models and considering possible reaction mechanisms, simplified calculations can be made to predict values for cross-sections. A comparison of these values with those determined experimentally then gives an indication as to the validity of the model and demonstrates its limitations.

In early work the "black" or "perfectly absorbing" nucleus model accounted well for observed phenomena but it soon became evident that this picture was inadequate. The variations in neutron cross-sections with energy were shown to be analogous to optical diffraction effects pointing to the existence of a fine structure in the nucleus not accounted for by the black nucleus model. The implication that the nucleus was appreciably transparent led to the development of the "cloudy crystal ball" model which provided for the event that in the extreme case, a neutron might traverse the nucleus without any strong interactions taking place. At low energies this occurrence is not unreasonable since all the energy levels in the nucleus are already occupied and the incoming neutron cannot be accommodated. For fast neutrons the high excitation of the nucleus which results, gives rise to a large number of

available levels and the nucleus again becomes "opaque". So great is the number of levels in fact, that a statistical treatment can be used to describe the state of the excited nucleus, allowing calculations to be made. This is the basis of the statistical model.

On the assumption that the nucleus is strongly absorbing, interactions can be explained by means of the formation of a compound nucleus. The neutron is rapidly absorbed, losing its identity; the binding and kinetic energies become distributed throughout the whole nucleus, much in the same way as energy is shared between the molecules in a liquid drop. The subsequent decay of the excited nucleus is independent of its mode of formation and occurs when sufficient energy becomes concentrated upon a particular nucleon to allow its escape. Again, in analogy with a liquid drop, this process is often pictured as an evaporation. Since the metastable compound nucleus exists for a relatively long period, an explanation of the sharp resonances discernible at low bombarding energies, is provided.

At high energies however, this mechanism becomes inadequate and experimental cross-sections are found to deviate from those calculated. Consideration of the implications of the optical model has led to the conception

of another mechanism which can be used to explain many anomalous results. The model is extended so as to allow for inelastic interactions by considering in greater detail the structure of the target nucleus. Two types of structure have been widely used. In the first, the nucleus is considered to consist of two components held together by mutual attraction. The incoming particle then interacts with one of these components (a nucleon or a group of nucleons) inelastically. A second representation which includes even more detail is that the nucleus consists of a core surrounded by other nucleons. Within the core the nucleons are in completed shells while those remaining are in incomplete shells and are available to take part in strong interactions. This is the basic concept of the shell model which particularly allows the consideration of surface effects, especially in the case of heavy nuclei. Included in both these representations are the possibilities of either "pick-up" or "knock-out" processes.^{1,2)}

The distinction between the compound nucleus and direct mechanisms is that in the latter the energy is not distributed evenly throughout the excited nucleus and the interactions are essentially one-step processes occurring in a time interval of about 10^{-22} seconds, the time taken for a fast neutron to traverse the nucleus. Experimentally, direct interactions also exhibit a strong dependence upon

the direction in which the reaction products are emitted. Despite the fact that the two mechanisms are quite different, both often have to be considered to contribute to the overall reaction, each to an extent determined by the incident neutron energy and the mass of the target nucleus. A theory of direct interactions occurring throughout the volume of the nucleus was initially developed for quantitative use by Brown and Muirhead³⁾ and has more recently been refined by Tobocman.⁴⁾

These concepts of nuclear structure and nuclear reactions are gross simplifications of the true situation. They have, however, proved invaluable by providing necessary alternatives to the solution of the many-body problem.

Neutron sources.

Information about the structure of the nucleus is derived from the variation of neutron cross-sections with energy, and if accurate results are to be obtained, so that useful comparisons can be made with theory, neutron sources of variable energy and high resolution are required. In this respect the neutron has certain disadvantages in comparison with charged particles. Fluxes of the latter, which fulfill these requirements can conveniently be generated with accelerators, whereas neutrons are only available indirectly from nuclear reactions. This makes the production of fluxes of monoenergetic neutrons with variable

energy a difficult problem. In the low energy region such neutrons are available up to 10,000 eV using crystal diffraction and time-of-flight selection techniques. For fast neutrons the difficulties of generation over a continuous energy range become more apparent. Early workers employed sources which relied upon (α, n) and (γ, n) reactions in various nuclei, the bombarding particles being obtained from naturally occurring radioactive nuclides such as radium. However the sources had a large energy spread and a low neutron yield so that results obtained using them were far from accurate. With the development of particle accelerators, fast neutrons are now available from a wider variety of nuclear reactions and with much more useful resolution. Beam currents have also been extended into the milliampere range so that good fluxes can be realised. Since individual nuclear reactions which can be employed in this way only provide neutrons over a limited energy range, work on fast neutron cross-sections has of necessity, become concentrated around particular energies.

The principal sources have been reactions occurring in the light nuclei. Medium weight nuclei are now however being investigated as possible sources so that the gaps in the spectrum, where information is somewhat scanty, might be more accurately filled in. Examples of such

sources are the (p,n) reactions induced in ^{45}Sc , ^{63}Cu and ^{65}Cu which provide, with available proton energies, neutrons from 1 to 700 KeV. A disadvantage of such reactions is that they have small cross-sections so that high beam currents are required to produce useful fluxes. They do however represent an important class of reactions in which the neutron energy can be controlled by varying the incident proton energy, the excited states in the product nucleus being relatively widely spaced. In cases where higher states are excited the resulting mixed spectrum of neutrons can be resolved by time-of-flight methods and this has allowed the use of reactions such as $^9\text{Be}(\alpha, n)^{12}\text{C}$ ($E_n \approx 8\text{MeV}$) and $^{15}\text{N}(d, n)^{16}\text{O}$ ($E_n \approx 11.6\text{ MeV}$).⁵⁾

Up until the present time, work has been largely carried out using neutrons derived from reactions in the very light nuclei. One of the first accelerator sources was the $^7\text{Li}(p, n)^7\text{Be}$ reaction which provided neutrons from 120 KeV to approximately 400 KeV. The perfection of suitable deuterium and tritium targets for use in accelerators then widened the scope of fast neutron spectroscopy considerably. Of the possible reactions those which have been used most extensively are the $\text{D}(d, n)^3\text{He}$ ($E_n \approx 3-14\text{ MeV}$), the $\text{T}(d, n)^4\text{He}$ ($E_n \approx 13-20\text{ MeV}$) and the $\text{T}(p, n)^3\text{He}$ ($E_n \approx 1-13\text{ MeV}$) reactions. Investigations

into the $H(t,n)^3He$ reaction have also recently been started and there is interest in the $D(t,n)^4He$ reaction.⁶) In the work described here, 14 MeV neutrons from the $T(d,n)^4He$ reaction have been used.

Nuclear reactions at a neutron energy of 14 MeV.

At an energy of 14 MeV a large number of neutron-induced reactions are energetically possible. For most nuclei the $(n,2n)$ (n,p) and (n,α) reactions are predominant. The magnitudes of $(n,2n)$ cross-sections are of the order of tens of millibarns for light nuclides, increasing to a few barns at the heavy end of the mass range. The cross-sections of the charged particle reactions generally follow a trend in the opposite sense being relatively large for light nuclides (up to hundreds of millibarns) and small for the heavy nuclei (of the order of a few millibarns). Despite competition from these three reactions, the (n,γ) capture process is still appreciable and for many nuclides has a value of several millibarns.⁷) In the heaviest elements fission of the nucleus also occurs and because of its theoretical and practical importance, has received much attention at this neutron energy.

The methods for the measurement of cross-sections, other than those for scattering processes, can be divided into two general groups: those which involve the detection

of the secondary particles emitted during the reaction and those where the radioactivity of the residual nuclei is measured.

Among the techniques included in the first approach, the use of nuclear emulsions and the detection of the secondary particles in scintillation crystals and semiconductor counters have been well developed. The most important feature of the method is that it allows the angular distribution as well as the energy spread of the emitted particles to be determined, thereby providing a means of distinguishing between direct and compound nucleus mechanisms. Because such a distinction can be made, much effort is being directed towards the development of the technique so that it might have a wider application. At the present time, results are restricted largely to those elements which form part of the detector i.e. the (n, α) reactions in Si, K, Na, I, Br and Cs, so that ways must be found of loading the detector⁸⁾ with the desired element, or improving methods of external detection of the secondary particles, to widen the scope of investigations. Patzak and Vonach⁹⁾ have for instance, measured the $^{27}\text{Al}(n, \alpha)^{24}\text{Na}$ and $^{59}\text{Co}(n, \alpha)^{56}\text{Mn}$ reactions by using a photoplate mounted in a vacuum chamber. Another major problem is that of distinguishing the events of interest from a high background

in the crystal or semiconductor detector. Several workers^{10,11)} have developed pulse shape discrimination techniques to overcome this.

Many of the products of neutron -induced reactions are radioactive. (n,2n) reactions generally give rise to nuclides which decay by positron emission or electron capture, while the charged particle reactions result in β^- -active isotopes. The technique of radioactivation analysis can thus be applied to measure cross-sections. Reliance is placed upon the determination of the half-lives and characteristic emissions, as a means of identifying and measuring the products. Often, complicated mixtures of activities result when any one element is irradiated and the problem of resolving individual components leads to difficulties in making accurate measurements. Some of these difficulties may be overcome by using radiochemical procedures when the products can be separated to some extent.

A third possible approach which is worthy of mention is the use of mass-spectroscopy. In principle this is a powerful method of separating the products but although it has been used in some fission studies¹²⁾, the problems of low yield and absolute quantitative measurement associated with fast neutron cross-sections as yet preclude its use in this field.

Much information has now been accumulated about the absolute cross-sections of the $(n,2n)$ (n,p) and (n,α) reactions at 14 MeV. One striking feature is the large number of discrepancies which exist between values obtained in different laboratories, mainly due to errors in the estimation of counter efficiencies. Part of the present work has been concerned with the resolution of some of these differences by using radiochemical separations and accurately calibrated counters.

In spite of disagreements, a comparison of the general trend of results with theory has proved to be of great value and several aspects of neutron reactions are now better understood. The compound nucleus theory has largely accounted for the $(n,2n)$ cross-sections but with the improvement of techniques, neutron shell effects¹³⁾ and the possibility of competition from the tertiary $(n,3n)$ reaction^{14,15)} have been treated in greater detail. Other anomalies have indicated that direct interactions must also be considered.^{16,17)} The measurement of isomeric cross-section ratios which allows a closer assessment of the reaction mechanisms by considering the spins of the products, together with a more detailed study of excitation functions^{18,19)} reflect the trend of further investigations.

The analysis of (n,p) cross-sections has proved to be a

complicated problem and has led to some apparent disparity in the interpretation of the results. Recently, Gardner²⁰) has derived a series of empirical equations from experimental data which predict the cross-sections quite successfully over a wide mass range. One outstanding conclusion which he reaches is that since the form of the equations is the same for both the low and high-Z nuclides, values of cross-sections measured at 14 MeV alone, can throw little light on reaction mechanisms. For the high-Z nuclides the contribution from direct mechanisms would be expected to alter the form of the equations relating the cross-sections. Also he noticed no marked fluctuations in cross-sections due to proton shell effects. In the regions of closed shells the number of stable isotopes increases thereby removing the lightest isotope further from stability. For such an isotope the (n,p) cross-section would be expected to be relatively large. In contrast, Chatterjee²¹) picks out shell effects by plotting (n,p) cross-sections against the proton number of the residual nucleus and shows that maxima exist at each of the closed shells. A modified statistical model in which the level density of the residual nucleus becomes shell-dependent is used successfully to predict these shell effects. Colli²²) has also made a general assessment of the (n,p) results and has shown that the compound nucleus mechanism can account

for the cross-sections of nuclides up to $A=60$ and that direct effects increase to a maximum up to $Z \approx 40$ and then decrease due to the increasing Coulomb barrier.

The (n, α) reactions are similar to the (n, p) reactions in that variations in the cross-sections have been attributed to compound nucleus and direct effects over the range of elements. It is generally thought that the compound nucleus mechanism predominates for the light elements. Saetta-Menichella et al²³⁾ and Facchini et al²⁴⁾ have recently examined (n, α) cross-sections and excitation functions in relation to the statistical model and have found that there is close agreement for nuclides up to $A \approx 80$. Mani et al²⁵⁾ have also made similar comparisons in the range $A = 20 - 120$ and have arrived at the same conclusion. As for the (n, p) reactions, the fine structure of the nucleus also gives rise to noticeable effects. In a series of papers, Chatterjee^{26,27)} has analysed the trends in (n, α) cross-sections and noted proton shell, and to a lesser extent, neutron shell effects in the residual nucleus. Over the small range of $6 \leq Z \leq 30$, Gardner²⁸⁾ has derived empirical equations on the basis of the statistical model, which fit the results. He suggests however, that the shell effects originate in the target, rather than the residual nucleus.

For the heavy nuclides the (n, α) cross-sections become larger than those predicted by the compound nucleus theory. At the present time a quantitative theoretical treatment of direct reactions involving α -particles is not available, so that comparisons with experimental cross-sections cannot be made. However, in analogy with the (n, p) reactions these deviations in the cross-sections have been attributed to direct effects. This immediately implies that relatively complicated groups of nucleons exist in the nucleus in contrast to the much simpler situation in (n, p) reactions. If, for instance, the direct interaction had a knock-out mechanism then a group equivalent to ${}^4\text{He}$ would be involved and if the interaction was of the pick-up type, the group would be ${}^3\text{He}$. Further these groups would have to be situated in or near the nuclear surface to facilitate interaction, as the mean free path of the secondary particle in the nucleus would be very short. The existence of such groups would however seem to be somewhat improbable and an equally reasonable explanation for the fact that the evaporation theory cannot account for the observed cross-sections would be that deviations from the assumed statistical distribution of the energy levels in the residual nucleus occur. It is obviously of great interest to examine these and similar reactions in greater detail to test these possibilities.

As well as the $(n, 2n)$ (n, p) (n, α) and (n, γ) reactions,

several others are energetically possible at 14 MeV. These involve groups of nucleons and include such reactions as: - (n,np) (n,pn) $(n,2p)$ (n,d) (n,dn) (n,t) $(n,\alpha n)$ $(n,n\alpha)$ $(n,3n)$ and $(n,^3\text{He})$. Consideration of their Q-values indicates that the probability of their occurrence is relatively low and for this reason they are referred to as the rare reactions and are expected to have small cross-sections of certainly no more than a few millibarns. Some of the product nuclides of the reactions as written are ambiguous and distinctions as to the actual reaction route are best made by secondary particle techniques. In other cases however, the reactions can be studied by activation analysis and since the cross-sections can be measured with reasonable accuracy in this way, it is possible to obtain useful evidence of the type of mechanism involved. In particular, a comparison of (n,α) and $[(n,\alpha n) + (n,n\alpha)]$ cross-sections allows a discussion of the mechanism by considering the extent of each of these reactions. If the interaction is initially with an α -particle in the nuclear surface then the residual nucleus would be expected to be left in a low state of excitation with the resulting low probability of neutron emission. The ratio of the (n,α) to $[(n,\alpha n) + (n,n\alpha)]$ cross-sections would be expected to be high in this case. Also the possibility

of interaction occurring initially with a neutron, or an overall compound nucleus mechanism can be discussed.

2. The present studies.

The principal object of the present studies has been to measure $(n, \alpha n) + (n, n \alpha)$ cross-sections which lend themselves to the radiochemical approach. As an introduction to the methods employed, it is felt that some discussion of the simple theoretical aspects of the measurement of partial neutron cross-sections in general, is necessary, so that the experimental requirements may be better assessed.

The measurement of activation cross-sections.

Consider the ideal case when an infinitely thin sample is irradiated with a constant flux of monoenergetic neutrons:-

The number of product nuclei appearing per second =

$$\frac{dN_p}{dt} = \phi \sigma N_s$$

where N_s = total number of stable target nuclei exposed to the neutron flux

ϕ = neutron flux (neutrons/sec/cm²)

σ = cross section for the nuclear reaction at the neutron energy concerned. (cm²).

After irradiation of the sample for T seconds, the number of product nuclei, if stable, would be given by:-

$$N_p \text{ stable} = \phi \sigma N_s T$$

If however, the product nuclei are radioactive, with a decay constant λ_p , the rate of production will be partially offset by losses through radioactive decay. For a very long irradiation, the number of active nuclei N_p , will increase until saturation is reached, when the rate of production just equals the rate of decay:-

$$\frac{dN_p}{dt} = N_p \lambda_p \quad \text{so} \quad N_p \lambda_p = \phi \sigma N_s$$

Now, $N_p \lambda_p$ equals I_{p0} , the absolute activity of the product nuclide at saturation, so that:-

$$I_{p0} = \phi \sigma N_s$$

If equilibrium is not reached, the activity I_{pT} , of the product nuclide after an irradiation of T seconds can be expressed as:-

$$I_{pT} = I_{p0} (1 - e^{-\lambda_p T})$$

$$\text{therefore } I_{pT} = \phi \sigma N_s (1 - e^{-\lambda_p T}) \quad \dots\dots\dots(1)$$

Equation 1 is the basic relationship for the measurement of activation neutron cross-sections. Of the various quantities in this equation, λ_p , T and N_s present the least difficulty with regard to accurate determination, Since reliance

is primarily placed upon the observed value of λ_p to identify the product nuclide, this value is already pre-supposed. Identification is achieved by comparing observed values of λ_p with those accepted in the literature.

The limit of accuracy with which the time of irradiation T , can be determined is set by the rapidity with which the neutron flux can be stopped and started. The way in which this is done is described in the section on neutron sources. Suffice it for the moment to note that this takes an appreciable time, estimated to be between one and two seconds. Since, however, the shorter irradiation times are of the order of ten minutes the error in this quantity would not be expected to be serious. N_g , the number of target nuclei can also be determined accurately by weighing with an error of less than 0.02%.

In contrast, the remaining quantities I_{pT} , the absolute activity and ϕ , the neutron flux are much more difficult to measure accurately. So much so, that it is the errors in these quantities which govern the overall accuracy with which σ can be determined.

Indirect methods have been adopted in the present work to measure both these quantities. Practical considerations have necessitated the use of calibrated counters or counters for which the absolute efficiency has been calculated, while

neutron fluxes have been found using the secondary standard method. Here, a reference element is introduced into the sample material and arrangements made so that both are exposed to the same neutron flux, as nearly as possible. By comparing the activities induced in each component and with a knowledge of the absolute cross-section of a specific reaction in the reference element the unknown cross-section can be calculated.

For the reference element (r) a similar expression to equation 1 can be written, making the same assumptions:-

$$I_{Tr} = \phi \sigma_r N_{sr} (1 - e^{-\lambda_{pr}T}) \dots\dots\dots(2)$$

Combining equations (1) and (2) the neutron flux ϕ , is eliminated:-

$$\frac{I_T}{I_{Tr}} = \frac{\sigma_N N_S (1 - e^{-\lambda_{pT}T})}{\sigma_r N_{sr} (1 - e^{-\lambda_{pr}T})} \dots\dots\dots(3)$$

Thus a direct determination of ϕ is not necessary.

The application of chemistry to the activation method

The initial difficulty associated with the measurement of absolute activities arises from the variety of reactions which are induced by 14 MeV neutrons. Irradiation of a given element, which often consists of several stable isotopes, inevitably

results in a complicated mixture of radioactive nuclides. At the extreme, the total activity of the irradiated sample can be measured and attempts made to determine individual activities by resolution of the gross decay curves. Often, however, several components of the mixture have similar decay constants and characteristic emissions so that this becomes very difficult. Since the neutron-charged particle reactions give rise to isotopes of elements different from the sample element, the application of chemistry allows some separation of the products to be made, thus considerably simplifying the problem. Such a technique has largely been employed in the present work and has proved particularly useful for the separation of the rarer reaction products with low activities.

A decision as to which cross-sections could usefully be measured in this way was based on several considerations. Nuclides with half-lives shorter than a few minutes could not be measured due to the time taken to complete chemical separations. Also, nuclides with half-lives longer than a few days were largely ruled out since their activity would be too low with the available neutron flux. Despite chemical separation, the resulting sources would in many cases be expected to contain several activities so that the half-lives would have to differ substantially to allow accurate analysis of

the decay curves by graphical methods. In this respect, the resolution of activities with half-lives differing by not much less than a factor of two was considered to be practical. For smaller differences the identification of the activities is liable to become uncertain.

Application of such considerations revealed that the number of $[(n, \alpha n) + (n, n \alpha)]$ cross-sections which could be measured was limited to about thirty, over the range of elements. An additional restriction in this case being the avoidance of interference from the (n, α) reaction on the adjacent $(Z, (A-1))$ isotope of the sample element.

Introduction to the present work

At the commencement of studies, Bormann et al²⁹) had reported values for several $[(n, \alpha n) + (n, n \alpha)]$ cross-sections. Their results seemed to be somewhat higher than would have been expected and thus prompted further investigation. Initial experiments showed that their results for copper and gallium could not be reproduced. Other elements have also been examined and upper limits set for the cross-section. In the case of silver, a value for the ^{109}Ag $[(n, \alpha n) + (n, n \alpha)]$ ^{105}Rh reaction, for which a cross-section had not previously been reported, has been obtained.

The cross-sections have been measured relative to the

$^{27}\text{Al}(n, \alpha)^{24}\text{Na}$ and $^{56}\text{Fe}(n, p)^{56}\text{Mn}$ reactions for which absolute values were available ³⁰). Counting equipment has been calibrated to allow the accurate determination of absolute β^- -activities. γ -spectroscopy, using NaI(Tl) crystals has also been employed where possible, to aid the identification of product nuclides.

Together with the main project, several (n, α) (n, p) and $(n, 2n)$ cross-sections have also been measured where the number of previously reported values was small or where inconsistencies occurred. In a number of cases the results have been found to disagree markedly with those of other workers. The use of internal gas-counting techniques, associated with the study of rubidium, has allowed the estimation of the $^{85}\text{Rb}(n, p)^{85\text{m}}\text{Kr}$ and $^{87}\text{Rb}(n, p)^{87}\text{Kr}$ cross-sections for which no previous values were available.

In the following chapter, the general experimental methods are described. Chapter 3 deals in detail with the various cross-sections measured and the results are collected and discussed in the final chapter.

CHAPTER 2

A description of general experimental techniques

1. The sources of neutrons

14 MeV neutrons were produced by the $T(d,n)^4He$ reaction which occurs when tritium targets are bombarded with deuterons. The reaction has a Q-value of + 17.58 MeV and the large reaction cross-section, with a resonance peak at 109 KeV incident deuteron energy; allows the generation of high fluxes of neutrons within a narrow energy range. Two different accelerators have been used to generate beams of deuterons during the course of this work, similar tritium targets being bombarded in each case.

The 150 KeV Cockcroft-Walton accelerator in the Londonderry Laboratory for Radiochemistry at Durham, was capable of providing deuteron beams of up to 150 μ amps which gave fluxes in the region of 10^8 n/sec/cm². Much higher fluxes have been realised on the S.A.M.E.S. 400 KeV electrostatic accelerator at Canterbury where beams of 800 μ amp were obtainable at 220 KeV, resulting in fluxes approaching 10^9 n/sec/cm².

The approach to the measurement of cross-sections has been the same in both laboratories except for the modifications to the procedure used for the $^{56}Fe(n,p)^{56}Mn$ reference reaction

which are later described in the section on the calibration of the liquid counter. (p. 65).

1.a. The Cockcroft-Walton accelerator

This machine has been well described by previous workers^{31,32}) and only a brief description of its operation need be given.

The high accelerating voltage was developed by a voltage quadrupling circuit and fed to a two-stage accelerating tube mounted in a vertical position. At the lower end of the tube, the deuteron beam was allowed to fall onto the tritium target which was soldered to a brass target block. Water cooling was applied to the target block to reduce the loss of tritium, some 30 watts of heat being dissipated under operating conditions. Samples were irradiated externally at 0° to the incident deuteron beam and as close to the target as possible. The irradiation geometry is shown diagrammatically in fig. 1. In order to reduce the flux of scattered neutrons through the sample, the target block was situated several feet from the walls of the concrete irradiation chamber. Other parts of the accelerator such as the ion source and the pumping arrangements were similar to those on the electrostatic machine described in the following section.

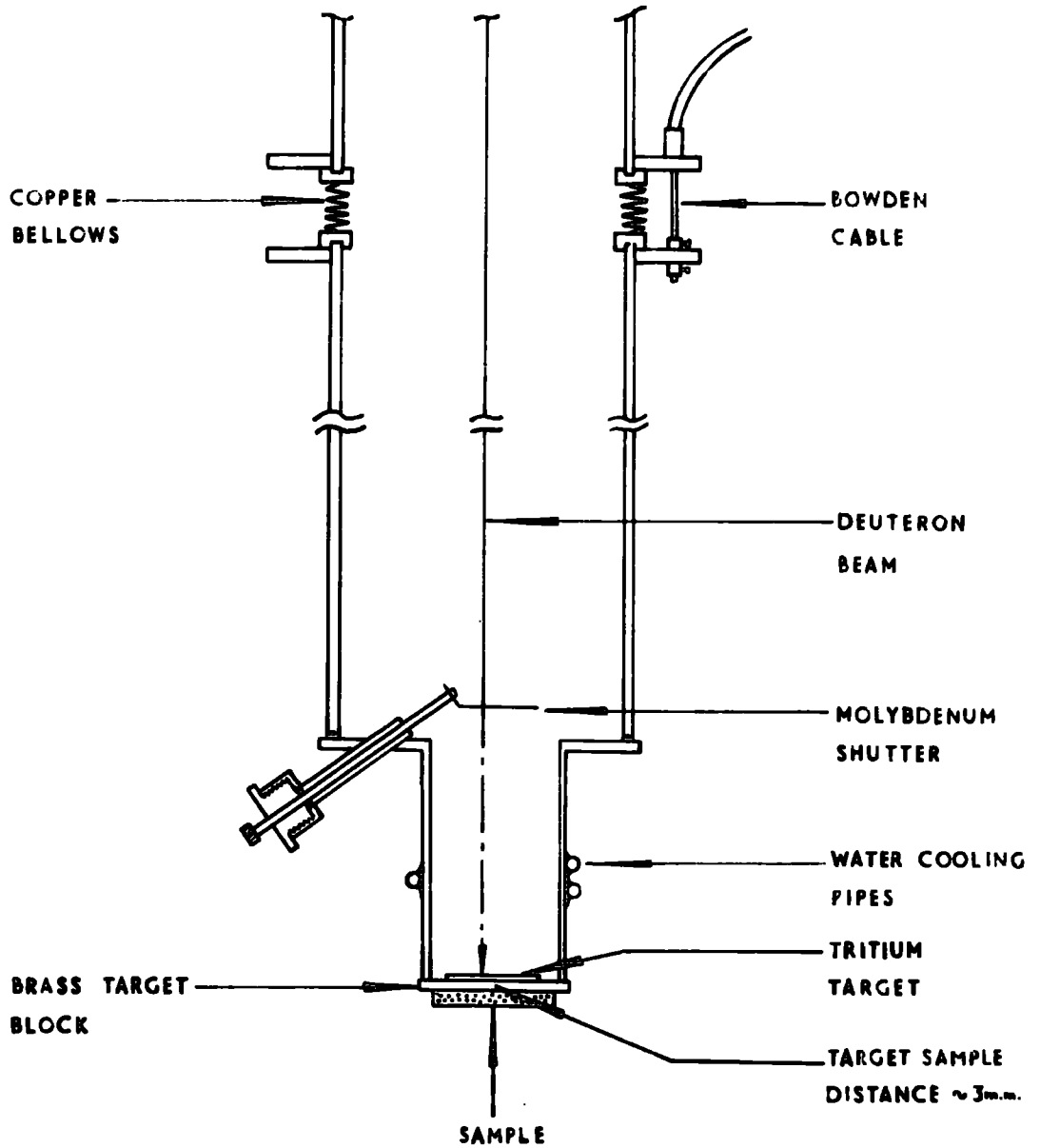


FIG 1 THE IRRADIATION GEOMETRY OF THE
 COCKCROFT-WALTON ACCELERATOR.

1.b. The electrostatic accelerator.

Housed in the laboratories at Canterbury, this machine was built by the Société Anonyme de Machines Electrostatiques and its design is shown in fig. 2. The high positive accelerating voltage was supplied by an electrostatic generator type K-400-3, capable of delivering 3 mA at 400 KeV. This generator worked on the Van der Graaff principle of "voltage amplification" and was extremely compact in its design. An insulated cylinder ~ 40 cm. in diameter and ~ 170 cm long was rotated at high speed about a vertical axis. A D.C. excitation voltage of 50 KeV was fed to this by a set of electrostatic brushes. The accumulated charge was removed from the cylinder by similar brushes and fed via a $3M\Omega$ series damping resistor to the high voltage electrode. All the working parts of the generator were contained in a steel vessel, pressurised to approximately 20 atmospheres with hydrogen. This gas, while providing a good insulation at the voltages involved allowed also a very efficient exchange of charge at the brushes.

The high voltage electrode which was connected to the first stage of the horizontal accelerating tube, contained the ion source in which deuterons were produced by the excitation of deuterium gas with radio frequency energy from a 100 watt self-excited oscillator operating at approximately

100 Mc/s. After extraction and admission to the tube, the deuterons underwent eight stages of acceleration to 220 KeV, this being the lowest voltage at which a stable beam could be maintained. The emergent beam at the earthed end of the tube was focussed electrostatically and passed down an extension into the shielded experimental area, where it was allowed to impinge on the tritium target. A pressure of approximately 10^{-6} m.m. Hg was maintained in the accelerating tube and extension by a silicone oil diffusion pump and a mechanical backing pump.

Some 200 watts was dissipated at the target during operation, necessitating efficient water cooling. The target arrangement is shown in fig. 3 - efficient cooling was provided by the copper block while the target-sample distance was kept as short as possible. Irradiation times were controlled by switching the deuteron beam with the extraction voltage applied to the ion source.

1.c. Tritium targets.

Tritium targets were of the type described by Wilson and Evans³³) and were obtained from the U.K.A.E.A. Each consisted of approximately 0.6 c.c. of tritium gas at S.T.P. adsorbed in a thin layer of titanium metal ($\sim 300 \text{ } \mu\text{g/cm}^2$) evaporated onto a copper foil. In use the targets were divided into four equal segments, one segment at a time being soldered to the

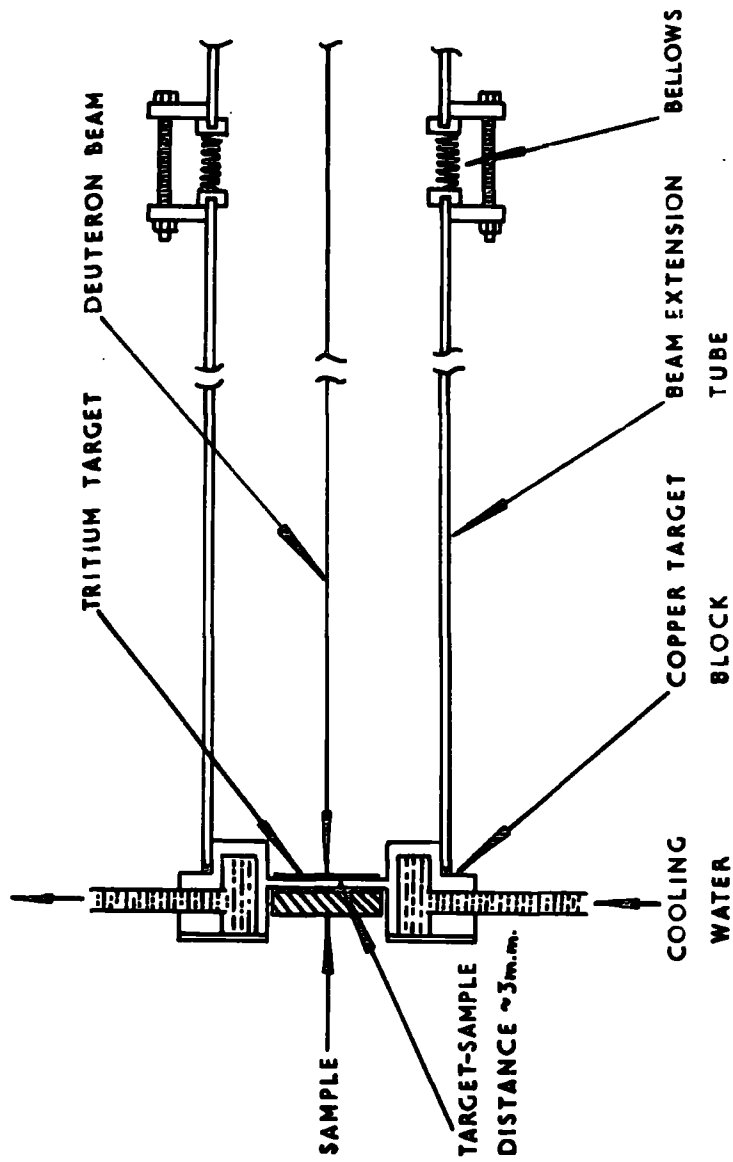


FIG 3 THE IRRADIATION GEOMETRY USED ON THE
 S.A.M.E.S. ELECTROSTATIC ACCELERATOR.

target block with Wood's alloy. The segments were found to have a useful life of approximately 5000 μ amp hours after which time the neutron yield fell to some 10% of its initial value, due mainly to the loss of tritium.

As deuterium accumulated in the ageing targets, the contribution to the flux by 3 MeV neutrons from the $D(d,n)^3\text{He}$ reaction increased. The effect of these low energy neutrons upon the measurements was considered to be negligible.

1.d. Relative flux measurements.

During irradiations, variations over and above the general decrease in the neutron yield also occurred as a result of fluctuations in the deuteron beam. A proton-recoil scintillation counter, mounted several feet from the target on each machine was used to monitor these relative changes in flux, since a correction for their effect was required in the calculations. In some irradiations on the electrostatic machine, a silicon detector, (Ortec) mounted at nearly 180° to the incident deuteron beam, to count the recoiling ^4He particles, was used for this purpose. The neutron monitors were biased so as to reject pulses due to neutrons or the ^3He recoil fragments from the (D,D) reaction. Counts were taken at intervals short in comparison to the half-life of the shortest induced activity and corrected for dead-time losses.

1.e. Neutron energies.

Upon interaction with the tritium target, the bombarding deuterons become degraded in energy, resulting in a spectrum ranging from the nominal accelerated energy to zero. Deuterons can react with tritium over the whole of this range producing neutrons down to an energy of approximately 14.1 MeV. Consideration of the excitation function for the reaction (Fig. 4) indicates however that most of the neutrons (certainly more than 80%) are produced by deuterons with energies from 80 KeV upwards. The angular energy distributions of neutrons for this useful lower limit of production and for the accelerated energies employed are plotted in fig. 5. For the geometry indicated, where an estimate has been made of the average angle subtended by the sample at the target, the neutron energies for each source are:-

Accelerator	Neutron energy range (MeV)	Average energy (MeV)
Cockcroft-Walton	14.4 - 15.0	14.7
Electrostatic	14.4 - 15.2	14.8

2. The secondary standards.

Because of the small magnitude of many of the cross-sections measured, full use of the neutron fluxes available was made by irradiating samples as close to the tritium targets as possible. Under such conditions of poor

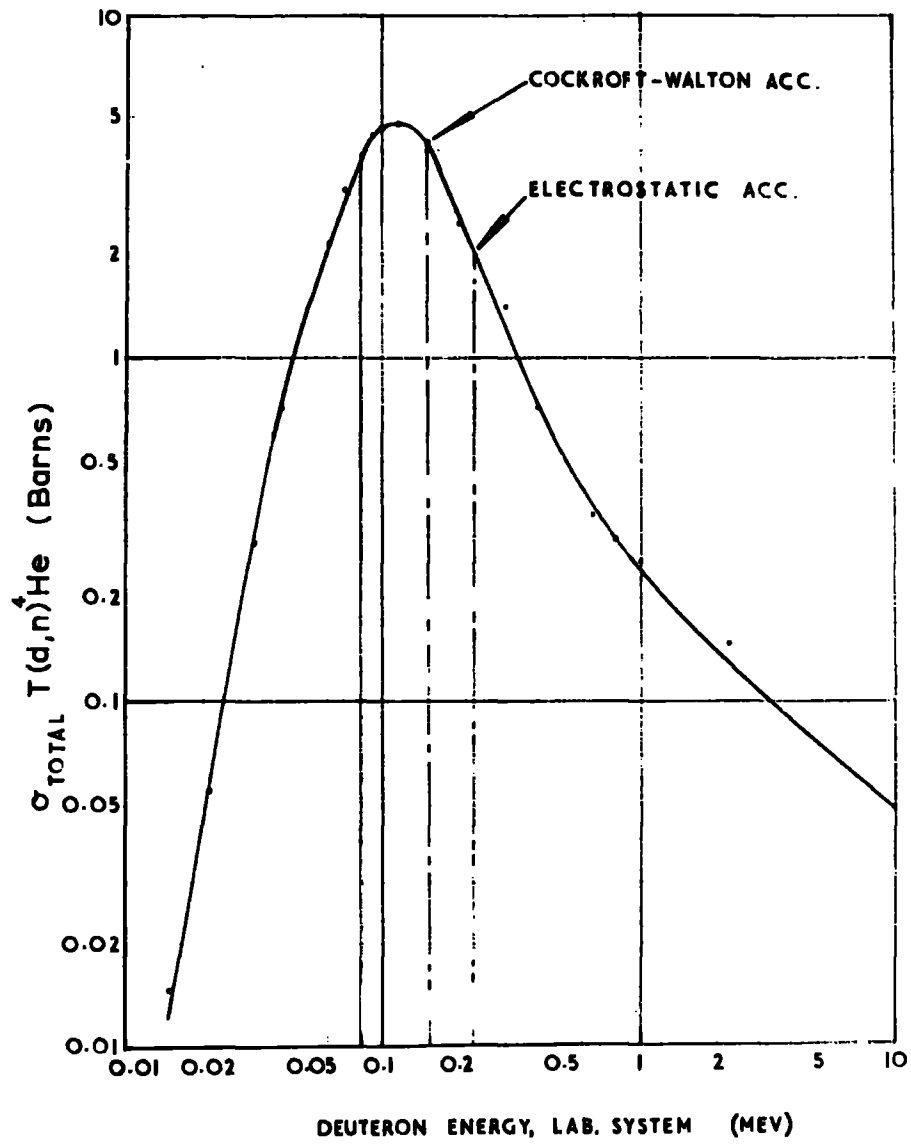


FIG 4 THE TOTAL CROSS-SECTION OF THE $T(d,n)^4He$ REACTION AS A FUNCTION OF DEUTERON ENERGY.³⁴⁾

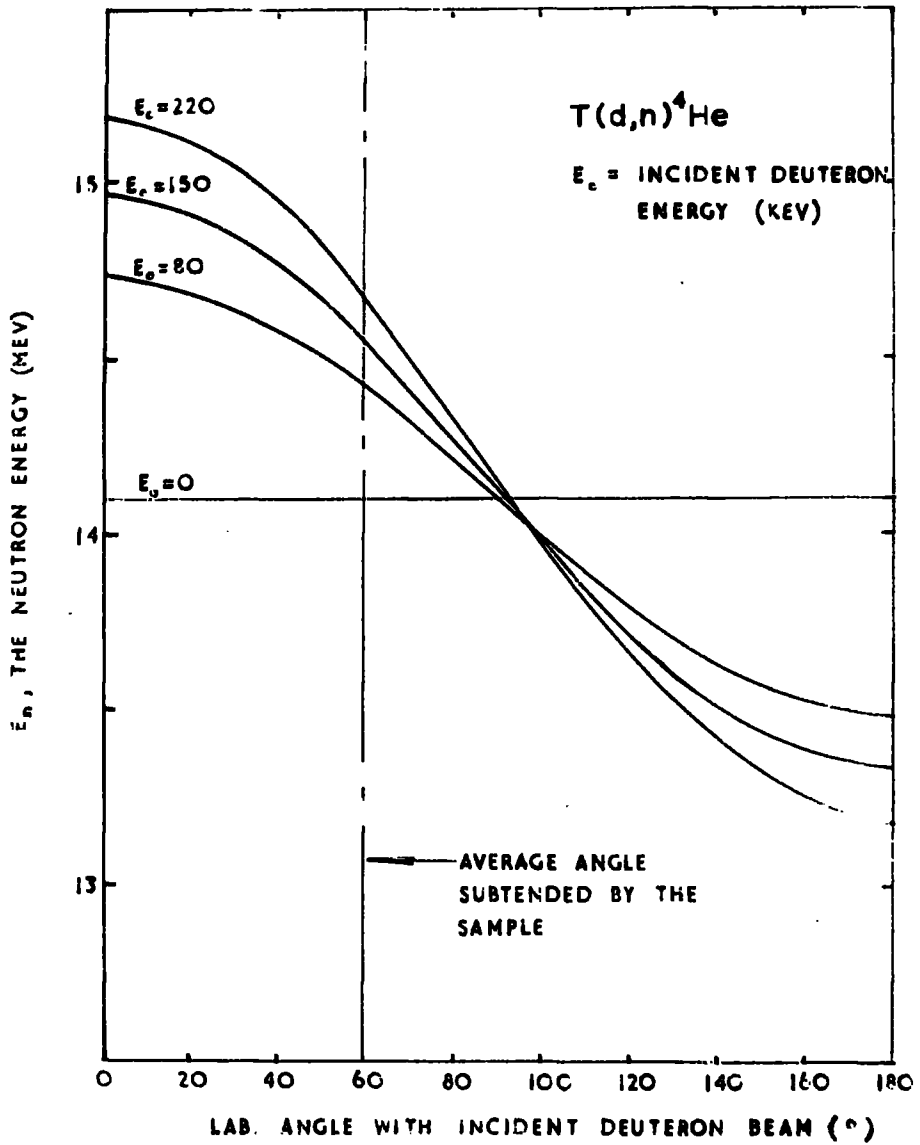


FIG 5 THE NEUTRON ENERGY AS A FUNCTION OF THE ANGLE OF EMISSION.³⁵⁾

irradiation geometry, the more direct methods of determining the absolute neutron flux by recoil and associated particle counting techniques, were unsuitable. These methods require good geometry in order to reduce errors caused by assuming that the neutron source is at a fixed point and that there is no variation of flux through the sample. The use of secondary standards was thus resorted to, and cross-sections were measured relative to the well-established $^{56}\text{Fe}(n,p)^{56}\text{Mn}$ and $^{27}\text{Al}(n,\alpha)^{24}\text{Na}$ reactions, both of which met the requirements for use as references. They have relatively high fast-neutron cross-sections and the target elements can be obtained in high states of purity. Furthermore, the resultant activities have convenient half-lives (^{56}Mn 2.58 hrs; ^{24}Na 15 hrs.) and are not ambiguously contaminated by other products, while the reaction threshold energies are sufficiently high to discriminate against degraded neutrons.

The cross-sections of the reference reactions had been previously measured absolutely by Hemingway et al³⁰⁾ in the Londonderry Laboratory at Durham, in a series of meticulous experiments involving a variation of the associated particle technique. Briefly, the recoil α -particles from the $\text{T}(d,n)^4\text{He}$ reaction were intercepted in an accurately known solid angle, at an average of 147° to the incident deuteron beam

by means of an aluminium catcher foil. To cut off ${}^3\text{He}$ recoil fragments from the $\text{D}(\text{d},\text{n}){}^3\text{He}$ reaction, the foil was coated with a thin VYNS plastic film. The volume of helium accumulated, (about 10^{-7} cc at S.T.P.) was then found by micro gas analysis and gave an absolute measure of the neutron yield. At the same time, foils of aluminium and iron were irradiated in as nearly as possible the same geometry as the catcher foil, and after dissolution, the induced β -activity in each was measured in a halogen-quenched liquid counter, absolutely calibrated against a 4π β -counter. The absolute cross-sections of the reactions were then found at 13.5 MeV after making a correction for the motion of the reaction products in the laboratory system.

In another series of experiments, the excitation functions of the ${}^{27}\text{Al}(\text{n}, \alpha){}^{24}\text{Na}$ and ${}^{56}\text{Fe}(\text{n},\text{p}){}^{56}\text{Mn}$ reactions were measured over the energy range 13.5 to 14.8 MeV and related to the previous absolute measurements. The values used in the present work were taken from the excitation functions and are given in the following table.

TABLE 1 Absolute cross-sections of the reference reactions³⁰⁾

<u>Reaction</u>	<u>t_{1/2} product</u>	<u>E_n MeV</u>	<u>σ mbs</u>
²⁷ Al(n,α) ²⁴ Na	15.0 hours	14.7	104.7 ± 5.6
⁵⁶ Fe(n,p) ⁵⁶ Mn	2.58 hours	{ 14.7	97.7 ± 4.6
		{ 14.8	96.7 ± 4.5

As described in greater detail in section 4.a. (p.41) of this chapter, both sandwiched-foil and homogeneous mixture techniques have been used to introduce the reference elements into the sample. The aluminium foil had been shown by comparison with a 99.999% pure sample, using activation analysis to be of a sufficiently high standard of purity³⁰⁾. The iron foil and granules were of 99.8% purity, the latter being supplied by the Bureau of Analysed Samples Ltd. (B.C.S. 149/1). When calculating unknown cross-sections, it was assumed that the neutron flux through the sample and the reference element was the same. That this is valid for homogeneous mixtures, when using powdered samples, had previously been shown³²⁾. Sandwiched foil assemblies were also kept as thin as possible to reduce uncertainties and for both the methods the errors introduced by this assumption are not thought to be more than a few percent.

An additional source of interference when using the

homogeneous mixture method was the contamination of the sample material by recoil fragments from the $^{56}\text{Fe}(n,p)^{56}\text{Mn}$ reaction. Approximately 1 part in 1500 of the total ^{56}Mn activity had been found to be transferred in this way³⁰). The use of chemical separation procedures however reduced the possibility of interference by this activity in the final sources and no adverse effects were noticed.

After irradiations the iron granules were separated rapidly and cleanly from the powdered sample by means of an electromagnet. Both the iron granules and the foils (~ 0.5 gm) were dissolved in a standard mixture of H_2SO_4 and HNO_3 containing manganese carrier and aliquots of the solution were taken for counting. The liquid counter was calibrated absolutely for ^{56}Mn in the standard solution, against a 4π proportional counter. During the work it was found necessary for convenience to use modified dissolution procedures and to determine the relative efficiency of the counter in each case.

A full description of the experiments carried out is to be found in section 5.c.(ii) (p. 65) where the efficiencies found for the different procedures are all related to the absolute value given here in the following table.

Aluminium foils were similarly dissolved in HCl containing sodium chloride carrier, the solution made up to a standard volume, and aliquots taken and counted in the same liquid tube as used for the iron. The absolute efficiency for ^{24}Na was also obtained by calibration against a 4π proportional counter.

The following table gives the absolute counting efficiencies, which are thought to be accurate to within 2%.

TABLE 2. Efficiency of the liquid counter⁵⁶).

<u>Nuclide</u>	<u>Detection coefficient</u>
^{24}Na	0.0532
^{56}Mn	0.0795

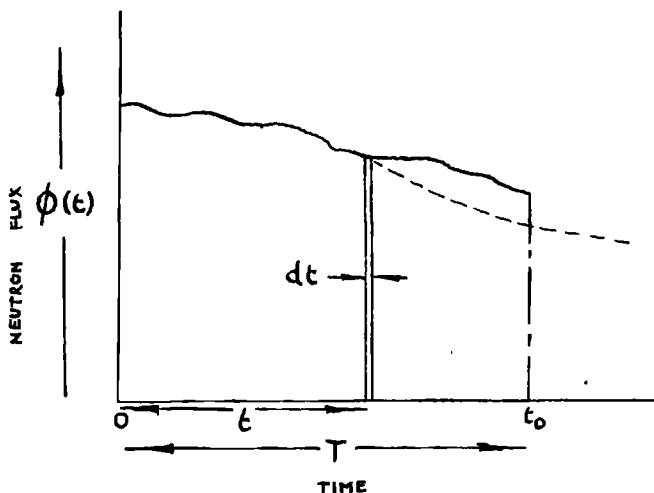
In the aluminium and iron reference elements the reactions $^{27}\text{Al}(n,p)^{27}\text{Mg}$ (9.5 minutes) and $^{57}\text{Fe}(n,p)^{57}\text{Mn}$ (1.7m.) also occur to a noticeable extent. These shorter lived activities were always allowed to decay before liquid counting was commenced and so did not interfere with the measurements. The decay of the activities of interest from the reference reactions was always followed for at least three half-lives and in all cases obeyed a purely exponential law with a half-life in agreement with the accepted value.

3. Methods of calculation

3.a. Corrections for the variation in neutron flux

Certain assumptions were made when deriving a theoretical relationship for the measurement of cross-sections in chapter 1. That the neutrons are monoenergetic is reasonably valid since the energy spread has been shown to be small under experimental conditions. Also the problem of infinitely thin samples is overcome by the use of homogeneous mixture and sandwiched-foil techniques. The neutron flux during irradiations, cannot, however, be assumed constant and a slightly modified theoretical approach allowing for this, must be used to derive a more rigorous relationship similar to equation 3.

Considering an irradiation lasting for a time T , the variation in the neutron flux $\phi(t)$, can be depicted diagrammatically:—



Stable target nuclei (s) undergo nuclear reaction giving rise to a radioactive product (p) with a decay constant λ p. The product decays to a stable nuclide. The rate of production of active nuclei, now irregular, is given as before, by:-

$$\frac{dN_p}{dt} = N_s \sigma \phi(t)$$

and the number of active nuclei produced during dt:-

$$dN_p = N_s \sigma \phi(t) dt$$

After radioactive decay the number of these nuclei remaining at the end of the irradiation (t_0) is:-

$$dN_p(t_0) = N_s \sigma \phi(t) e^{-\lambda(T-t)} dt$$

The neutron flux, $\phi(t)$ is proportional to the counting rate, A_n , of the monitor since this is fixed relative to the sample and neutron source:-

$$\begin{aligned} \phi(t) &\propto A_n(t) \\ &= \frac{A_n(t)}{\gamma} \end{aligned}$$

- Where γ is a factor accounting for the geometrical arrangement and the detection coefficient of the monitor.

Therefore, for the whole irradiation:-

$$N_p(t_0) = \frac{N_s \sigma}{\gamma} \int_{t=0}^{t=t_0} A_n(t) e^{-\lambda(T-t)} dt$$

Providing the intervals, dt , are short compared with the half-life of the product nuclide, the integral may be replaced by the summation:-

$$\sum (A_n e^{-\lambda(T-t)}) \delta t = X$$

$$\text{and, } N_p(t_0) = \frac{N_s \sigma X}{\gamma}$$

$$\text{Now, } A_p(t_0) = C_p \lambda_p N_p(t_0)$$

Where $A_p(t_0)$ is the observed activity of the product at the end of the irradiation, determined by extrapolation of the decay curve. C_p is the detection coefficient of the product nuclide.

$$\text{Thus:- } A_p(t_0) = \frac{C_p \lambda_p N_s \sigma X}{\gamma}$$

A similar expression can be written for the reference reaction (r) assuming the total neutron flux to be the same:-

$$A_{pr}(t_0) = \frac{C_{pr} \lambda_{pr} N_{sr} \sigma_r X_r}{\gamma}$$

Combination of these expressions eliminates the unknown, γ and allows the calculation of σ :

$$\frac{A_p(t_a)}{A_{pr}(t_0)} = \frac{c_p \lambda_p^{N_s} \sigma X}{c_{pr} \lambda_{pr}^{N_{sr}} \sigma_r X_r} \dots\dots (4)$$

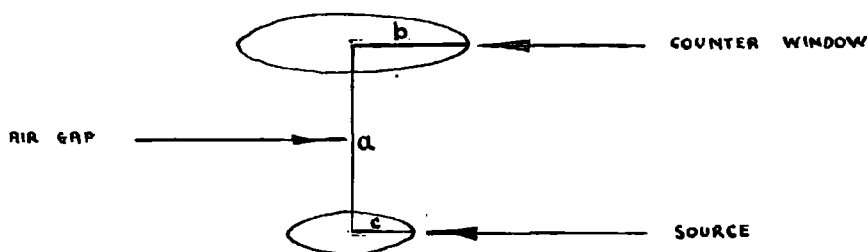
3.b. Calculation of proportional counter efficiency.

Calibration of the end-window proportional counter when a VYNS window was used in the early work (Irradiation of copper and gallium) was not possible. Absolute β -activities were determined by correcting observed values for geometry, mass absorption and backscattering. The relationship employed was:-

$$A_{abs} = \frac{A_{obs}}{G \cdot f_w \cdot f_B}$$

where: A_{abs} = absolute disintegration rate.
 A_{obs} = observed counting rate.
 f_w = mass absorption correction factor.
 f_B = back scatter correction factor.
 G = physical geometry.

The fraction of β -particles entering the correct solid angle for counting (G), was calculated from the measured dimensions using an equation due to Blackman.³⁶) For the geometrical arrangement,



the geometry can be written as the series:-

$$G = 0.5 \left[1 - \frac{1}{(1+\beta)^{\frac{1}{2}}} - \frac{3}{8} \frac{\beta \gamma}{(1+\beta)^{\frac{3}{2}}} - \gamma^2 \left(-\frac{5}{16} \frac{\beta}{(1+\beta)^{\frac{1}{2}}} + \frac{35}{64} \frac{\beta^2}{(1+\beta)^{\frac{3}{2}}} \right) \right. \\ \left. - \gamma^3 \left(\frac{35}{128} \frac{\beta}{(1+\beta)^{\frac{1}{2}}} - \frac{315}{256} \frac{\beta^2}{(1+\beta)^{\frac{3}{2}}} + \frac{1155}{1024} \frac{\beta^3}{(1+\beta)^{\frac{5}{2}}} \right) \right]$$

Where $\beta = \frac{b^2}{a^2}$, $\gamma = \frac{c^2}{a^2}$,

and, a = distance between source and window

b = radius of the counter window.

c = radius of the source.

For the geometrical arrangement used, G had a value in the region of 0.28.

The mass absorption correction factor f_w , was estimated from data compiled by Gleason Taylor and Tabern³⁷):-

$$f_w = e^{-\mu d}$$

where: μ = mass absorption coefficient in mg/cm^2
 d = total thickness traversed by the β -particles
 (source $\frac{1}{2}$ -thickness + air gap + window
 thickness in mg/cm^2 .)

μ was taken as μ_0 , the mass absorption coefficient near zero thickness which was given by the equation:-

$$\mu_0 = 0.017 (E_{\beta \text{ max}})^{-1.43}$$

where: $E_{\beta \text{ max}}$ = the maximum β energy.

Gleason et al have shown that this equation is a good approximation over the β -energy range 0.15 to 3.5 MeV. For nuclides decaying via several β 's of different energy, the absorption correction factor was calculated for each transition and the total absorption factor found by summing the individual factors weighted by the percentage abundances of the transitions.

Saturation backscattering was assumed and the correction factor was taken from the paper by Burt³⁸), where f_B was plotted as a function of $E_{\beta \text{ max}}$ for aluminium.

4. Chemical separation methods.

4.a. The choice of sample material.

The choice of sample material was governed by several factors. Samples of a high chemical purity were required

and, in particular contaminants giving rise to interfering activities unresponsive to chemical separation or incapable of resolution from expected activities were avoided as far as possible. Physical stability and a well-defined chemical composition were also essential so that the number of target nuclei in the sample could be determined accurately by weighing. Some "Analar" grade substances were used, but in several cases the purity was of a higher standard.

Two opposing requirements determined the size of samples. On the one hand the number of target nuclei had to be as high as possible in view of the small cross-sections expected for the rare reactions and on the other, too large a size would have increased the uncertainty in the neutron energy. Generally the weight of samples was from 1 to 2 gms.

The ideal form was metallic foil. When this was used, discs 2 cm. in diameter and up to 1 mm thick, were sandwiched between foils of aluminium ($\sim 7 \text{ mg/cm}^2$) or iron ($\sim 120 \text{ mg/cm}^2$) of slightly larger diameter (2.1 cm.). The small uncertainty in the neutron flux in the sample material itself caused by this arrangement was taken to be negligible. To prevent possible contamination during irradiation, the foils were separated by approximately 0.05 mm thick polythene spacers. A polythene foil was also interposed

between the target block on the accelerator and the sample for the same reason. Before assembling the stack each foil was cleaned and weighed. Stacks had maximum thicknesses of approximately 3 mm. When the sample was in the powder form it was homogeneously mixed with 0.5 gm. of pure iron granules and sealed in a thin polythene bag. Care was taken to ensure a uniform sample thickness as far as possible and maximum thicknesses were in the region of 5 m.m. In some cases, nitrates, sulphates and carbonates were irradiated. The ten minute activity due to the $^{14}\text{N}(n,2n)^{13}\text{N}$ reaction did not interfere with counting measurements as it was either allowed to decay or eliminated during the separation procedure. Also the thresholds of the reactions $^{16}\text{O}(n,2n)^{15}\text{O}$ (2.1 m) and $^{12}\text{C}(n,2n)^{11}\text{C}$ (20.5 m) were above the neutron energy used, thus causing no interference.

4. b. Chemical separation procedures:

Irradiated samples were dissolved in solutions containing known weights (approximately 10 mg) of inactive carriers for each of the (n,p) and (n, α) reaction products. Carrier solutions were prepared from reagents of "primary standard" quality as far as possible and were determined where necessary by gravimetric and titrimetric methods. Aliquots of the carrier solutions (~ 1 mg/ml) were pipetted

into the dissolving solutions.

In order to ensure complete exchange, oxidation-reduction cycles and digestions were performed. This was especially necessary for elements with several valency states, since it was possible for any one or all, to be present due to the occurrence of "hot-atom" reactions. It was always arranged that the carriers were present in the dissolving solution before the sample was added, to avoid the loss of activity by adsorption onto the glass-ware. With these conditions fulfilled, the exchange was assumed to be complete.

The various elements were then separated chemically and after purification, sources prepared for counting. Procedures for separation were developed from general information available in the literature, a particularly useful source being the National Academy of Sciences series on the Radiochemistry of the Elements. Solvent extraction and precipitation methods were suitably adapted to deal with the separation of milligramme quantities from gramme quantities and to meet the time requirement for short-lived nuclides.

4.c. The preparation of sources for end-window counting

Solid sources for end-window proportional counting were prepared by filtration at the pump, of the final

precipitates from the chemical separation procedures onto glass fibre discs (Whatman GF/A, 2.1 cm diam.). The precipitates were confined to a circle of radius 0.8 cm. in the centre of the discs by using a polythene filter chimney. Source materials were chosen for physical stability (non-hygroscopic non-volatile) and for the provision of a uniform layer subject as little as possible to cracking upon drying and mechanical losses during handling. After drying, the sources (approx. 20 mg.) were mounted on aluminium planchets (2.5 cm. diameter, $\sim 80 \text{ mg/cm}^2$ thick) for counting.

The chemical yield, for which the observed activities had to be corrected, was determined for precipitates of gravimetric standard by weighing. Initially, the blank glass fibre discs were pretreated using the washing and drying procedures dictated by the chemical separations (alkaline washes were avoided) and weighed together with the planchets. A tare consisting of a similarly treated disc and planchet was used as a relative measure to minimise errors due to the effects of atmospheric changes. The weighing procedure was carefully standardised, the sources normally being kept in a desiccator (silica gel). During counting a special holder was used to store the sources which prevented damage and the accumulation of dust. Using a Stanton MC1A semi-micro balance, weighing was carried out to the nearest 0.01 mg and it was estimated that chemical yields could

be determined to within $\pm 1\%$.

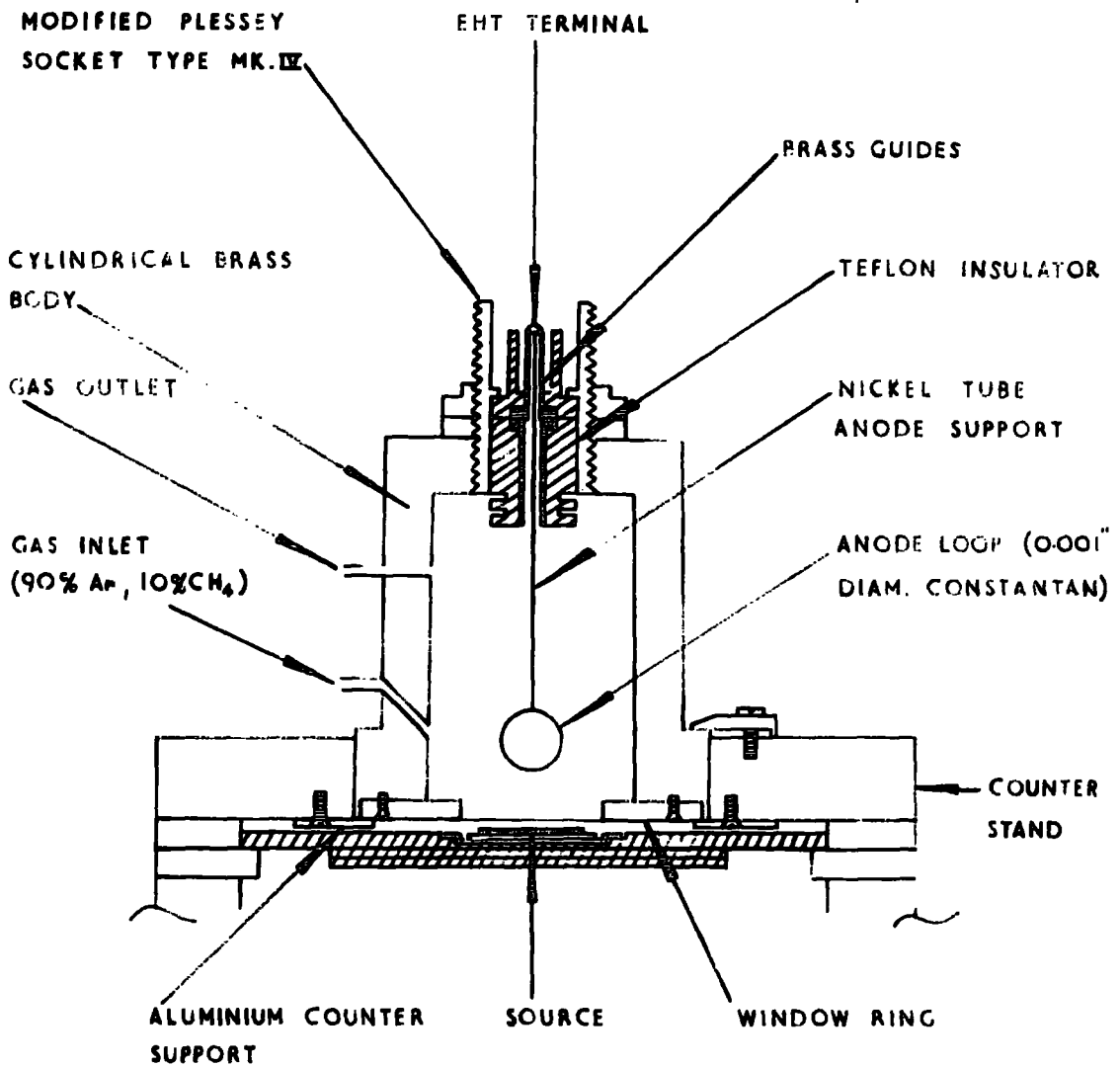
When precipitates were not of gravimetric quality the chemical yield was determined after the completion of counting by dissolving the source and applying a suitable titrimetric method. Titrations were on the semi-micro scale and the same accuracy was estimated as for the gravimetric method.

5. Counting techniques

5.a. End-window proportional counting

An end-window proportional counter calibrated absolutely against a 4π proportional counter was used to measure the β -activity of the separated reaction products. Although it would have been desirable to use the 4π counter directly, difficulties associated with the rapid preparation of suitable internal sources made it inconvenient for the measurements undertaken. External sources for end-window counting could be prepared with the rapidity required when dealing with short lived nuclides and also allowed accurate determination of chemical yields since several milligrammes of material were involved.

The construction of the counter is shown diagrammatically in Fig. 6. Counters of a similar type had been extensively used by previous workers in this laboratory but, during the



(SIDE ELEVATION , NEAR SCALE)

FIG 6 DIAGRAM OF THE END-WINDOW
 PROPORTIONAL COUNTER.

present studies, two modifications to the arrangement were tried with the object of improving both the individual accuracy of the counter and also the reproducibility of results obtained with different counters of the same design. A new type of demountable counter stand was tested and used and a new window material tried.

5.a.(1) A description of the counter and its operation

The counter was operated on the gas-flow principle, the internal pressure being very slightly above atmospheric pressure. Before admission to the tube, the gas mixture, consisting of 10% methane and 90% argon was dried by passing it over silica gel (with indicator) and magnesium perchlorate. A Fischer and Porter flowmeter was used to control the flow and for rates in excess of 10 ml./min. the efficiency was found to be reproducible. During use a flow-rate of 30 to 40 ml./min was maintained. Fresh gas was admitted at the window end of the counter where the anode loop was situated.

The arrangement of the associated electronic equipment is given as a block diagram in fig. 7. Pulses from the counter tube ($\sim 50 \mu V$) were fed via a high voltage 47 pF condenser to the "ring-of-three" preamplifier which gave a voltage gain of approximately 100 times. Further amplification was provided by a linear pulse amplifier (max. voltage gain

$\sim 10^6$ times) which fed 15-25 volt pulses to the scaling unit. A mains filter was incorporated in the linear amplifier supply to prevent the pick-up of spurious pulses.

The scaler was capable of accepting pulses at a maximum repetition frequency of 180,000 p.p.m. It also incorporated a variable bias line to discriminate against amplified noise and a variable resistance-capacity network, by means of which the dead time could be preset over the range 0 to 10 m sec. The EHT was supplied by a 2000 volt pack (10 mA max), voltage stabilised to within $\pm 0.1\%$. The output from this was fed to a potential divider which allowed the EHT supplied to the counter anode to be adjusted over the range 500-2000 volts. A twin π -section resistance-capacity filter in series with the potential divider and counter served to remove spurious pulses. All interconnecting cables were screened and returned to earth at the lead castle, care being taken to avoid earth loops.

The following settings were used during normal operation:

<u>Scaler</u>	Dead-time	:	50 μ sec
			5 μ sec (for counting rates in excess of 36,000 c.p.m.)
	Discriminator bias	:	15 volts.

Linear pulse amplifier

Differentiating time : 0.4 μ sec
 Integrating time : 0.4 μ sec
 Polarity : Anode
 Attenuation : 10 d B

Potential divider

Voltage : 1750-1850 volts

By mounting the counter inside a $1\frac{1}{2}$ " thick lead castle the background counting rate was kept to a minimum. Normally the background was in the region of 10 cpm. Sources were generally counted for a sufficiently long period to reduce the statistical error to less than 1% and observed counting rates were corrected for dead-time losses and background counts. Most of the counting was carried out manually with a stopwatch but in some cases an automatic recorder was used. For sources with higher counting rates, two 1009E scalers were connected in series the dead-time being set to 5 μ sec and 0 μ sec on the first and second scalers respectively.

The correct functioning of the counting set was frequently checked with a standard β -source (Ra D,E). Counting rates with this source were in the region of 13,800 cpm and were found to be reproducible to within 3%

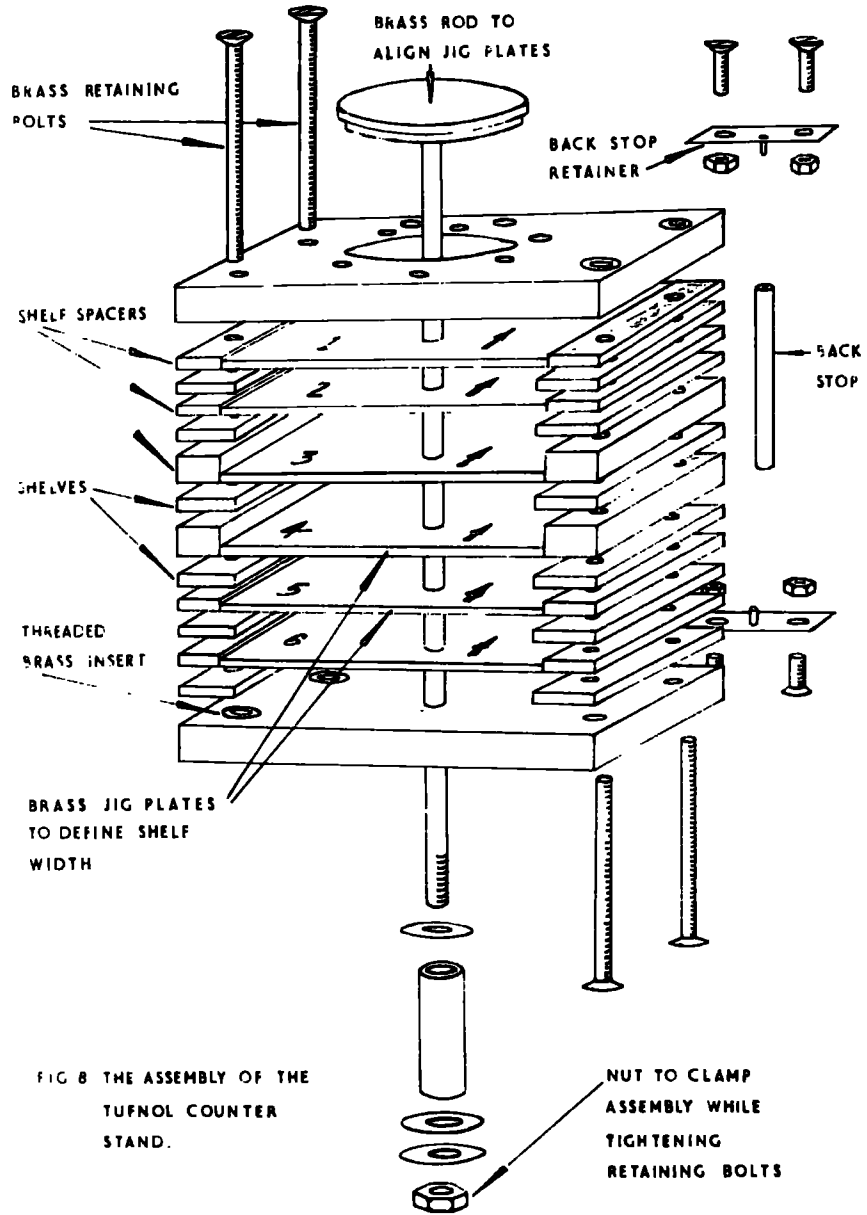
for a counting interval of 5 minutes. Using the same source, plateaux were also regularly determined, the working voltage being taken as the mid-point. Plateaux usually had slopes of approximately 0.05% /volt and extended for 150 volts under normal working conditions. Two preamplifiers, both of the same circuit design, were used at different times and after initial setting-up, no change in the characteristics of the counting set due to each, was noticed.

5.a.(ii) The demountable counter stand.

Previously, counter stands had been made from machined perspex and considerable skill was required on the part of the constructor to enable the counting efficiency to be reproduced to within 1% for different stands. Since it was often desirable to compare results obtained with different counters in the laboratory, a reliable and convenient method of reproducing the geometry to within this tolerance was required. The availability of tufnol strip (a material of low Z) which possessed an accurately machined thickness allowed an alternative form of construction which fulfilled this requirement. The design of the stands adopted using this material was also such that they could be assembled by a comparatively unskilled operator.

The assembly of the Tufnol stand is shown as an exploded diagram in fig. 8. Its geometrical reproducibility was tested by taking counts with a standard Ra(D,E) source before dismantling and after reassembling. When strips were taken at random for reassembly the efficiency was not reproduceable to within 1% for the top two shelf positions, these being the most sensitive to slight changes in geometry. A selection procedure was therefore introduced whereby the eight strips used for spacers and shelves in these positions, on all stands, had identical thicknesses to within 0.0005". Measurements were made with a micrometer screw, several readings being taken along the length of each strip. Using selected strips the required accuracy was achieved. The lower four shelves did not show the same sensitivity and strips accurate only to within 0.001" could be used in these positions.

Lateral movement of the source trays was also critical and the width of each shelf had to be accurately adjusted by means of a jig, during assembly, so that the trays were a moderately tight fit. To position the source under the counter window the trays rested against a stop at the back of the stand. The window end of the counter tube was held against an annular aluminium support on the underside of the top-piece, by three steel retaining clips,



In this position it was flush with the undersurface of the top-piece. To ensure reproducibility a routine procedure was developed for the assembly of the stands.

5. a. (iii) The melinex window.

In the early work on copper and gallium, a VYNS window was used. Since the counter was subsequently calibrated after a melinex window had been fitted its efficiency was calculated by the method already described, for the work on these two elements. (p.39).

The preparation of VYNS windows has been described in detail elsewhere^{32,40}). Briefly, the film is prepared by dropping a solution of the plastic in cyclohexanone onto a clean water surface. Four layers of this film are then stretched across the window ring and a thin layer of gold evaporated onto the inner surface to make it electrically conducting. Such windows have the advantage that they are extremely thin ($\sim 80 \mu\text{g}/\text{cm}^2$) and are thus eminently suited to β -counting. They are however, very fragile and easily broken, necessitating frequent repair.

Recently, aluminised melinex film has become commercially available and has been used for the counter window in part of this work. The material provides a window which is much more rugged than VYNS film, while

still having a thickness of only 1 mg/cm^2 . Melinex windows have proved to be satisfactory as regards electrical conductivity and no depreciation in counter performance compared with gold-plated VYNS windows has been noticed. In contrast to VYNS windows their preparation is also extremely simple;-

A square of melinex is held taught by a rubber "O-ring" in a special frame designed for the purpose. (Fig. 9). The brass window ring, after cleaning with acetone, is coated with a solution of cellulose acetate in acetone ("Britfix" cement) and placed on the melinex with a small weight on top. The whole is then left for 24 hours to dry thoroughly, when the excess melinex is trimmed off and the window examined for defects. During the preparation the melinex is kept free from dust and grease by careful handling. As the film tends to become electrostatically charged very easily the working conditions must be kept as "dust-free" as possible. It was found that a slight contraction of the cement takes place on drying giving a satisfactorily tight covering. Typical defects include an excess of cement which is squeezed out onto the effective area of the window or a deficiency of cement which gives rise to air leaks.

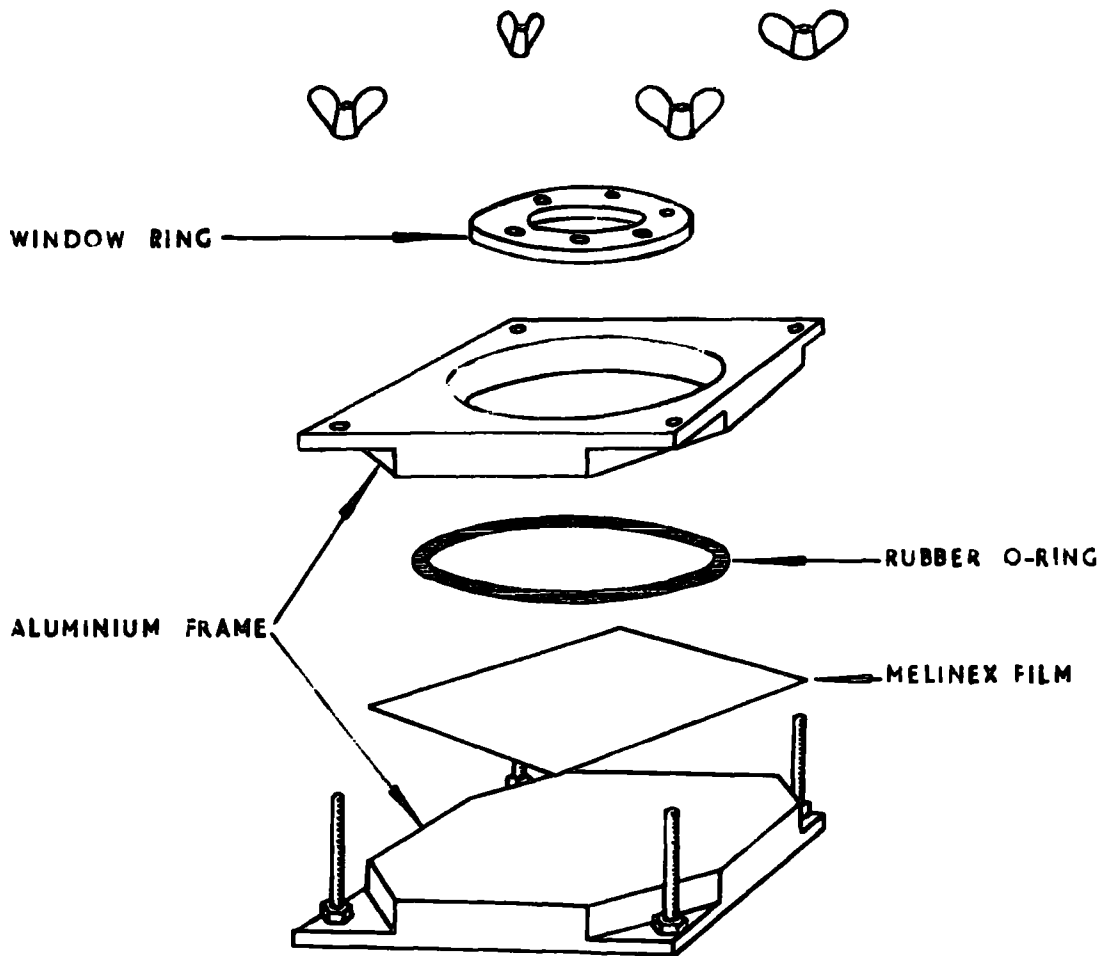


FIG 9 EXPLODED DIAGRAM OF THE APPARATUS
USED FOR THE PREPARATION OF THE
MELINEX COUNTER WINDOW.

5 a.(iv) Calibration.

The following calibration refers to the counter fitted with a melinex window as used for the work on rubidium, thallium, silver and germanium.

Since a 4π counter was used as the absolute standard, it was not practicable to calibrate the end-window counter for each individual product nuclide due to the difficulties associated with isolating pure samples and preparing sources of the short lived isotopes for absolute counting. Instead, calibration curves at different source weights were constructed using manageable isotopes according to the method described by Bayhurst and Prestwood³⁹). They suggest that the errors introduced by the interpolation of efficiency from curves where the β end-point energy is plotted against efficiency, can be reduced by considering alternatively the average β -energy. When β end-point energies are used, no allowance is made for the increase in negatron efficiencies with increasing Z or for the higher counting efficiencies of positrons and this leads to a considerable spread in values. The average β -energy is a quantity more closely related to the shape of the β -spectrum and since the shape depends upon the end-point energy, the atomic number, and the charge of the emitted particle, a much better estimate of β -efficiency for a given nuclide

can be made from an average β -energy vs. efficiency curve. Where several β -groups occur, the overall efficiency can be found by adding the efficiencies of each group weighted by their percentage abundance.

In the present calibration, the average energy \bar{E}_β , for allowed transitions was obtained from curves of \bar{E}_β plotted as a function of E_0 , the end-point energy, calculated by Bayhurst and Prestwood. The "equivalent allowed E_0 " for first-forbidden transitions was found from another curve in the same paper which had been determined by a summation method comparing the shapes of the two spectra for given E_0 values.

The method of calibration allowed the estimation of β -counting efficiencies to within 3%. Bayhurst and Prestwood have also shown that the efficiency obtained in this way, has a negligible dependence upon the nature of the source material.

Eight nuclides were used to provide data for the construction of calibration curves, pure "carrier-free" solutions of each being supplied by the Radiochemical Centre, Amersham. The range of maximum β -energies covered was from 0.254 to 3.58 MeV. After dilution, 4 π sources were made by evaporating weighed aliquots of the active solutions onto thin ($\sim 20 \mu\text{g}/\text{cm}^2$) VYNS films^{32,40}).

The films were gold-plated on one side and treated on the opposite side with a dilute solution of insulin (1 mg/10 cc H₂O + 1 drop HCl) to improve the hydrophillic properties of the surface and so facilitate uniform spreading and crystallisation. The area covered by the solution was approximately 0.2 cm² in the centre of the film. After drying under lamps, the almost weightless ($\sim 30 \mu\text{g}$) sources were counted in a 4 π gas-flow proportional counter. The gas mixture and electronic equipment used with this counter were similar to those used for the end-window counter (Fig. 7). Up to six 4 π sources were prepared and counted for each nuclide. In some cases the absolute activity was determined by β/γ coincidence counting, a 3" flat NaI(Tl) crystal being used in conjunction with the 4 π counter for this purpose. Counter plateaux were obtained for each individual nuclide and in general the operating voltage was in the region of 1700 volts. The specific β -activity of the diluted solution was calculated from these measurements and the standardised solution used to prepare solid sources for end window counting.

A weighed aliquot of the standardised solution was added to another solution containing a known weight of inactive carrier, and the mixture digested to allow

complete exchange. Solid sources, ranging in weight from 1 to 40 mg were then prepared for end-window counting by the standard method described previously (p.44). In most cases precipitation from the whole solution was carried out, sources of different weight being made by taking measured volumes of a slurry for filtration. In other cases where it was more convenient, precipitation was carried out separately on individual aliquots just before filtration. This latter procedure was less desirable as there was the possibility of the slightly varying conditions leading to errors in the specific activity of the sources. However no adverse effects were noticed. The procedures used for each nuclide were standard and the source materials are given in table 11. After correcting for decay and any contribution by γ -rays the efficiency of the end-window counter was calculated:-

$$\beta\text{-efficiency} = \frac{\text{observed counting rate}}{\text{absolute } \beta\text{-disintegration rate.}}$$

Thickness curves of β -efficiency against source weight were then plotted. The results for the eight nuclides are recorded in tables 3 to 10 and figures 10 to 17. The purity of the samples was checked by following the decay of the nuclide in each case and the half-lives were found to agree with accepted values. From the thickness curves,

TABLE 3. End-window counter calibration: Thickness curves

⁴⁵Ca.

Source wt. mg.	1.12	2.45	2.84	4.05	9.50	12.67	19.75	52.58
Curve								
A	0.245	0.226	0.221	0.224	0.182	0.166	0.139	0.070
B	0.253	0.233	0.225	0.222	0.186	0.166	0.136	0.069
C	0.257	0.234	0.227	0.221	0.185	0.166	0.135	0.069

Curve: A: Nucleonic Accessories planchets with backscatterer.

B: Brillhart planchets with backscatterer.

C: Brillhart planchets without backscatterer.

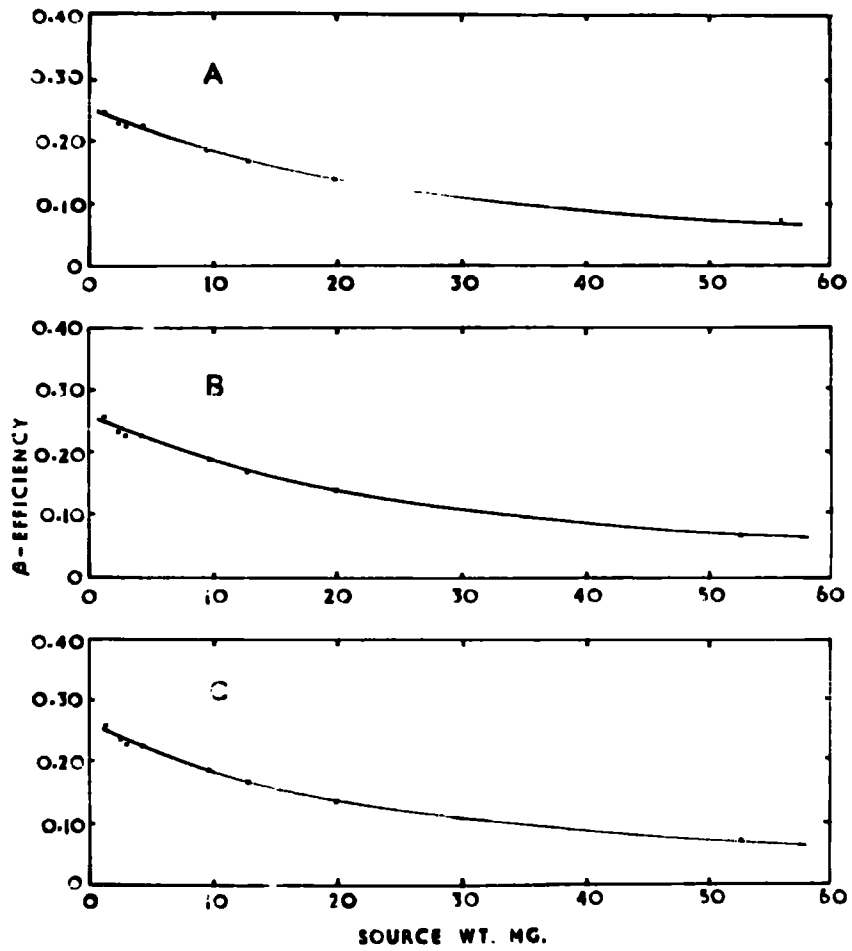


FIG 10 END-WINDOW COUNTER CALIBRATION: THICKNESS CURVES FOR ^{45}Ca .

TABLE 4. End-window counter calibration: Thickness curves
for 185W.

Source wt. mg.	1.81	2.31	6.39	8.77	17.74	20.51	25.24	32.70	41.51	53.56
Curve										
A	0.297	0.288	0.275	0.259	0.215	0.209	0.194	0.171	0.157	0.133
B	0.286	0.273	0.273	0.265	0.218	0.214	0.197	0.175	0.158	0.134
C	0.298	0.282	0.278	0.262	0.213	0.214	0.197	0.172	0.157	0.133

Geometry: A: Nucleonic Accessories planchets with backscatterer.

B: Brillhart planchets with backscatterer.

C: Brillhart planchets without backscatterer.

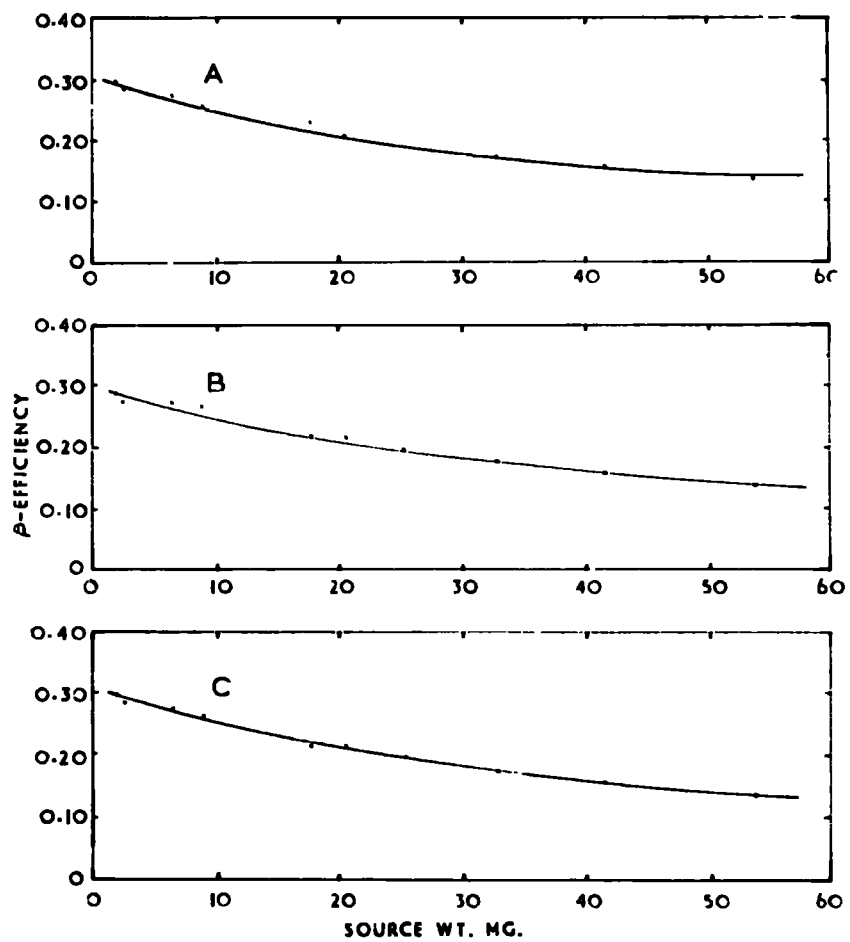


FIG II END-WINDOW COUNTER CALIBRATION: THICKNESS CURVES FOR ^{185}W .

TABLE 5. End-window counter calibration. Thickness curve for

¹³¹I.

Source wt. mg.	2.11	4.97	10.59	10.68	18.46	23.76	27.95	37.37	45.70
β - Efficiency	0.312	0.328	0.297	0.293	0.276	0.252	0.229	0.216	0.212

Curve A: Nucleonic Accessories planchets with backscatterer.

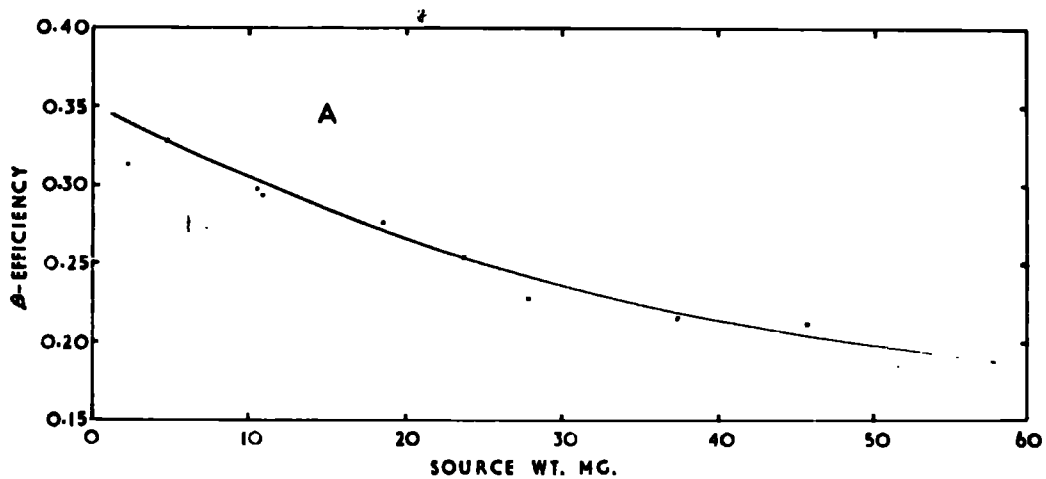


FIG 12 END-WINDOW COUNTER CALIBRATION: THICKNESS
CURVE FOR ¹³¹I.

TABLE 6. End-window counter calibration. Thickness curves for ²²Na.

Source wt. mg.	1.91	5.69	8.18	11.35	12.93	16.42	19.12	28.62	34.39	45.81
Curve										
A	0.358	0.355	0.348	0.345	0.342	0.334	0.324	0.301	0.292	0.261
B	0.366	0.355	0.354	0.349	0.346	0.335	0.331	0.305	0.294	0.265
C	0.359	0.353	0.348	0.350	0.346	0.333	0.327	0.307	0.293	0.266

A: Nucleonic Accessories planchets with backscatterer

B: Brilliant planchets with backscatterer

C: Brilliant planchets without backscatterer

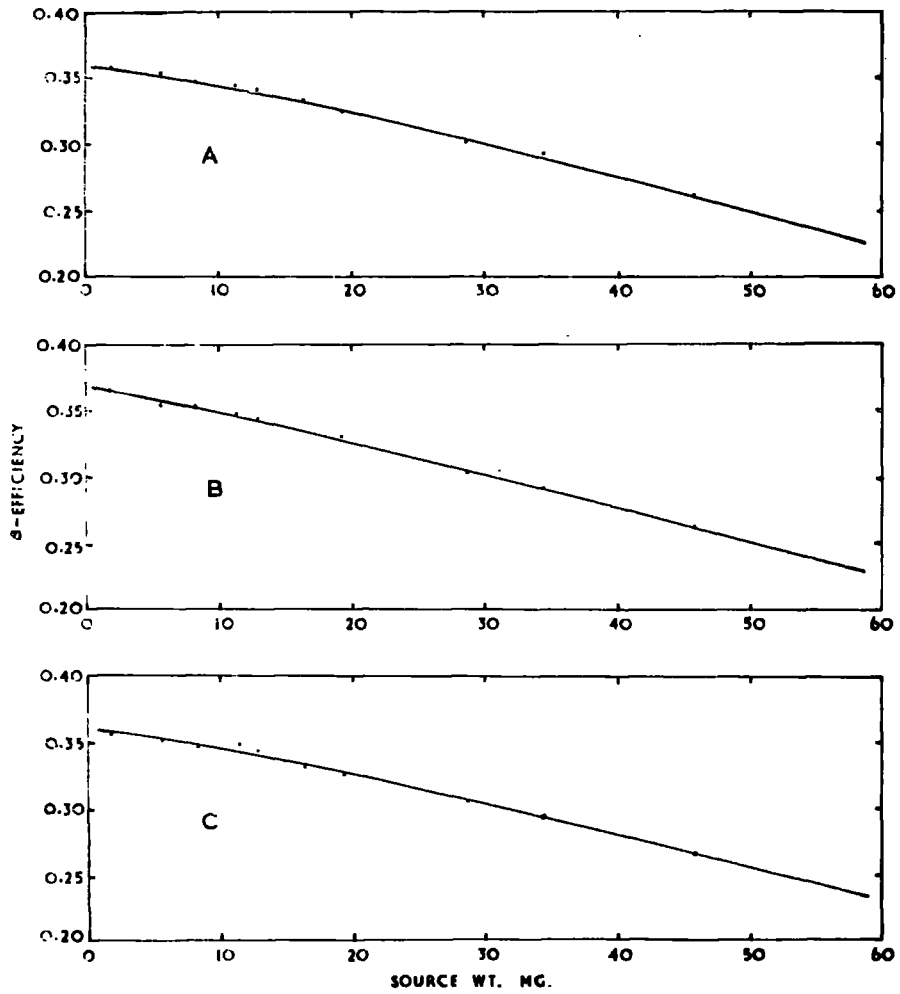


FIG 13 END-WINDOW COUNTER CALIBRATION: THICKNESS CURVES FOR ^{22}Na .

TABLE 7. End-window counter calibration: Thickness curves
for ^{24}Na .

Source wt. mg.	1.11	2.77	5.42	8.44	12.85	19.98	27.18	28.17	32.18	47.53
Curve										
A	0.351	0.351	0.367	0.363	0.367	0.370	0.372	0.370	0.370	0.360
B	0.346	0.360	0.364	0.367	0.364	0.368	0.375	0.371	0.359	0.358
C	0.343	0.350	0.360	0.366	0.360	0.360	0.364	0.361	0.362	0.356

Geometry: A: Nucleonic Accessories planchets with backscatterer.

B: Brillhart planchets with backscatterer.

C: Brillhart planchets without backscatterer.

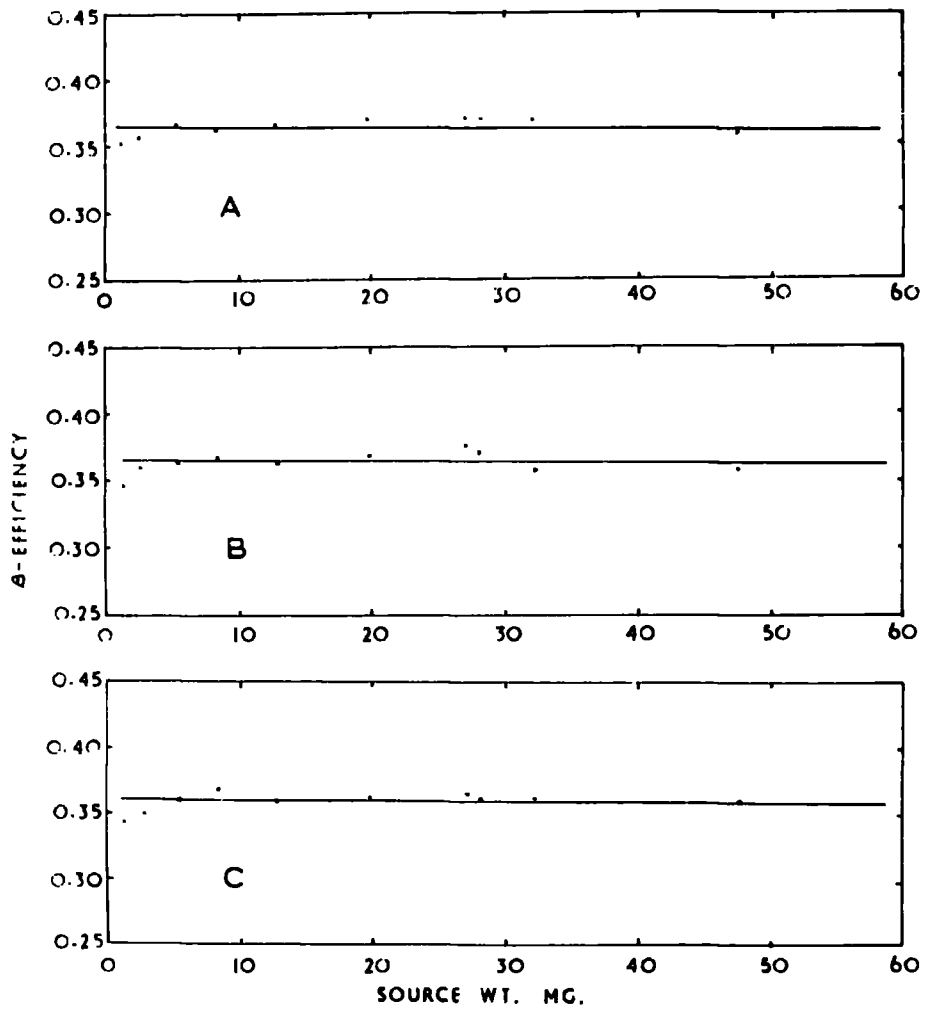


FIG 14 END-WINDOW COUNTER CALIBRATION: THICKNESS CURVES FOR ^{24}Na .

TABLE 8. End-window counter calibration. Thickness curves for ⁹¹Y.

Source wt. mg.	Curve	2.39	5.78	7.06	9.05	13.53	18.72	20.89	35.97	41.33	50.34
Efficiency	A	0.362	0.359	0.349	0.360	0.356	0.358	0.362	0.356	0.349	0.347
Efficiency	B	0.351	0.357	0.354	0.361	0.356	0.359	0.362	0.353	0.350	0.350
Efficiency	C	0.352	0.352	0.342	0.350	0.349	0.351	0.353	0.347	0.345	0.341

Geometry: A: Nucleonic Accessories planchets with backscatterer.

B: Brillhart planchets with backscatterer.

C: Brillhart planchets without backscatterer.

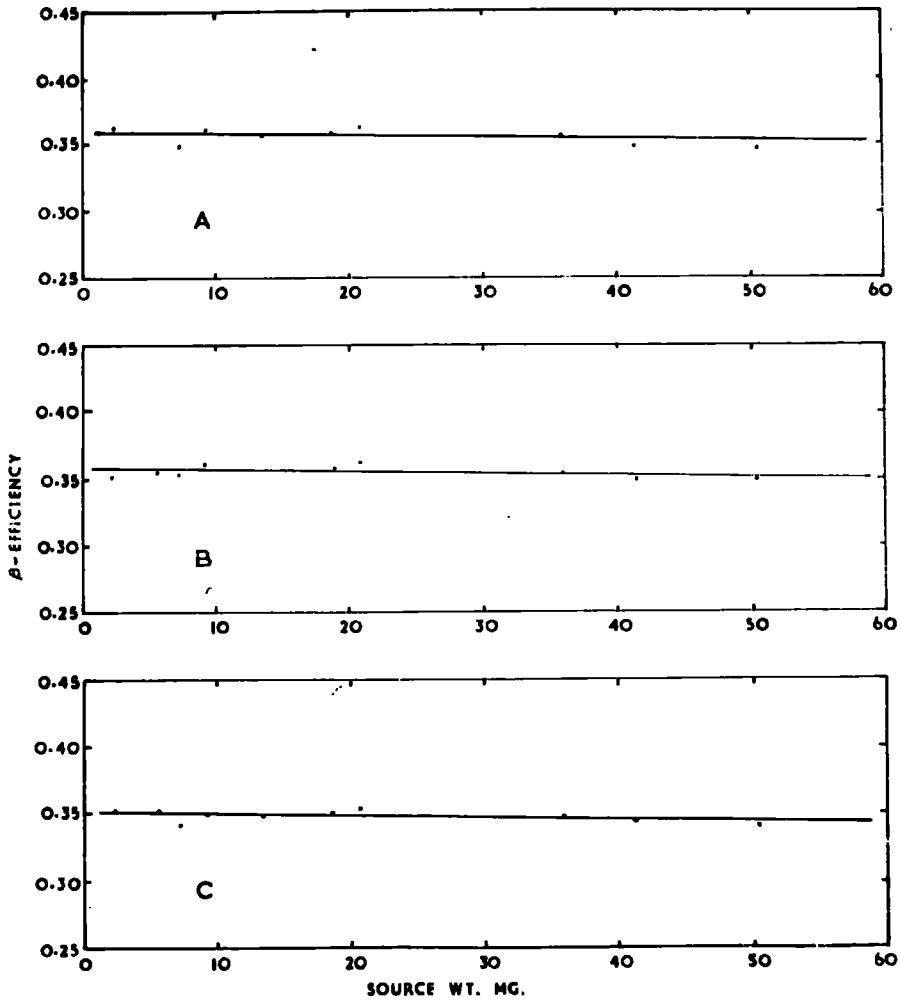


FIG 15 END-WINDOW COUNTER CALIBRATION: THICKNESS CURVES FOR ^{91}Y .

TABLE 9. End-window counter calibration: Thickness curves
for ⁹⁰Y.

Source wt. mg.	2.69	4.55	5.72	8.38	13.45	18.40	27.90	49.81
Curve								
A	0.356	0.350	0.369	0.349	0.345	0.368	0.352	0.366
B	0.368	0.355	0.374	0.364	0.360	0.375	0.370	0.370

Curve A: Nucleonic Accessories planchets with backscatterer.

B: Brillhart planchets with backscatterer.

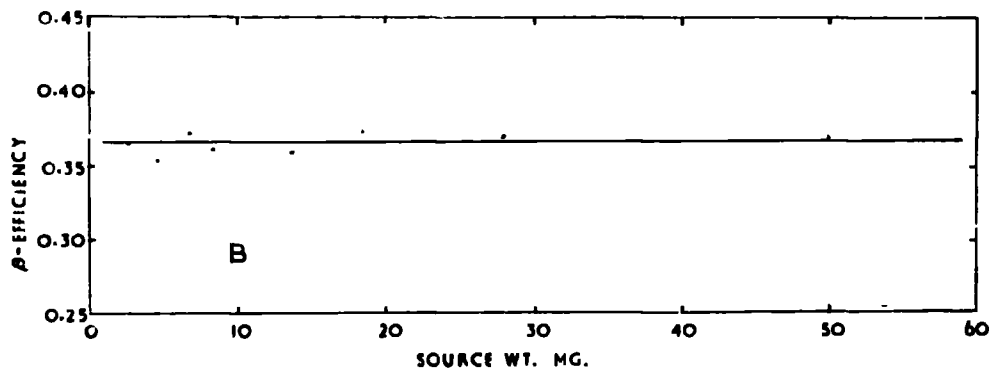
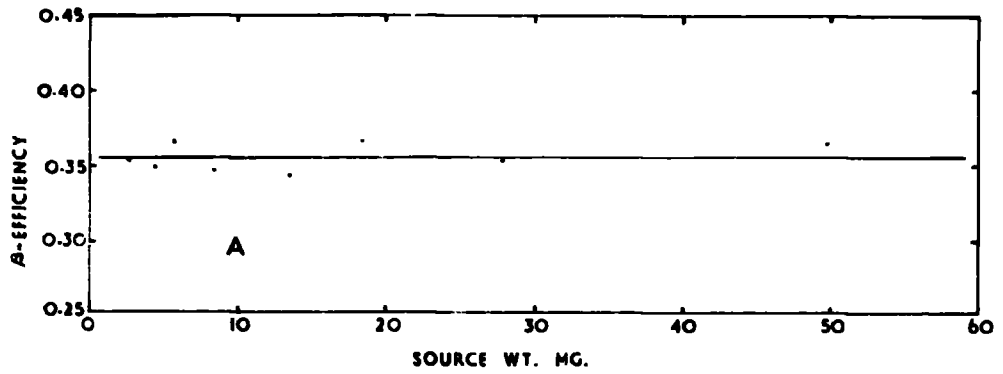


FIG 16 END-WINDOW COUNTER CALIBRATION: THICKNESS CURVES FOR ^{90}Y .

TABLE 10. End-window counter calibration: Thickness curves
for ⁴²K.

Source wt. mg.	1.40	4.01	7.68	10.42	13.84	15.29	18.86	20.51	24.98	49.18
Curve										
A	0.384	-	0.357	0.356	0.360	0.355	0.358	-	0.365	0.369
B	0.377	0.361	0.356	0.360	0.362	0.353	0.357	0.362	0.356	0.368
C	0.344	0.322	0.329	0.326	0.328	0.327	0.334	0.328	0.337	0.345

A: Nucleonic Accessories planchets with backscatterer.

B: Brillhart planchets with backscatterer.

C: Brillhart planchets without backscatterer.

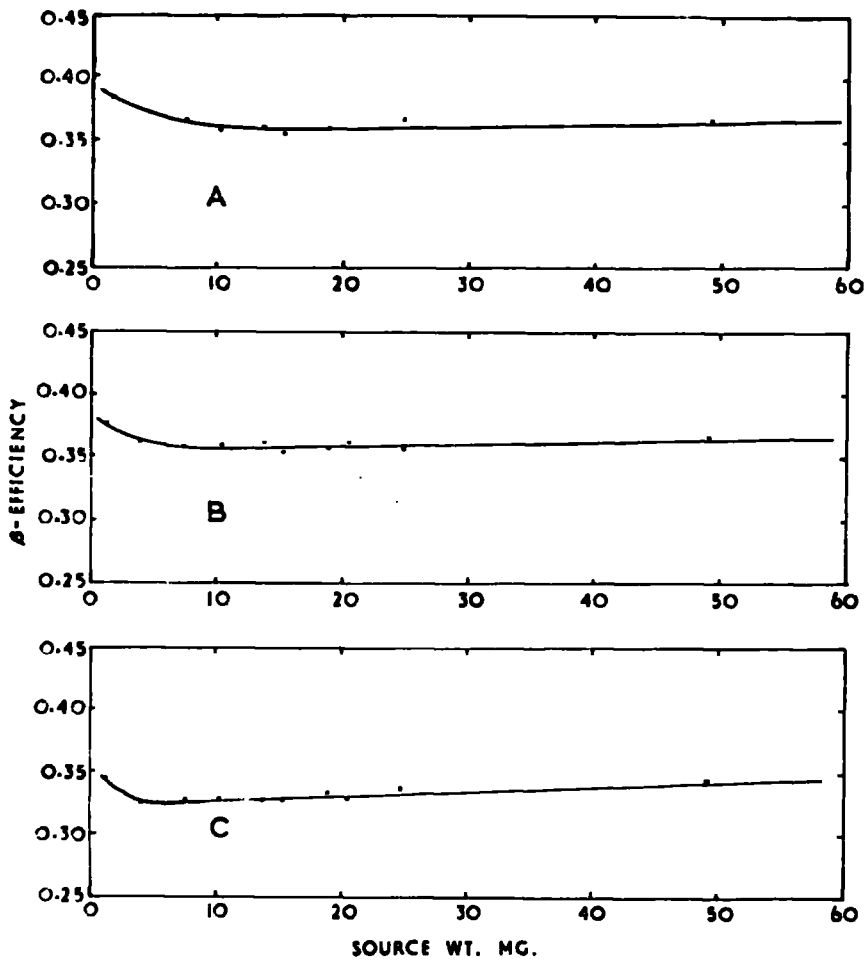


FIG 17 END-WINDOW COUNTER CALIBRATION: THICKNESS CURVES FOR ^{42}K .

the efficiencies at various source weights were read off and plotted against the average β -energy, \bar{E}_β . Four of these calibration curves are shown in figs 18 and 19. In practice, several other similar curves were plotted at intermediate and greater weights to enable the efficiency to be interpolated over the whole range of sources encountered.

Two types of aluminium planchet, differing slightly in their dimensions were used during the course of the work. These were:-

- i) Manufactured by Brillhart Ltd to A.E.R.E. drawing No. A.36688.
- ii) Manufactured by Nucleonic Accessories Ltd., similar to A.E.R.E. drawing No. A.36688.

The Brillhart planchet was found to be 0.19 mm shallower than the Nucleonic Accessories planchet and this meant that the β -sources were closer to the counter window in this case. Since all β -counting had been carried out in the first, and most sensitive, shelf position it was essential that the efficiency was determined for each type of planchet. The results showed however, a variation of no more than 3% over the energy range considered.

β -counting was also performed with and without a supplementary aluminium backscatterer (800 mg/cm^2) mounted behind the source and this necessitated the calibration of the

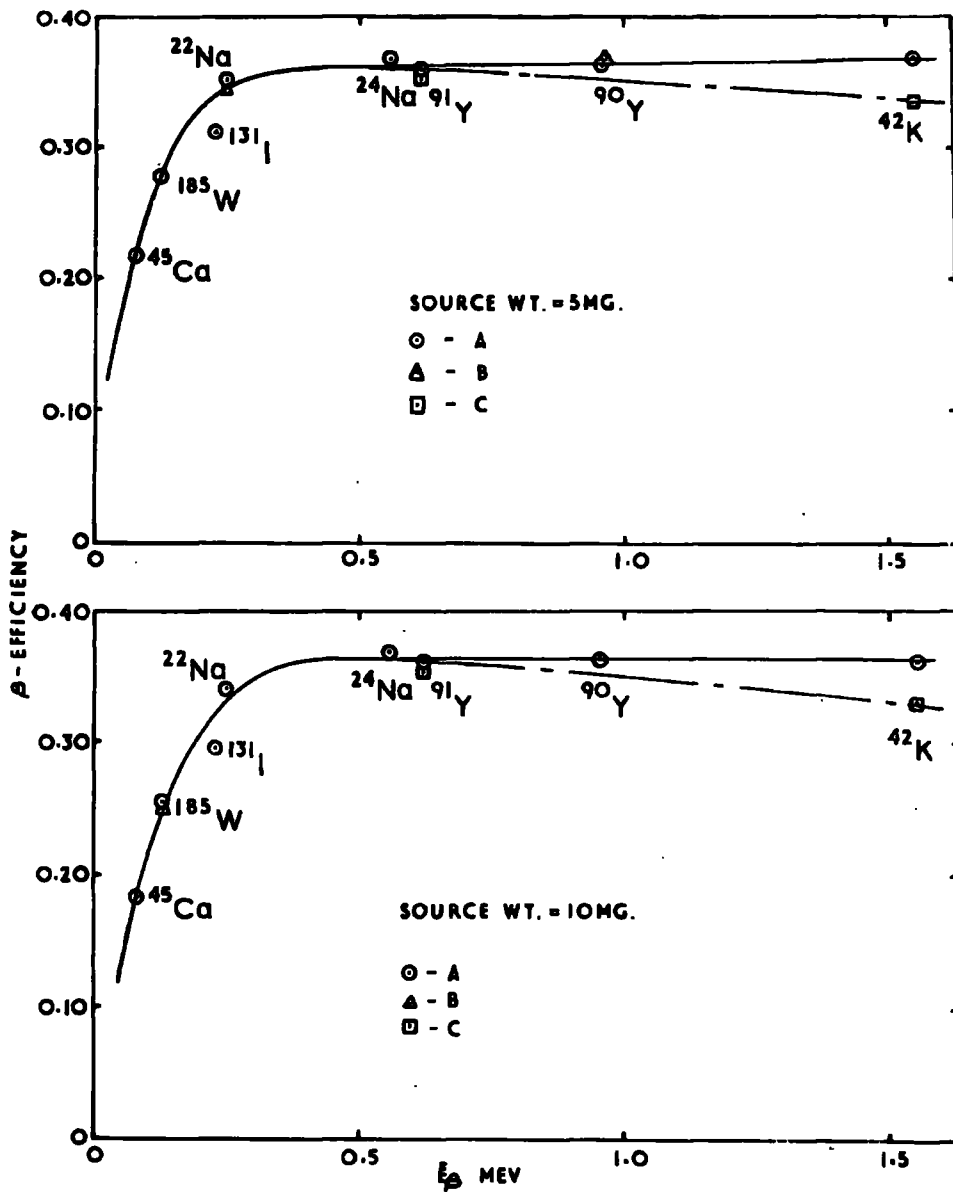


FIG 18 END-WINDOW COUNTER CALIBRATION: β -EFFICIENCY AS A FUNCTION OF E_{β} , THE AVERAGE ENERGY.

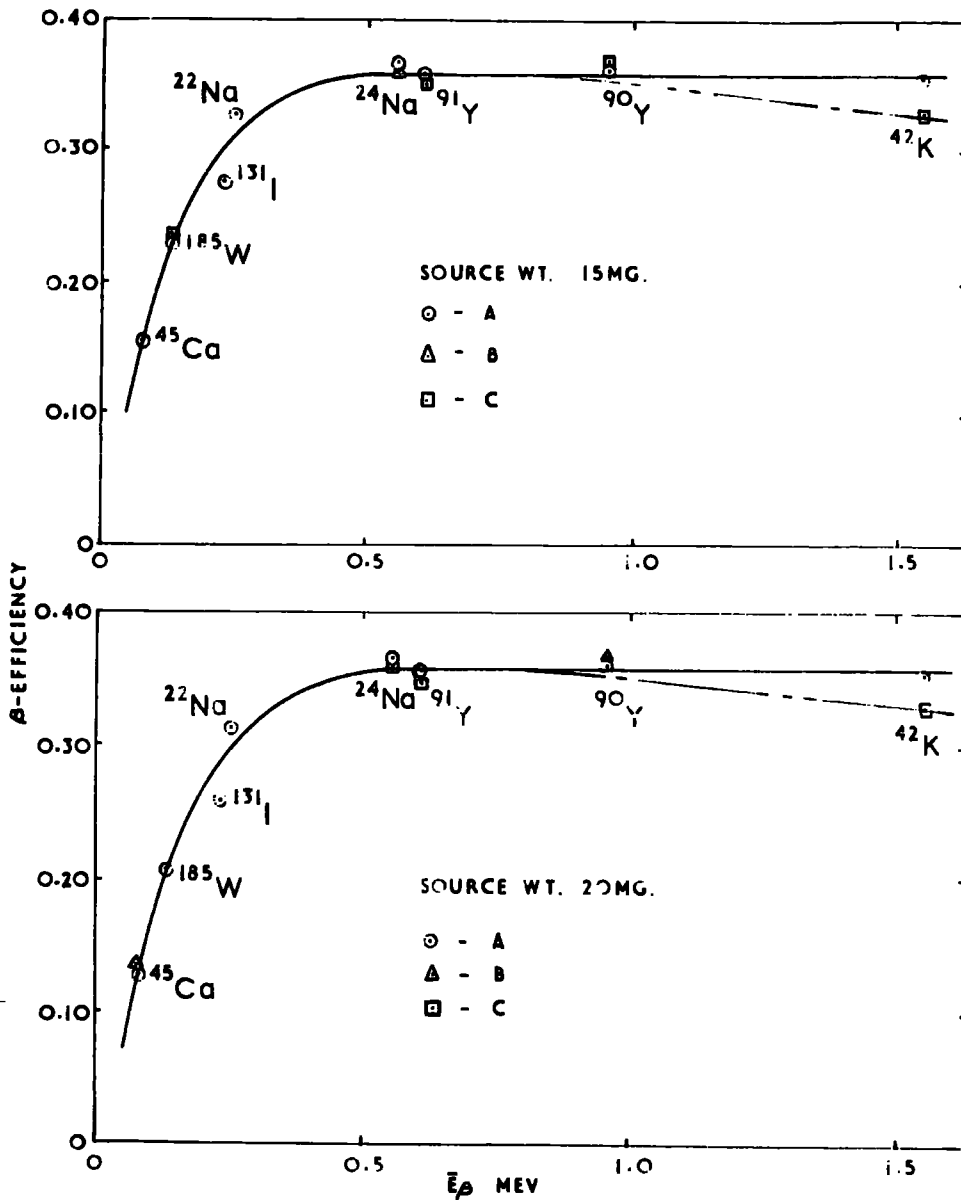


FIG 19 END WINDOW COUNTER CALIBRATION: β-EFFICIENCY AS A FUNCTION OF \bar{E}_β , THE AVERAGE ENERGY.

counter under each of these conditions. It was found that only for β -end-point energies above 2 Mev did the backscattering correction become appreciable reaching a value of 3% at 3.58 Mev.

5.b. Scintillation counting.

Scintillation counting using NaI(Tl) crystals was employed in order to identify many of the product nuclides by means of their γ -spectra. Only in one or two cases was the determination of absolute disintegration rates from γ -counting attempted by calculation of the counter efficiencies.

5.b(1). The operation of NaI(Tl) crystals

The three types of crystal to be described were all operated under similar conditions and a general description of scintillation counting is initially given. By mounting the crystals in $1\frac{1}{2}$ " lead shielding the background level was reduced. The same basic electronic circuitry was always used but amplifier outputs could be fed either to a single channel analyser or to a multichannel pulse amplitude analyser for more detailed investigation of γ -spectra.

A block diagram showing the electronic circuits is given in fig. 20. Pulses from the anode of the photo-multiplier, which gave an effective amplification

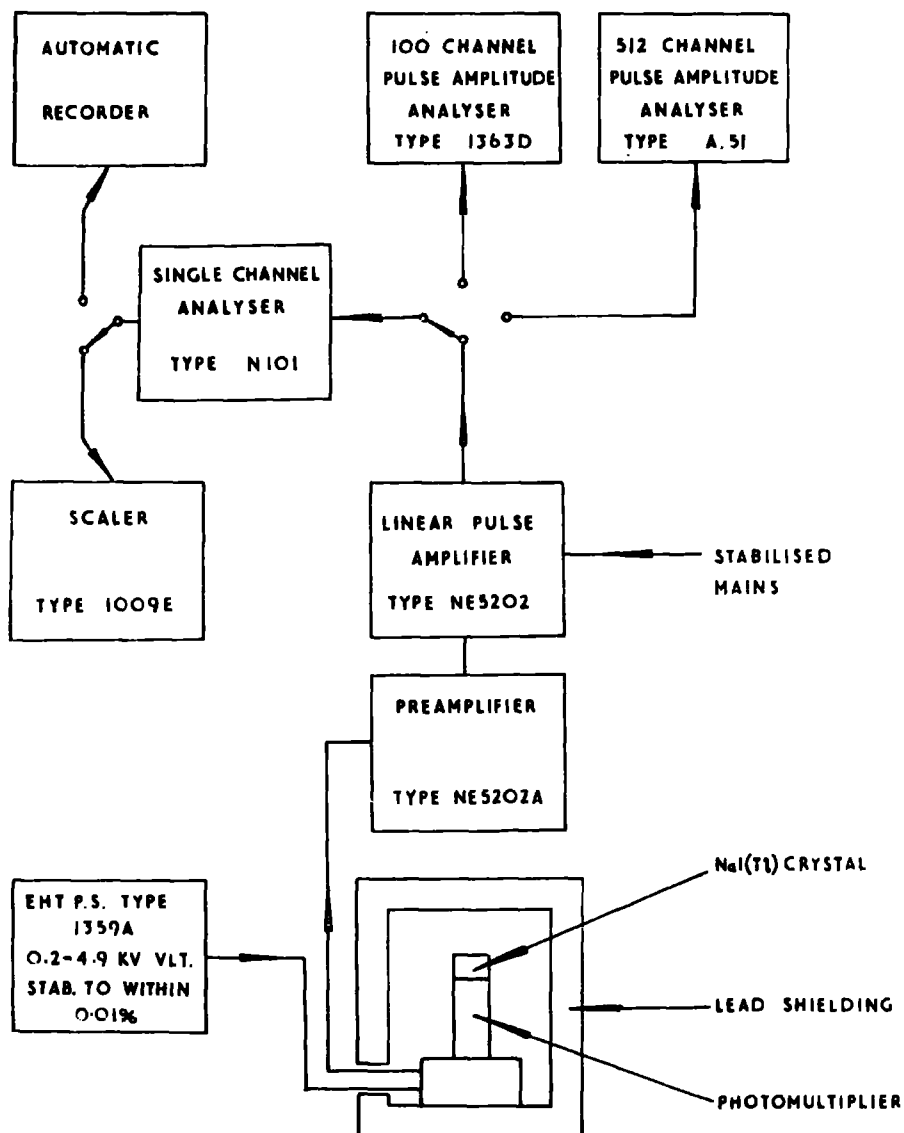


FIG 20 BLOCK DIAGRAM OF THE CIRCUITS USED FOR SCINTILLATION COUNTING.

TABLE 11. End-window counter calibration: β -efficiency as a function of E_{β} , the average energy.

Nuclide	E_{β} Max. MeV	\bar{E}_{β} MeV	Source Material	β -Efficiency at different source weights				Geometry
				5mg.	10mg.	15mg.	20mg.	
^{45}Ca	0.254	0.076	$\text{CaC}_2\text{O}_4 \cdot \text{H}_2\text{O}$	0.217	0.184	0.155	0.128	A
				0.215	0.182	0.155	0.135	B
				0.217	0.183	0.155	0.134	C
^{185}W	0.428	0.127	$\text{WO}_2(\text{C}_9\text{H}_6\text{ON})_2$	0.278	0.255	0.228	0.207	A
				0.274	0.250	0.232	0.210	B
				0.278	0.256	0.234	0.210	C
^{131}I	0.25, 0.33 0.61, 0.81	0.188	CuI	0.324	0.295	0.275	0.258	A
$^{22}\text{Na}^{\#}$	0.542	0.225	NaCl	0.351	0.340	0.328	0.314	A
				0.344	0.341	0.329	0.318	B
				0.348	0.337	0.326	0.316	C
$^{24}\text{Na}^{\#}$	1.39	0.560	NaCl	0.368	0.368	0.368	0.367	A
				0.370	0.369	0.368	0.367	B
				0.364	0.363	0.361	0.361	C
^{91}Y	1.537	0.620	$\text{Y}_2(\text{C}_2\text{O}_4)_3 \cdot 9\text{H}_2\text{O}$	0.360	0.360	0.358	0.358	A
				0.358	0.356	0.355	0.355	B
				0.353	0.351	0.350	0.348	C
^{90}Y	2.26	0.960	$\text{Y}_2(\text{C}_2\text{O}_4)_3 \cdot 9\text{H}_2\text{O}$	0.363	0.363	0.362	0.361	A
				0.368	0.368	0.368	0.368	B
^{42}K	3.58	1.55	$\text{K}[\text{B}(\text{C}_6\text{H}_5)_4]$	0.370	0.360	0.355	0.355	A
				0.365	0.360	0.360	0.360	B
				0.335	0.330	0.330	0.330	C

Geometry: A: Nuclear Accessories planchets with backscatterer.

B: Brilhart planchets with backscatterer

C: Brilhart planchets without backscatterer

$\#$ Observed efficiency corrected for 1.96% contribution by γ -rays.

$\#$ Observed efficiency corrected for 2.40% contribution by γ -rays.

of some 10^7 times, were fed to a cathode follower preamplifier and then to a linear pulse amplifier, capable of a voltage gain of 200 times. When single channel analysis was required, the amplifier output was taken to the appropriate unit which could also be used as a discriminator. As an analyser, the voltage range within which pulses were selected could be adjusted in steps from 0 to 7.5 volts. The lower limit of this "window" could be set in relation to the complete spectrum of pulses by means of a bias control over the range 0-50 v. When used in the discriminator mode the upper limit of selection was removed and the lower limit again adjusted with the bias control. In this way photo-peaks within the crystal, corresponding to particular γ -ray energies could be selected. Pulses from the analyser were then fed to a scaler type 1009E where the dead time was preset, generally at a value of 50 μ sec.

For multichannel analysis the output from the linear amplifier was taken either to a 100 channel or a 512 channel, pulse amplitude analyser.

The first of these analysers (type 1363D) employed a magnostription delay line store. This could accommodate 2^{13} pulses in each channel. A visual indication of the

analyser operation was provided by a cathode ray tube on which the information stored was displayed in binary code. This information could be printed out on a modified adding machine in octal code. To carry out calculations, the octal numbers were converted to decimals using exact conversion tables. The dead-time of the machine, governed primarily by the time taken to sort pulses, was comparatively long (1.8 m sec) and limited the acceptable pulse repetition frequency to a maximum of approximately 10^4 p.p.m. A "live-time" integrating unit controlled the counting time and since only live-time was registered, the observed counting rates did not have to be corrected for dead-time losses. The actual mean time of a count had, however, to be determined externally with a stop watch when necessary. A biasing control, useful in eliminating amplified noise, was available to preset the lower limit of the spectrum.

The 512 channel analyser (type A.51) employed a faster method of sorting pulses resulting in a smaller dead-time and acceptable pulse repetition frequencies up to 6×10^4 p.p.s. Each channel could accommodate 2^{16} pulses, the information being stored in a magnetic core memory. Stored information was displayed on a cathode ray tube in decimal code and could be printed out rapidly either as a typewritten sheet or a perforated

eight-hole tape. The counting time, controlled by a "live-time" unit could be set from approximately 1 minute to 546 minutes. The dead-time could also be set in steps up to a value of 150 μ sec. A subtraction facility was available so that backgrounds could be removed from a total spectrum already stored.

5.b.(ii) The energy calibration of crystals.

When setting up a scintillation counter the γ -spectra of known nuclides were used in order to calibrate the energy scale. Generally the EHT voltage was set at 800 v and the gain of the amplifier adjusted to the required value. For single channel analysis, counts were taken with a window width of 1 or 2 volts over a range of bias settings and a graph of counting rate against bias voltage plotted. The bias voltages at the photopeak maxima were then read from this graph and plotted as a function of the γ -ray energy. A linear curve was obtained which allowed the subsequent interpolation of unknown γ -ray energies. A similar procedure was used for multichannel analysis, the channel width being suitably adjusted and a curve of channel number as a function of energy plotted.

Some of the nuclides used were as follows:-

<u>Nuclide</u>	<u>$t_{1/2}$</u>	<u>E_{γ} Mev</u>
^{75}Se	127d	0.14, 0.27
^{22}Na	2.6y	0.51, 1.28
^{137}Cs	33y	0.662($^{137\text{m}}\text{Ba}$)
^{54}Mn	324d	0.84
^{60}Co	5.2y	1.17, 1.33

5b.(iii) The 2" x 1 $\frac{3}{4}$ " well crystal.

The well crystal (type NE7~~78~~8) provided a good geometrical efficiency so that sources with low activity could be counted. This increased efficiency over a flat crystal was, however, obtained at the expense of some loss in resolution and inaccuracies introduced by summation effects. Both solid and liquid sources were counted, polythene capsules, $\frac{1}{16}$ " thick, being used as containers. Solid sources were placed at the bottom of the capsule to reduce geometrical losses while the volume of liquid sources was adjusted to be as small as possible. ~ 3 mls. of solution was considered to be the maximum when absolute disintegration rates were to be determined. The contribution by particles from negatron emitters was found to be negligible. For the most part, the β -particles were absorbed by the capsule and the crystal casing. The resulting bremsstrahlung radiation was also unnoticeable for the nuclides investigated.

In the case of certain energetic positron emitters, where it was desired to count the annihilation radiation, the sources were placed in a brass capsule $\sim 1000 \text{ mg/cm}^2$ thick to ensure complete annihilation.

5.b.(iv) The $1\frac{1}{2}$ " x 1" and 3" x 3" flat crystals.

$1\frac{1}{2}$ " (type NE 6D4) and 3" (type NE 12DM212) flat crystals were used for sources with a higher specific activity. Solid sources were of the same form as used for β -end-window counting and the geometry was determined by similar tufnol stands mounted on the crystals. Normally sources were counted at a distance of approximately 1 cm allowing aluminium absorbers to be used when necessary.

5.c. Geiger counting.

A halogen-quenched liquid Geiger tube (type MX 124/01) previously calibrated against a 4π counter, was used to measure the activity of ^{56}Mn and ^{24}Na from the reference reactions. Internal gas-counters were also used to observe the (n,p) krypton activities resulting from the irradiation of rubidium.

5.c.(i) The operation of Geiger counters.

The block diagram in fig. 21 shows the electronic equipment used for Geiger counting. Pulses from the counter tubes ($\sim 10\text{v}$) were fed to a trigger probe unit

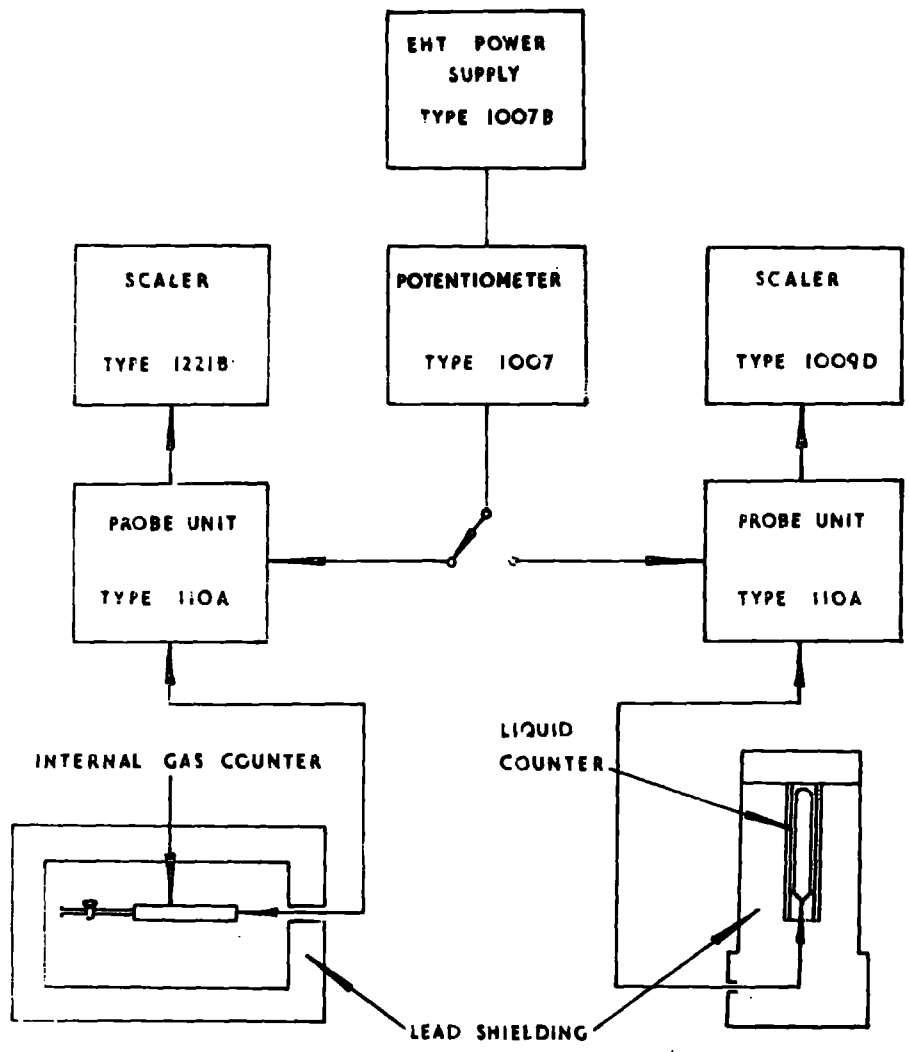


FIG 21 BLOCK DIAGRAM OF THE CIRCUITS USED FOR GEIGER COUNTING.

and thence to the scalers where the discriminator bias was set at 5 v to eliminate noise. The dead-time was electronically controlled in the probe circuit at a value of 500 μ sec. This limited the maximum counting rates which could be handled with accuracy, to approximately 10^4 c.p.m. The operating potential was supplied by a voltage stabilised pack ($2000 \pm 0.1\%$ v) via a potentiometer to the anodes of the counters and could be adjusted over the range 0 to 2000 volts. Both types of counter were operated behind lead shielding to reduce the background level.

5.c.(ii) Calibration of the liquid counter.

The efficiency of the liquid counter depended critically upon the density of the solution. ^{56}Mn and ^{24}Na counting efficiencies had previously been determined for standard dissolution procedures by comparison with a 4π counter. (see p. 35). These procedures had been developed for use with the fluxes available from the Cockcroft-Walton accelerator but the higher fluxes available on the S.A.M.E.S. electrostatic machine necessitated modifications to the dissolution procedure used for iron, so that the ^{56}Mn could conveniently be counted within 2 to 3 half-lives of the end of irradiations. A different solvent was also used in some irradiations on the Cockcroft-Walton machine. It was necessary to determine the efficiency for these modified procedures which were at different dilutions to that used

in the original calibration. Aluminium was never used as a monitor under the higher flux conditions so recalibration of the counter for ^{24}Na was not necessary.

The three methods used for the dissolution of iron were as follows:—

- (i) 0.5 gm iron was dissolved in a mixture of 50% 5N HNO_3 /50% 5N H_2SO_4 with inactive Mn(II) carrier present (1.78 gm. $\text{MnSO}_4 \cdot 4\text{H}_2\text{O}/1$). The solution was then made up to 12 ml with the acid mixture and 10 ml taken for counting. (This procedure was used in the absolute ^{56}Mn calibration).
- (ii) 0.5 gm iron was dissolved in 5 ml 8 M HCl containing 0.25 gm $\text{MnCl}_2 \cdot 4\text{H}_2\text{O}$ and 3 drops 100 vol H_2O_2 . The solution was then made upto 12 ml and 25 ml with H_2O . A 10 ml. aliquot was then transferred to the counter with a pipette.
- (iii) 0.5 gm. iron was dissolved in 20 ml of the acid/carrier mixture used in (i) and diluted with H_2O to 100, 250, 500 or 1000 mls. depending upon the neutron flux and length of irradiation on the electrostatic accelerator. 10 ml. of the diluted solution was taken for counting.

The following experiment was carried out to compare procedures (i) and (ii):—

1.5 gm of iron granules, contained in a thin polythene bag were irradiated at 60° to the incident deuteron beam of the Cockcroft-Walton accelerator for 30 minutes. This angle was chosen to reduce the chance of inhomogeneous activation since the granules were to be divided before dissolution. After irradiation the granules were well mixed and divided into three aliquots of 0.5 gm. Two aliquots were dissolved as in procedure (ii) and made up to 12 and 25 ml. respectively. The remaining aliquot was treated as in (i). After counting, the observed specific activity of ^{56}Mn in the iron at a fixed time was calculated in each case, yielding the relative efficiencies for the two dilutions in procedure (ii). The results are given in table 12.

TABLE 12. The efficiency of the liquid counter for ^{56}Mn

Dissolution procedure	Specific ^{56}Mn act. cpm/gm Fe	^{56}Mn detection coeff.
(i) 12 ml $\text{HNO}_3/\text{H}_2\text{SO}_4$	2.0042×10^4	0.0795*
(ii) 12 ml $\text{H}_2\text{O}_2/\text{HCl}$	2.0490×10^4	0.0813
(iii) 25 ml $\text{H}_2\text{O}_2/\text{HCl}$	2.0860×10^4	0.0827

* From absolute calibration.

Procedures (i) and (iii) were compared in a similar manner:-

2.25 gm of iron granules was irradiated at 0° to the incident deuteron beam on the electrostatic accelerator. 2.08 gm of the granules was dissolved in exactly 50 ml of the acid/carrier mixture to give a solution identical to that obtained in (i). 12 ml of this solution was taken and diluted to 20 ml with the acid mixture and then to 100 ml with water, giving a solution identical to the 100 ml solution in (iii). 10 ml aliquots of this solution were diluted to 25, 50 and 100 ml respectively, to give the remaining dilutions in (iii). The solutions were then counted starting with the most dilute, and the relative efficiencies for ^{56}Mn calculated. The decay of ^{56}Mn was followed to check the purity of the sample and the observed activities were corrected for decay by calculation. Collected results from triplicate experiments are given in table 13.

TABLE 13. The efficiency of the liquid counter for ^{56}Mn

Dissolution procedure	Run	Specific ^{56}Mn activity cpm/gm Fe.	^{56}Mn detection coefficient	Mean detection coefficient
(1) 12 ml. $\text{HNO}_3/\text{H}_2\text{SO}_4$	1	2.4466 x 10^6		0.0795
	2	2.6310 x 10^5		
	3	4.8456 x 10^5		
(111) 100 ml. $\text{HNO}_3/\text{H}_2\text{SO}_4/\text{H}_2\text{O}$	1	2.4958 x 10^6	0.0811	0.0809
	2	2.6628 x 10^5	0.0805	
	3	4.9388 x 10^5	0.0810	
(111) 250 ml. $\text{HNO}_3/\text{H}_2\text{SO}_4/\text{H}_2\text{O}$	1	2.5568 x 10^6	0.0831	0.0828
	2	2.7730 x 10^5	0.0838	
	3	4.9756 x 10^5	0.0816	
(111) 500 ml. $\text{HNO}_3/\text{H}_2\text{SO}_4/\text{H}_2\text{O}$	1	2.5972 x 10^6	0.0844	0.0832
	2	2.7592 x 10^5	0.0834	
	3	4.9922 x 10^5	0.0819	
(111) 1000 ml. $\text{HNO}_3/\text{H}_2\text{SO}_4/\text{H}_2\text{O}$	1	2.5730 x 10^6	0.0836	0.0831
	2	2.7500 x 10^5	0.0831	
	3	5.0326 x 10^5	0.0827	

* From absolute calibration.

5.c.(iii) Internal gas-counting.

An account of the purification and isolation of radioactive krypton from irradiated rubidium nitrate is given in detail in the following chapter (p.104).

The construction of the type of counter used in this work is shown in fig. 22. A stainless-steel tube approximately 1.59 mm thick and 2.54 cm in diameter formed both the cathode and the body of the counter. This was intended to increase the efficiency over the normal glass-enveloped counter by making almost the whole counter volume sensitive. The ends of the counter were made from polystyrene to provide insulated supports for the central anode wire. "Black-wax" (Apiezon W) was used to seal the end-pieces and the counter could be filled via the glass tube and tap. 9 cm. (Hg) of pure argon and 1 cm of pure ethyl formate (the quenching agent) were used to fill the counter. A slight tension was maintained in the coaxial anode wire (0.001" diam. tungsten) by a small spring at one end. A T-piece of 0.5 mm diameter tungsten wire spot-welded to the anode enabled it to be retained by the spring. Connection to the EHT supply was made via the tungsten/glass seal at the opposite end of the counter.

A slightly smaller counter of similar design was also

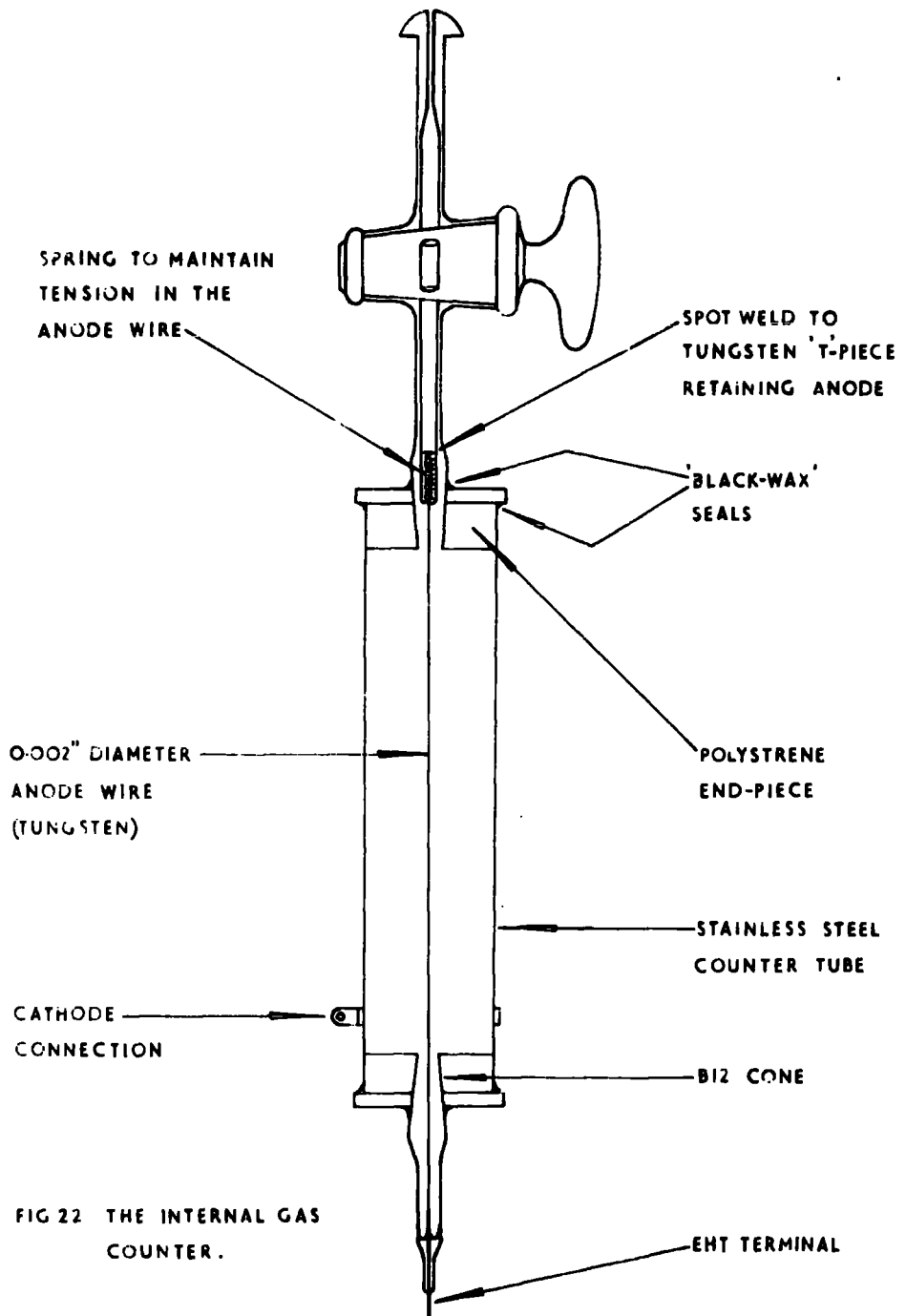


FIG 22 THE INTERNAL GAS COUNTER.

used. This differed from the one described by having the anode wire and its external connections, supported directly by the polystyrene end-pieces. A B7 cone was inserted through one end-piece to the side of the terminal to facilitate filling. The same gas mixture and operational conditions were used and the counter had similar characteristics to the one described.

Plateaux for each counter were determined using an external standard β -source. The position of the source was fixed at a point half-way along the length of the counter and close as possible to it. Optimum operating voltages were in the region of 1000 volts and were found to be reproduceable to within 70 volts for individual fillings. For active fillings the choice of operating voltage was based in the first place upon data obtained previously with the external source. When the krypton activities had decayed, the plateau was checked with the standard source and the background counting rate also determined. Background rates varied from 20 to 40 cpm.

Care had to be taken when handling this type of counter to avoid leaks. Only slight mechanical strain on the end-pieces was sufficient to disturb the seals and allow the ingress of air. The repair of leaks was somewhat tedious involving gentle warming of the seals

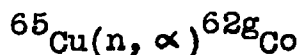
and sometimes the further application of "black-wax", followed by prolonged testing on the vacuum line.

CHAPTER 3

A description of the individual cross-section measurements
and the results

1. The reactions of copper.

The following reactions occurring in copper were investigated:-



Foils of "Analar" copper (99.985% pure), 2 cm. in diameter and 0.125 mm thick were sandwiched between aluminium foils and irradiated for periods of fifteen minutes. "Analar" cupric oxide (99.24% pure) mixed with iron granules was also irradiated for periods of thirty minutes.

Both the irradiated foils (approximately 0.25 gm) and the cupric oxide (approximately 2 gm) were dissolved in solutions containing cobalt (II) and nickel (II) carriers. The bulk of the copper was initially removed by precipitation and the cobalt isolated by solvent extraction, solid sources of cobalt sulphide subsequently being prepared for end-window β -counting. ${}^{61}\text{Co}$, which decays completely via a 0.07 MeV gamma transition to the ground state of ${}^{61}\text{Ni}$, was also counted as aqueous solutions using a 2" x 1 $\frac{3}{4}$ " NaI (Tl) well crystal.

The chemical separation procedure

The separation scheme was developed from general analytical methods, and more detailed information available in the Nuclear Science Series. ^{41,42,43}

Step 1 The irradiated copper was dissolved in a boiling mixture of 10 ml. 8 NHCl and 4 ml 100 volume H₂O₂ to which 10 ml each of the nickel and cobalt carriers had been added. After cooling, 5N NH₄OH was added until a pale green precipitate just persisted and the solution was then diluted to 100 ml. SO₂ was passed until the precipitate just redissolved to give a pale green solution.

Step 1 a The cupric oxide was dissolved in a mixture of 20 ml 5 NHCl and 10 ml each of the carriers by boiling and treated as described in the first and following steps.

Step 2 Solid NH₄SCN was added to precipitate copper (I) thiocyanate which was filtered at the pump using a Whatman 50 paper and washed with 5-10 ml of 1% NH₄SCN. The filtrate and washings were retained. If a brown colouration appeared at this precipitation stage, the mixture was further treated with SO₂ until a white precipitate and a slightly pink supernate were obtained.

Step 3 To the filtrate was added approximately 1 gm of NH₄SCN and 1 ml of concentrated HCl. The cobalt thiocyanate

complex was extracted into 60 ml of a mixture of equal volumes of amyl alcohol and diethyl ether in three equal portions and the aqueous layer discarded. Before each of the last two extractions, a further 1 ml of concentrated HCl was added to maintain the acid concentration in the aqueous phase. The blue organic extract was washed with 10 ml 1% NH_4SCN and the cobalt back-extracted into 20 ml of 5N NH_4OH , giving a yellow aqueous solution.

Step 4 A sulphide precipitation under acid conditions was initially performed on the stripped cobalt solution to eliminate traces of copper. The pH was adjusted to approximately 6 by the addition of 5N HCl. 5 ml. of 5% aqueous thioacetamide was then added and the mixture heated to boiling. Any precipitate which formed was removed with the aid of "Super-Cell" filtering agent. The filtrate was made alkaline with 20 ml of 5N NH_4OH and the whole again heated to boiling to precipitate cobalt (II) sulphide. After filtration, the precipitate was washed with 10 ml H_2O and 10 ml diethyl ether. A solid source was prepared for end-window counting and dried at 80°C . Counting was started after approximately one hour.

Step 4a For γ -counting, an ⁹aqueous cobalt source was prepared by evaporating the filtrate remaining after the removal of copper in the previous step, to a volume of approximately 2 ml and placing this in a polythene capsule.

The preparation of the carrier solutions

Nickel hold-back carrier was prepared by dissolving "Analar" $\text{NiCl}_2 \cdot 6\text{H}_2\text{O}$ to give a solution with a concentration of approximately 1 mg Ni/ml.

The cobalt carrier was prepared in a similar manner using "Analar" $\text{CoCl}_2 \cdot 6\text{H}_2\text{O}$ and the concentration, which was also in the region of 1 mg Co/ml was determined by titration.

The determination of cobalt

The concentration of the cobalt carrier was determined by direct titration against EDTA according to the method described by Flaschka⁴⁴) using murexide as the indicator.

To 5 ml aliquots of the carrier solution were added 10 ml of 1N $\text{NaOOC}\cdot\text{CH}_3$, 2 drops of a saturated murexide solution and 2N NH_4OH dropwise until a colour change from orange to yellow was observed. The mixture was then titrated immediately against 0.1M EDTA disodium salt from a semi-micro burette to the purple end-point. During the titration 2N NH_4OH was added dropwise to neutralise the hydrogen ions formed, which otherwise imparted an orange colour, tending to mask the end-point. From the titres, which agreed to within 1% the concentration of the cobalt carrier was calculated.

A similar titration procedure was also used to determine the chemical yield of cobalt in the solid sources. Each source was dissolved in 3 ml of 8N HCl plus 2 drops of H_2O_2 and the solution boiled gently for approximately one hour to destroy excess peroxide. After cooling, the volume was adjusted to 5 ml and the solution titrated against EDTA, as just described for the carrier. The aqueous cobalt sources were determined in a similar manner, the dissolution step being omitted.

Observations

The β -decay of the solid cobalt sources was followed in the end-window counter until a residual activity of a few counts per minute above the background level remained. Due to the low counting rate this long-lived component was not identified with certainty although the most likely contaminant was thought to be 12.8 hour ^{64}Cu from the $^{65}Cu(n,2n)$ reaction.

Upon resolution of the decay curves, a short-lived activity of 13.8 minutes was observed, corresponding to ^{62g}Co from the $^{65}Cu(n, \alpha)$ reaction. A second component showed a half-life of 100 minutes which was in good agreement with the value accepted for ^{61}Co (99m). The initial observed activity of ^{61}Co was corrected for the residual activity,

which amounted to approximately 1% of this value. For the purposes of calculation, the observed counting rates were corrected for absorption, backscattering and geometry using the methods put forward by Burt³⁸⁾ and by Gleason et al.³⁷⁾ No evidence of the 1.6 minute ^{62m}Co , resulting from the $^{65}\text{Cu}(n, \alpha)^{62}\text{Co}$ reaction was seen, as counting was not started until some sixty minutes had elapsed after the end of each irradiation.

The γ -decay of the aqueous cobalt sources was followed in the NaI(Tl) well crystal at a photopeak corresponding to 0.07 MeV, using multichannel analysis. (fig. 23). In order to plot the decay, events occurring in the photopeak were summed and corrected for background counts. A half-life of 100 minutes was obtained attributable to ^{61}Co , which decays completely via a 0.07 MeV gamma transition to the ground state of ^{61}Ni . No sign of the 10.6 minute ^{60m}Co isomer, which decays via a 0.058 MeV gamma transition to ^{60g}Co , was seen. The absolute activity of ^{61}Co , the $(n, \alpha n) + (n, \alpha)$ product, was calculated by correcting for the crystal photopeak efficiency⁵⁶⁾ and the absorption of the gammas in the source, capsule and crystal casing.⁵⁷⁾

Discussion

^{61}Co can be produced by the $^{63}\text{Cu}(n, ^3\text{He})^{61}\text{Co}$ reaction

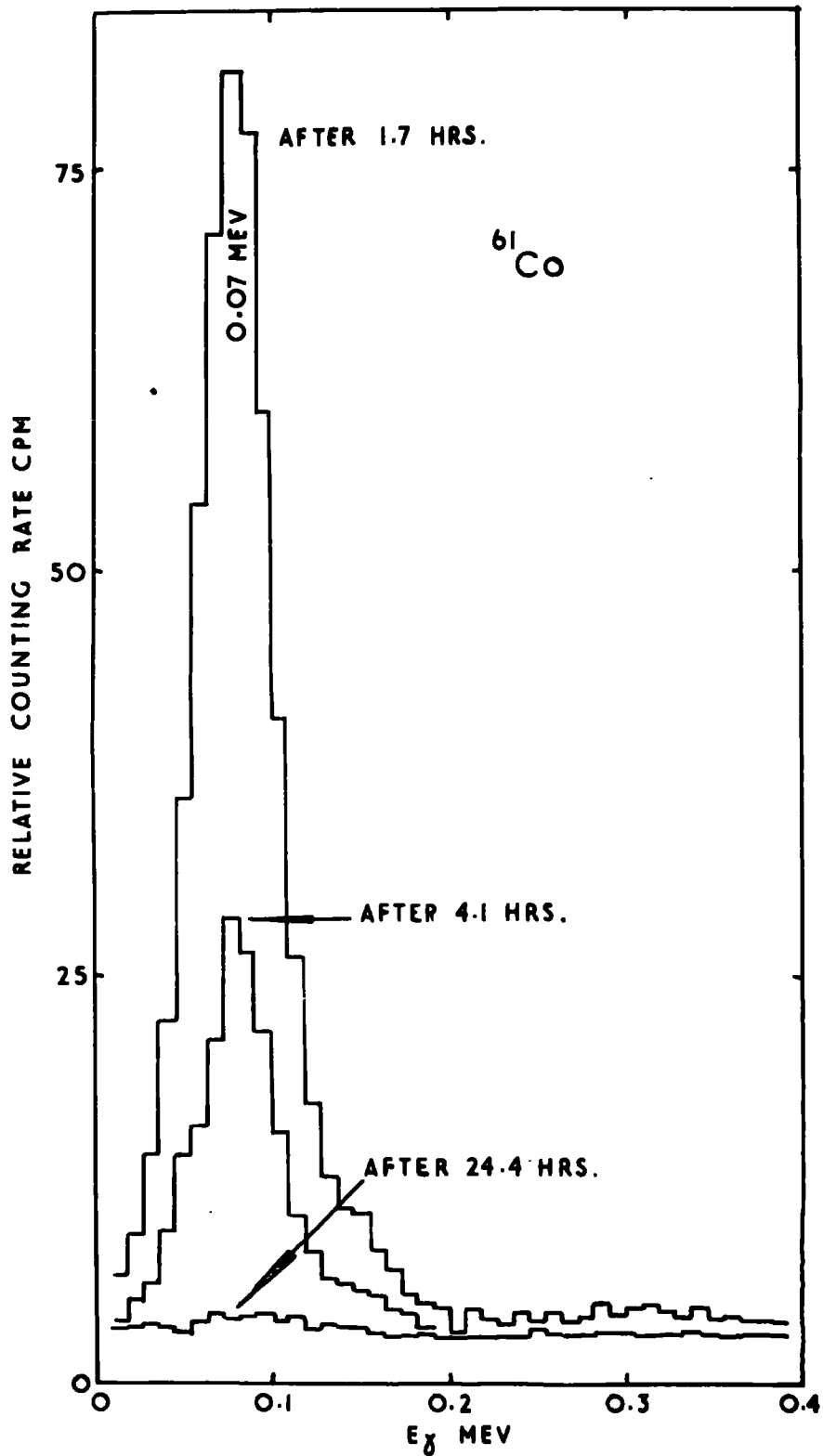


FIG 23 EXAMPLES OF THE OBSERVED γ -SPECTRA OF THE AQUEOUS COBALT SOURCE.

as well as the $^{65}\text{Cu}((n, \alpha n) + (n, n\alpha))^{61}\text{Co}$ reaction. No distinction could be made between these reaction routes by the present method, but since the cross-section for the former reaction was expected to be relatively small, (Bramlitt et al ⁴⁵/₄, have recently quoted a value of < 0.08 mb at 14.5 MeV) the assumption that ^{61}Co was produced only by the latter reaction was thought to be reasonably valid. Another possible interference was from the $^{65}\text{Cu}(n, ^3\text{He})^{63}\text{Co}$ reaction which gives rise to a β^- -active nuclide with a half-life of 1.4 hours. It would have been very difficult to distinguish this activity from 1.7 hour ^{61}Co but again, since the $(n, ^3\text{He})$ cross-section was expected to be small, the contribution by ^{63}Co was assumed to be negligible.

With regard to the estimation of the ^{62g}Co (13.8 m) activity, two possible sources of interference were considered. If indeed, the residual activity in the cobalt sources was due to ^{64}Cu , then some contribution by ^{62}Cu (9.8m) from the $^{63}\text{Cu}(n, 2n)^{62}\text{Cu}$ reaction might also have been expected. This would have had the effect of decreasing the observed half-life of the initial component of the decay curve. A similar effect would also have been caused by the presence of ^{60m}Co from the $^{63}\text{Cu}(n, \alpha)^{60}\text{Co}$ reaction, which decays by an appreciably converted 0.058 Mev internal transition to ^{60g}Co . The good agreement of the observed half-life for ^{62g}Co with the literature values

indicated that both these possible interferences were negligible and particularly in the second case, that the energy of the conversion electrons was probably below the cut-off energy of the counter.

The results are set out in the following tables (14 to 17) the errors given being the standard deviations. The value of 8.54 ± 0.53 mb for the $^{65}\text{Cu}(n, \alpha)^{62}\text{Co}$ cross section, is essentially a lower limit since only one of the β^- -active isomers was observed. Kantele and Gardner ⁴⁶) have measured this cross-section at 14.8 Mev and found a similar value of 7.5 ± 2 mb. The present result also agrees tolerably with that of Bramlitt ⁴⁷ (20 ± 10 mb) when the large error in the latter value is considered. There is however some disagreement with other workers as regards the $^{65}\text{Cu}((n, \alpha n) + (n, n\alpha))^{61}\text{Co}$ cross-section. Bommann et al ⁴⁸ give a value of 6 ± 2 mb at 14.7 MeV for this reaction which is altogether different from the 1.01 ± 0.05 mb observed. The more recent values of 2.9 ± 0.8 mb (Bramlitt) and 2.8 ± 0.3 mb (Kantele) at similar neutron energies, also disagree substantially with the present work.

2. The reactions of gallium.

The following reaction cross-sections of gallium were measured:-

TABLE 14 The reference reaction $^{27}\text{Al}(n,\alpha)^{24}\text{Na}$.

Expt. No.	No. of ^{27}Al nuclei	cpm A_0 obs	dpm A_0 abs	$(X_T \times \lambda_{pr})$
4	9.937×10^{20}	2.04×10^3	4.60×10^4	68.57
5	9.970×10^{20}	1.53×10^3	3.45×10^4	59.93

$t_{1/2}^{24}\text{Na} = 15.0$ hours.

$C^{24}\text{Na} = 0.0532$

$E_n = 14.7$ MeV

$\sigma^{27}\text{Al}(n,\alpha)^{24}\text{Na} = 104.7$ mb.

TABLE 15 The reference reaction $^{56}\text{Fe}(n,p)^{56}\text{Mn}$

Expt. No.	No. of ^{56}Fe nuclei	cpm A_0 obs.	dpm A_0 abs	$(X_T \times \lambda_{DT})$
6	4.556×10^{21}	4.80×10^3	1.45×10^5	788.3

$$t_{\frac{1}{2}} \text{ } ^{56}\text{Mn} = 2.58 \text{ hours.}$$

$$\sigma \text{ } ^{56}\text{Fe}(n,p)^{56}\text{Mn} = 97.7 \text{ mb}$$

$$E_n = 14.7 \text{ MeV}$$

$$C \text{ } ^{56}\text{Mn} = 0.0827$$

TABLE 16

The $^{65}\text{Cu}(n, \alpha)^{62}\text{gCo}$ cross-section

Expt. No.	No. of ^{65}Cu nuclei	A ₀ cpm	Chem Yield	A ₀ dpm	(xx)p	Ref. reaction	σ mb
		obs		abs			
4	7.612×10^{20}	1.13×10^4	0.23	1.40×10^5	3144	$^{27}\text{Al}(n, \alpha)^{24}\text{Na}$	9.07
5	7.170×10^{20}	1.34×10^4	0.44	8.70×10^4	2751	$^{27}\text{Al}(n, \alpha)^{24}\text{Na}$	8.00

$t_{1/2}^{62\text{gCo}} = 13.8$ minutes

$C_{\text{Calcd}}^{62\text{gCo}} = 0.35$

Mean value $\sigma = 8.54 + 0.53$ mb

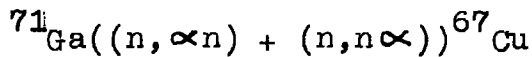
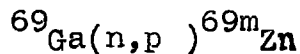
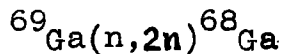
TABLE 17

The $^{65}\text{Cu}((n, xn) + (n, n\alpha))$ ^{61}Co cross-section

Expt. No.	sample material	No. of ^{65}Cu nuclei	A_0 obs	cpm	Calcd.	Chem.	A_0 obs	dpm	(Xx/p)	Ref. Reaction	σ mb
4	copper foil	7.612×10^{20}	2.20×10^2	0.34	0.23	2.81×10^3	594.9	$^{27}\text{Al}(n, \alpha)$	^{24}Na	0.91	
5	copper foil	7.170×10^{20}	3.25×10^2	0.34	0.44	2.17×10^3	520.1	$^{27}\text{Al}(n, \alpha)$	^{24}Na	1.09	
6	Cupric oxide	4.607×10^{21}	9.60×10^2	0.79	0.52	2.34×10^3	1192	$^{56}\text{Fe}(n, p)$	^{56}Mn	1.03	

$t_{1/2}^{61}\text{Co} = 100$ minutes

Mean value $\sigma = 1.01 + 0.05$ mb



Samples consisting of discs of 99.99% pure gallium metal, 2 cm in diameter and approximately 0.5 mm thick were irradiated for periods of either one or three hours. When aluminium was used as the neutron monitor, the discs were sandwiched between two, approximately 6 mg/cm^2 thick, aluminium foils.

The gallium discs were made by casting the metal, which melts at 29.8°C under ordinary conditions, in a perspex mould. Solid carbon dioxide was used to cool the melt to ensure reliable solidification, as supercooling of the metal was otherwise troublesome. The discs were cleaned by washing in chilled dilute HCl containing a few drops of 20 volume H_2O_2 and afterwards in cold water and acetone. After drying in a desiccator the discs were stored in cool surroundings. Discs with a tolerably uniform thickness could be prepared in this way.

After irradiation the gallium was dissolved in a

solution containing zinc and copper carriers and the three elements were separated by precipitation and solvent extraction techniques. Solid sources of copper (II) sulphide were prepared for end-window β - counting and weighed to determine the chemical yields. In initial experiments, solid sources of gallium 8- hydroxyquinolate and zinc sulphide were counted in the 2" x 1 $\frac{3}{4}$ " NaI(Tl) well crystal, the chemical yields also being determined by weighing. Aqueous sources of these elements were used in later work, when the chemical yields were found by titration. Using the separation procedure shortly to be described, the gallium sources could be counted after approximately 90 minutes and the zinc sources after about 2 $\frac{1}{2}$ hours.

The $^{69}\text{Ga}(n,2n)^{68}\text{Ga}$ cross-section was determined relative to the $^{27}\text{Al}(n,\alpha)^{24}\text{Na}$ reaction and for convenience was used as the internal reference reaction in some experiments.

Based upon information available in the Nuclear Science Series^{41,49,50} on the radiochemistry of the elements, the following chemical separation procedure was developed and used.

The chemical separation procedure.

Step 1 The gallium was dissolved in a mixture of 12 ml aqua regia and 10 ml each of the zinc and copper carrier solutions, by boiling for approximately ten minutes. After fuming the resulting solution to near dryness, the residue was taken up in 40 ml of 6N HCl and the gallium extracted into 60 ml of diethyl ether in three equal portions. Before each of the last two extractions, a further 1 ml of concentrated HCl was added to the aqueous layer to maintain the acid concentration. Both phases were retained. The ether extract was washed with 40 ml 6N HCl in two portions and the gallium back-extracted into 40 ml H₂O, from which traces of ether were finally removed by boiling.

Step 2 To the aqueous gallium extract was added 30 ml δ -hydroxyquinoline solution (1% in 50% acetic acid) followed by 30 ml of 3N NH₄OOCH₃, to precipitate the organic derivative. The lemon yellow precipitate was filtered at the pump, washed with 10 ml 50% acetic acid, 40 ml H₂O and dried at 90°C. A solid source of gallium was prepared for counting in the well crystal by packing a weighed amount of the precipitate into a thin polythene bag and placing this in a brass capsule which had a wall thickness of approximately 1gm/cm². The brass capsule was used to ensure the

annihilation of the positrons from ^{68}Ga .

Step 2a To prepare a liquid source for γ -counting, the aqueous gallium extract (essentially a solution of GaCl_3) was evaporated to a volume of approximately 2 ml and placed in a test-tube inside the brass capsule.

Step 3 The aqueous phase from step 1, containing zinc and copper, was washed with 40 ml diethyl ether and the washings rejected. After boiling to remove excess ether, the pH of the solution was adjusted to approximately 6 by the addition of 5N NH_4OH , using Universal indicator; 5 ml of a 5% aqueous solution of thioacetamide was then added and the mixture heated to boiling to precipitate copper (II) sulphide. Approximately 1 gm of "Super-Cell" filtering agent was added and the solution filtered, the filtrate being retained. The precipitate was washed well with H_2O and boiled with 20 ml of 6N HCl plus a few drops of 20 vol H_2O_2 to redissolve the copper sulphide. The solution was then filtered, any sulphur precipitate being retained by the "Super-Cell", and copper sulphide reprecipitated from the resulting filtrate in the same way as before. Finally, the precipitate was filtered and washed with 20 ml H_2O followed by 10 ml acetone. A source for end-window counting was prepared and dried in a vacuum desiccator. Counting of the source was started after approximately 2 hours.

Step 4 The filtrate from step 3, containing zinc, was made alkaline with 5N NH_4OH , 5 ml of 5% thioacetamide added and the mixture boiled and digested for 30 minutes to precipitate zinc sulphide. A sintered glass disc was used to filter the precipitate which was washed with 50 ml H_2O and then slurried with the same volume of water. A source was prepared on a glass fibre disc by filtration and was washed with 10 ml acetone and dried at 90°C . After weighing, the source was carefully folded and placed at the bottom of a polythene capsule for γ -counting in the well crystal.

Step 5 A liquid zinc source was prepared by dissolving the zinc sulphide precipitate in 2 ml 5 N HCl and placing the solution in a polythene capsule. The chemical yield of zinc was subsequently determined by titration.

The preparation of the carrier solutions.

The zinc carrier was prepared by dissolving "Analar" ZnO in a few mls of 5N HCl and diluting the solution to give a concentration of approximately 2 mg Zn/ml.

A standard solution of copper, with a concentration in the region of 1 mg Cu/ml, was prepared by dissolving "Analar" copper foil in 5 N HCl containing a small amount of H_2O_2 and diluting the resulting solution to the appropriate volume.

The titrimetric determination of gallium.

The chemical yield of the aqueous gallium sources was determined by titration against EDTA using pyrocatechol violet as the indicator, according to the method described by Welcher⁵¹).

Each source, consisting of an acidic solution of gallium chloride, was diluted to 500 ml with H₂O. To 20 ml aliquots of this solution were added:- 10 ml of buffer solution at pH 3.8 (176 ml 0.2N acetic acid + 24 ml 0.2N ammonium acetate), 6 drops of a 0.1% aqueous solution of pyrocatechol violet, and H₂O to make the volume up to approximately 70 ml. The mixtures were then titrated against 0.1M EDTA disodium salt to the end-point indicated by a colour change from blue to yellow. From the results the weight of gallium in each source was calculated.

The determination of zinc.

After the method described by Welcher⁵²), the chemical yield of zinc in the aqueous sources was determined by titration against EDTA using pyrocatechol violet as the indicator.

The zinc chloride solution was diluted to 50 ml and 10 ml aliquots titrated against 0.1M EDTA disodium salt

from a semimicro burette. To each aliquot was added sufficient buffer solution (equal volumes of 1N NH_4Cl and 1N NH_4OH) to redissolve the initial precipitate of $\text{Zn}(\text{OH})_2$ and 3 - 5 drops of 0.1% pyrocatechol violet solution. A colour change from blue to purple was taken as the end-point.

Observations.

The β -decay of the copper sources was followed for periods of up to ten days in the end-window counter. A purely exponential curve was obtained in each case, but some variation in the half-life of the activity was observed in different experiments. The mean value of five

determinations was found to be 63.6 ± 1.8 hours. This corresponded closely to the most recent value of 61.6 hours for ^{67}Cu , observed by Rudstam⁵³). However, a still lower value of 61 hours was given both by Easterday⁵⁴) and Hopkins⁵⁵.) In view of the discrepancies between the observed half-life and the values of these other workers it was decided that the most reliable course was to calculate the mean of the four results. This was done, a value of 61.8 hours being found and used for the purpose of calculating the cross-section.

The absolute activity of the ^{67}Cu was determined from the β -counting measurements, by correcting for absorption, geometry and backscattering, using data from the papers of Burt³⁸ and of Gleason³⁷ et al). Since the counting of the sources was not started until approximately two hours had elapsed after each irradiation, there was little possibility of observing the 5.2 minute ^{66}Cu from the $^{69}\text{Ga}(n, \alpha)$ reaction.

^{69}Zn decays completely via an internal transition of 0.435 MeV to the β^- -emitting ground state, $^{69}\text{Zn}(55\text{m})$. The decay of the zinc sources at a photopeak corresponding to this energy, was followed in the NaI(Tl) well crystal (fig 24) until the background level had been reached. The spectra were observed using the one hundred-channel pulse height analyser and decay curves were constructed from the

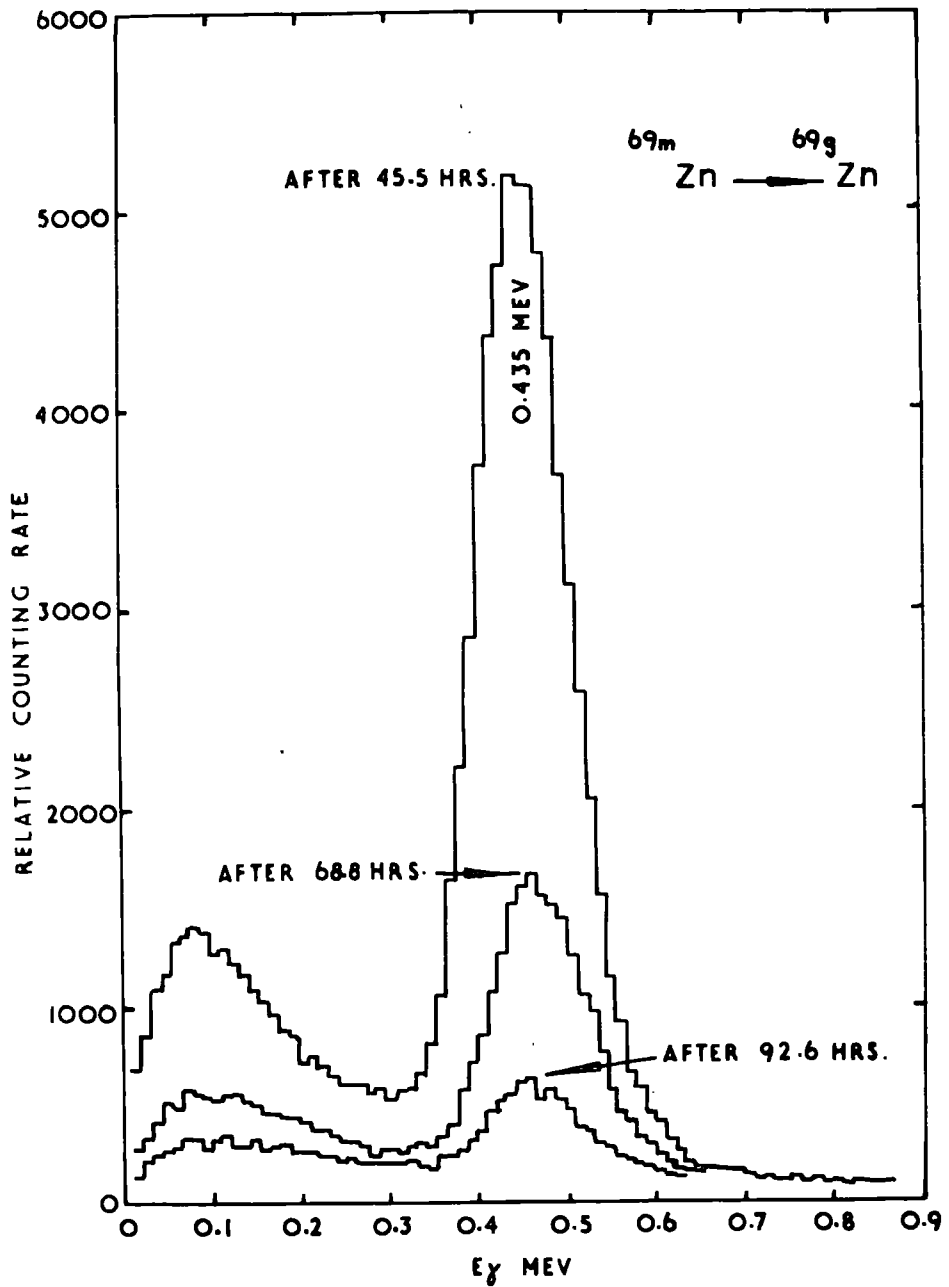


FIG 24 EXAMPLES OF THE OBSERVED γ -SPECTRA OF A ZINC SOURCE.

total counts, determined by summing the events occurring in the photopeak and correcting for background activity. A half-life of 13.7 ± 0.3 hours was obtained, in good agreement with the accepted values for ^{69m}Zn . Evidence of a small contribution by ^{71m}Zn , which decays via gammas of 0.38 and 0.49 MeV, to the initial portion of the decay curves was seen. No attempt was however made to estimate the $^{71}\text{Ga}(n,p)^{71m}\text{Zn}$ cross-section.

The gallium sources were counted at the positron annihilation peak of 0.51 MeV in the well crystal, using hundred-channel pulse height analysis. (fig 25). Decay curves were plotted in the same way as described for zinc and were found to consist of a single component with a half-life of 69 ± 1 minutes corresponding to ^{69}Ga . This nuclide decays predominantly by positron emission (86%, 1.89 MeV; 1.5%, 0.82 MeV) to ^{68}Zn . No shorter lived activity due to the 21 minute ^{70}Ga from the $^{71}\text{Ga}(n, 2n)^{70}\text{Ga}$ reaction was seen. ^{70}Ga decays almost completely by β -emission to the ground state of ^{70}Ge .

To obtain the absolute activities of ^{69m}Zn and ^{68}Ga , the observed counting rates were corrected for the crystal photopeak efficiency⁵⁶, the absorption of gammas in the source, its container and the crystal casing, and also the

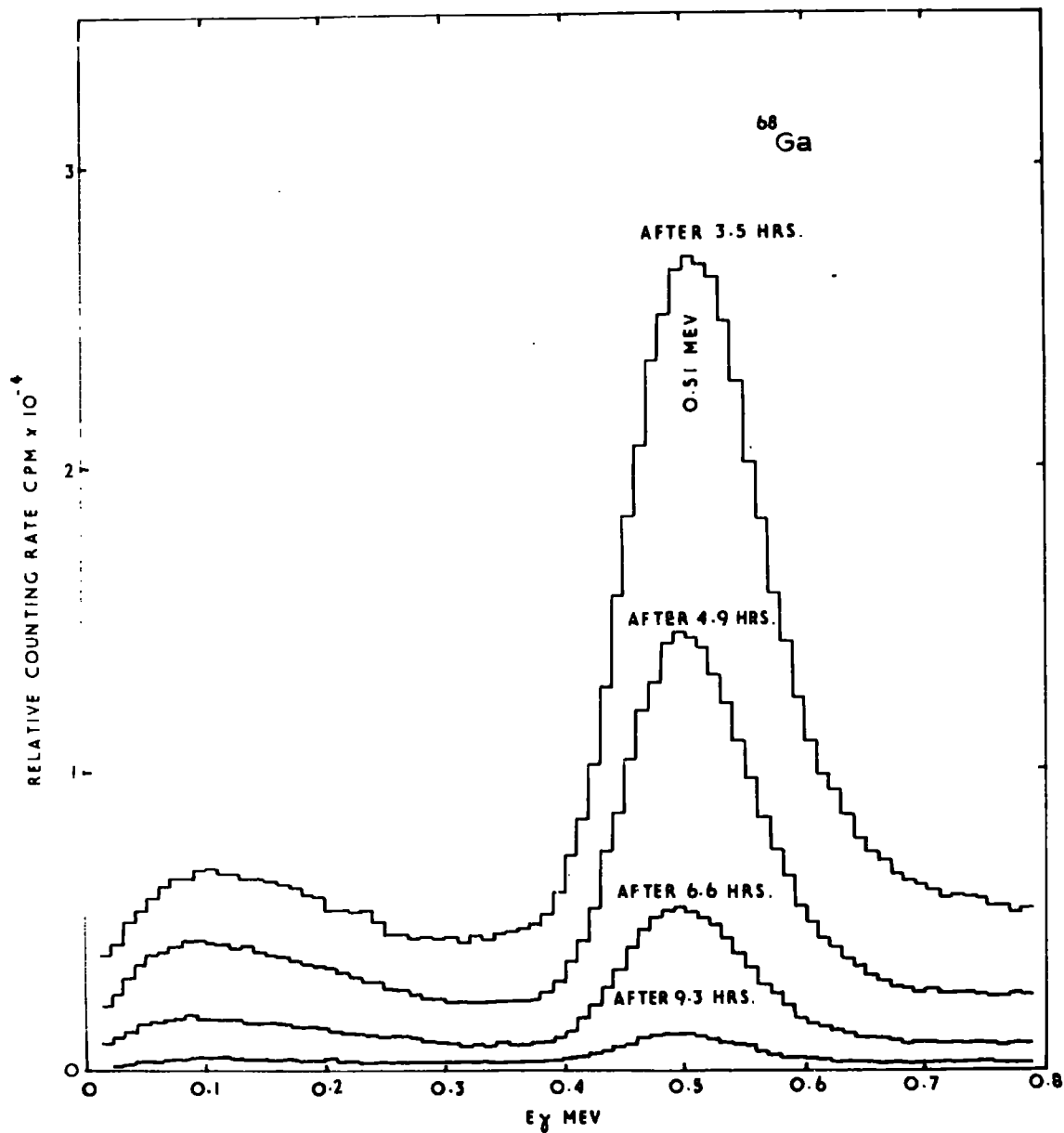


FIG 25 EXAMPLES OF THE OBSERVED γ -SPECTRA OF A GALLIUM SOURCE.

gamma ray and positron yields. Complete annihilation of the positrons from ^{68}Ga was assumed.

Discussion.

The cross-section results, together with the standard deviations, are given in tables 18 to 23 which follow. Where the internal reference reaction $^{69}\text{Ga}(n,2n)^{68}\text{Ga}$ was used instead of $^{27}\text{Al}(n,\alpha)^{24}\text{Na}$, this is indicated in the second column of the appropriate table.

For the $^{71}\text{Ga}(n,\alpha n) + (n,n\alpha)^{67}\text{Cu}$ cross-section, the value of 1.23 ± 0.22 mb observed, resolves the disparity existing between the result of Bormann et al²⁹) (6 ± 2 mb at 15.2 MeV) and that recently given by Bramlitt⁴⁷) (2 ± 1 at 14.7 MeV). It would seem that the value of the former workers is too high, although the excitation function of the reaction could conceivably be rising steeply in this energy region to reach such a magnitude at the slightly higher neutron energy. This however is unlikely, and it is suggested that these workers made some error in the assessment of their results, which were obtained without performing a chemical separation.

Due to approximations which it was necessary to make when calculating the absolute γ -counting efficiencies, it

TABLE 18

The $^{27}\text{Al}(n,\alpha)^{24}\text{Na}$ reference reaction

Expt. No.	No. ^{27}Al nuclei	$A_{0\text{obs}}$ cpm	$A_{0\text{obs}}$ dpm	$(X_T \times \lambda_{\text{PR}})$
7	1.105×10^{21}	1.54×10^3	3.47×10^4	118.4
8	8.418×10^{20}	5.81×10^3	1.31×10^5	207.7
9	8.217×10^{20}	6.50×10^3	1.47×10^5	363.2

$t_{1/2}^{24}\text{Na} = 15.0$ hours

C $^{24}\text{Na} = 0.0532$

$\sigma^{27}\text{Al}(n,\alpha)^{24}\text{Na} = 104.7$ mb

$E_n = 14.7$ MeV

TABLE 19

The $^{69}\text{Ga}(n,2n)^{68}\text{Ga}$ reference reaction

Expt. No.	No. ^{69}Ga nuclei	A_0 cpm obs	Chemical Yield	A_0 dpm obs	$(X_r \times \lambda_{pr})$
10	6.244×10^{21}	2.07×10^6	0.243	4.48×10^7	1717
11	5.660×10^{21}	1.55×10^6	0.234	3.49×10^7	1125
12	5.286×10^{21}	5.30×10^6	0.861	3.24×10^7	1706

$t_{\frac{1}{2}}^{68\text{Ga}} = 69$ minutes

C calcd. $^{68}\text{Ga} = 0.19$

TABLE 20

The $^{71}\text{Ga}((n,\alpha) + (n,n\alpha))^{67}\text{Cu}$ cross-section

Expt. No.	Reference reaction	No. of ^{71}Ga Nuclei	A_{obs} cpm	Calcd Eff.	Chem. Yield	A_{abs} dpm	$(\lambda \times \lambda_p)$	σ mb
10	$^{69}\text{Ga}(n,2n)^{68}\text{Ga}$	4.094×10^{21}	8.10×10^2	0.30	0.870	3.10×10^3	70.18	1.60
11	"	3.711×10^{21}	4.80×10^2	0.30	0.822	1.95×10^3	53.09	1.12
12	"	3.466×10^{21}	9.65×10^2	0.32	0.337	8.95×10^2	38.12	1.17
7	-	-	-	-	-	-	-	-
8	$^{27}\text{Al}(n,\alpha)^{24}\text{Na}$	2.604×10^{21}	2.85×10^2	0.32	0.792	1.12×10^3	55.23	1.29
9	"	2.545×10^{21}	1.54×10^2	0.33	0.445	1.05×10^3	92.43	0.95

$t_{1/2}^{67}\text{Cu} = 61.8$ hours

Mean value $\sigma = 1.23 + 0.22$ mb

TABLE 21

The $^{69}\text{Ga}(n,p)^{69m}\text{Zn}$ cross section

Exp. No.	Reference Reaction	No. ^{69}Ga nuclei	A cpm A _{oobs}	Calcd Eff.	Chem. Yield	dpm A _{oabs}	($\bar{x} \pm \lambda$) _p	σ mb
10	$^{69}\text{Ga}(n, 2n)^{68}\text{Ga}$	6.244×10^{21}	3.30×10^4	0.24	0.625	2.20×10^5	294.7	18.2
11	"	5.660×10^{21}	4.35×10^4	0.24	0.839	2.16×10^5	221.1	20.1
8	$^{27}\text{Al}(n, \alpha)^{24}\text{Ne}$	3.971×10^{21}	1.40×10^4	0.24	0.556	1.05×10^5	228.8	16.2

$t_{1/2}^{69m}\text{Zn} = 13.7$ hours

Mean value $\sigma = 18.2 \pm 1.6$ mb

TABLE 22

The $^{69}\text{Ga}(n, 2n)^{68}\text{Ga}$ cross section.

Expt. No.	^{69}Ga nuclei	A_0	A_0 cps	Chem. Yield	A dpm	$(\sum \lambda_p)$	σ mb
No.		obs	obs		$^{\circ}$ abs		
7	3.623×10^{21}	1.11×10^6	0.848	6.89×10^6	1171	641	
8	3.971×10^{21}	3.70×10^6	0.829	2.35×10^7	1420	582	
9	3.882×10^{21}	5.16×10^6	0.629	4.32×10^7	3700	640	

$t_{1/2}^{69}\text{Ga} = 69$ minutes

C $^{69}\text{Ga} = 0.19$

Mean value $\sigma = 621 \pm 28$ mb

TABLE 23

$^{56}\text{Fe}(n,p)^{56}\text{Mn}$ reference reaction

Expt. No.	No. of ^{56}Fe nuclei	A_{obs} cpm	Counting Eff	A_{abs} dpm	$(X_r \times \lambda_{pr})$
13	5.330×10^{21}	9.10×10^4	0.0813	1.34×10^6	537.7
14	4.379×10^{21}	6.38×10^4	0.0827	1.93×10^6	949.3
15	7.278×10^{21}	6.19×10^4	0.0827	1.87×10^6	537.3
16	6.677×10^{21}	8.45×10^4	0.0813	1.25×10^6	346.1

$t_{1/2}^{56}\text{Mn} = 2.58$ hours

$\sigma^{56}\text{Fe}(np)^{56}\text{Mn} = 97.7$ mb

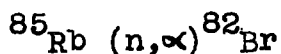
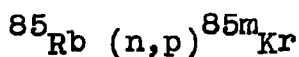
$E_n = 14.7$ MeV

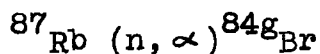
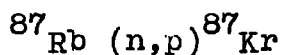
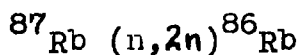
is doubted whether an accuracy of much better than $\pm 20\%$ can be claimed for the (n,p) and (n,2n) cross-sections. Even with this revised accuracy the $^{69}\text{Ga}(n,p)^{69\text{m}}\text{Zn}$ cross-section value of 18.2 ± 3.6 mb disagrees markedly with the previous result of Bormann et al²⁹⁾ (42 ± 3 mb at 15.2 MeV). Again it is possible, although somewhat unlikely, that the excitation function is varying rapidly in this energy region.

The result for the $^{69}\text{Ga}(n,2n)^{68}\text{Ga}$ cross-section (621 ± 124 mb) agrees most closely with the work of Paul and Clarke⁵⁸⁾, who obtain a value of 552 ± 155 mb at 14.5 MeV. Also there is agreement with the result of 735 ± 44 mb obtained by Cevolani⁵⁹⁾ at 14.1 MeV. Taken together, these results suggest that the cross-section varies little over this energy range. Contrary to this trend however, Rayburn⁶⁰⁾ and Khurana⁶¹⁾ quote the higher values:- 923 ± 70 mb at 14.4 MeV and 1070 ± 107 mb at 14.8 MeV respectively.

3. The reactions of rubidium.

The cross-sections of the following reactions of rubidium were measured:-





The description of the study of this element is divided into two sections. Initially, the work involving the isolation of the (n,α) bromine activities is covered, followed by the experiments to determine the (n,p) krypton production cross-sections.

3a. The measurement of the bromine activities.

Throughout the work, 99.9% pure rubidium nitrate was used as the sample material, approximately 1 gm of this being mixed with iron granules. After dissolution of the irradiated salt in a solution containing bromate carrier, a solvent extraction procedure was employed to separate the bromine, and solid sources of silver bromide were prepared for counting. Prior to use, the rubidium nitrate was dried in a desiccator (silica gel). Irradiations of one hour were carried out, the relative neutron flux being monitored at five minute intervals. The results obtained for the

(n,α) cross-sections disagreed markedly with those of previous workers⁶²) and prompted further tests on the chemical exchange between the bromine activities and the carrier, using available ⁸²Br as the tracer. Also the possibility of bromine escaping from the sample material and reacting with the iron present was not unreasonable in view of the oxidising nature of the medium. An investigation was carried out to ascertain whether or not this was taking place.

Using information available in the Nuclear Science Series^{63,64}) of volumes, the following separation scheme was developed.

The chemical separation procedure.

Step 1 After weighing, the rubidium nitrate was dissolved in 10 ml of bromate carrier solution and hydrogen sulphide was passed for about three minutes to reduce the bromate to bromide. Excess of the gas was then removed by boiling and 1 ml of 6 N HNO₃ added to the solution, followed by the dropwise addition of KMnO₄ until a pink colouration just persisted. The liberated bromine was extracted into 30 ml of carbon tetrachloride in three equal portions. At this stage a precipitate of sulphur and maganese dioxide was present in the aqueous layer, but this did not interfere

with the extraction.

Step 2. The combined carbon tetrachloride extract was washed with 10 ml of H_2O containing 1 ml of 6N HNO_3 and two drops of saturated $KMnO_4$. Bromine was back-extracted from the organic layer into a sodium hydrogen sulphite solution consisting of 5 drops of 1 M $NaHSO_3$ in 10 ml H_2O .

Step 3. To the aqueous extract was added 1 ml 6M HNO_3 and the mixture boiled to remove SO_2 . After cooling slightly, 2 ml of 0.1N $AgNO_3$ was added dropwise with stirring to precipitate $AgBr$ and the solution was allowed to digest for one minute. The precipitate was filtered and washed with 15 ml of H_2O followed by 15 ml of ethanol. A source was prepared for end-window counting and dried at $80^\circ C$. The source was weighed immediately before counting, which could be started after approximately one hour.

In order to avoid as much photodecomposition of the silver bromide sources as possible the last precipitation step was carried out under subdued lighting conditions and the sources were stored in the dark. The elimination of the krypton (n,p) products was expected to occur largely in step 1 and there was no evidence that the sources became contaminated with the activities.

The preparation of bromate carrier solution.

The solution was prepared by dissolving approximately 1 gm of dried (150°C) "Analar" potassium bromate in 500 ml H₂O to give a solution with a concentration of ~ 1 mg Br/ml. No chemical estimation was made since the reagent was of primary standard quality.

The determination of the chemical yield of bromine.

A titration method was used to determine the silver in the bromide sources to provide a check on the chemical yield of bromine previously determined by weighing. According to Flascha^k and Huditz⁶⁵) nickel ions are displaced quantitatively from potassium cyanonickelate (II) by silver ions in ammoniacal solution. The reaction can be represented:-



Using murexide as the indicator, the nickel can then be determined by titration against EDTA. Potassium cyanonickelate monohydrate was prepared in the laboratory⁶⁶) and the following procedure used to determine the silver bromide sources:-

Step 1. The AgBr source was treated with 20 ml of boiling 8N HNO₃ to ensure the complete dissolution of the small amount

of silver produced by unavoidable photo-decomposition. After dilution of the initial solution to 100 ml, 0.1M KBr was added dropwise to reprecipitate the bromide and 30 minutes were allowed for digestion. The solid material, which included the finely divided remains of the glass fibre disc, was filtered off and washed with a little 0.5N HNO_3 .

Step 2. After treatment of the solid residue with a solution of 1 gm of $\text{K}_2(\text{Ni}(\text{CN})_4) \cdot \text{H}_2\text{O}$ in 20 ml 9 N NH_4OH the resulting solution was made up to 50 ml in a graduated flask. 10 ml aliquots were diluted to 30 ml, 0.25 gm of murexide indicator (1 part ammonium purpureate: 100 parts "Analar" NaCl) added and the mixture titrated against 0.001M EDTA disodium salt from a semimicro burette. The end-point was indicated by the colour change from yellow to purple. The titrations were repeated in triplicate.

The chemical yields of bromine obtained by titration agreed to within 1% with those previously obtained by weighing.

Observations.

The decay of the bromide sources was followed in the end-window counter for a period of several days in each case. Two activities with half-lives of 32 minutes and 36 hours were resolved, corresponding to $^{84}\text{g}_{\text{Br}}$ and ^{82}Br respectively. Due to the time taken to prepare the sources, the 6 minute

^{84m}Br , also from the $^{87}\text{Rb}(n, \alpha)$ reaction, was not observed. There was no definite indication of the presence of 2.3 hour ^{83}Br from the $^{87}\text{Rb}((n, \alpha n) + (n, n\alpha))$ reaction, which was expected to occur as an intermediate component of the decay curves. In order to determine an upper limit for this reaction cross-section, the maximum value of detectable ^{83}Br activity was estimated by inspection of the decay curves. A hypothetical 2.3 hour activity was added, in increasing proportions, to the 32 minute component until a noticeable change in the slope of the curve was produced. It was found that a contribution equivalent to 2% of the initial ^{84g}Br activity was required and this was taken as the maximum value of ^{83}Br in each case, for the purposes of calculation.

Discussion.

The results are presented in the following tables (24 to 26), the errors quoted being the standard deviations from the mean. The upper limit of < 0.052 mb for the $^{87}\text{Rb}((n, \alpha n) + (n, n\alpha))^{83}\text{Br}$ reaction is somewhat lower than that of < 1.5 mb recently set by Bramlitt⁴⁷), but it is in support of his result. Levkovskii⁶⁷) has given a value of 0.39 for the cross-section ratio $^{85}\text{Rb}(n, \alpha)^{82}\text{Br} / ^{87}\text{Rb}(n, \alpha)^{84g}\text{Br}$ and this agrees with the present results (0.25 ± 0.24) when the large experimental error is taken

TABLE 24

The Upper limit of the $^{87}\text{Rb}(\text{ncn}) + (\text{ncn})^{83}\text{Br}$ reaction

Expt. No.	No. of ^{87}Rb nuclei	A_0 obs	cpm	Chem Yield	A_0 abs	dpm	$(X \times \lambda_p)$	σ mb
13	1.166×10^{21}	3.64×10	3.64×10	0.490	2.08×10^2	2.08×10^2	580.9	0.064
14	1.490×10^{21}	7.20	7.20×10	0.513	3.93×10^2	3.93×10^2	1050	0.053
15	1.073×10^{21}	3.50	3.50×10	0.610	1.61×10^2	1.61×10^2	592.9	0.052
16	2.105×10^{21}	3.80	3.80×10	0.452	2.35×10^2	2.35×10^2	381.4	0.053

$$t_{\frac{1}{2}}^{83}\text{Br} = 2.3 \text{ hours}$$

$$C^{83}\text{Br} = 0.357$$

$$\sigma < \underline{0.052 \text{ mb}}$$

TABLE 25

The ^{85}Rb (n, α) ^{82}Br cross-section

Expt. No.	No. of ^{85}Rb nuclei	A_0 cpm _{obs}	Counting Eff.	Chem. Yield	A_0 dpm _{abs}	($\Sigma x \lambda_p$)	σ mb
13	3.020×10^{21}	4.00×10^2	0.279	0.490	2.93×10^3	44.69	4.54
14	2.978×10^{21}	7.15×10^2	0.279	0.513	5.00×10^3	75.73	4.67
15	2.778×10^{21}	4.25×10^2	0.252	0.610	2.76×10^3	43.74	4.64
16	5.453×10^{21}	3.95×10^2	0.279	0.452	3.13×10^3	28.46	3.64

$t_{1/2}^{82}\text{Br} = 36$ hours.

Mean value $\sigma = 4.37 + 0.25$ mb

TABLE 26

The $^{87}\text{Rb}(n, \infty) ^{84}\text{gBr}$ cross section.

Expt. No.	No. of ^{87}Rb nuclei	A_0 cpm obs	Chem. Yield	A_0 dpm abs	$(Xx\lambda p)$	σ mb
13	1.166×10^{21}	1.82×10^3	0.490	1.03×10^4	1575	1.17
14	1.149×10^{21}	3.60×10^3	0.513	1.95×10^4	3076	1.16
15	1.073×10^{21}	1.75×10^3	0.610	7.99×10^3	1601	0.95
16	2.105×10^{21}	1.90×10^3	0.452	1.17×10^4	1001	1.00

$t_{1/2}^{84\text{gBr}} = 32$ minutes

$C^{82\text{Br}} = 0.359$

Mean value $\sigma = 1.07 + 0.01$ mb

into account.

A comparison of the results for both the (n, α) cross-sections with those available by other authors at the time of the work shows marked disagreement. For the $^{85}\text{Rb}(n, \alpha)^{82}\text{Br}$ cross-section Poularikas and Gardner⁶⁸⁾ give a value of 145 mb at 14.7 MeV, while Strohal et al⁶²⁾ quote $142 \pm$ mb at 14.6 MeV. In contrast, the observed value is 4.37 ± 0.25 mb. Similarly for the $^{87}\text{Rb}(n, \alpha)^{84g}\text{Br}$ reaction Strohal et al obtain 59 ± 12 mb, altogether different from the 1.07 ± 0.01 mb measured. These large discrepancies cannot be accounted for in the case of the work of Strohal et al, by differences in the values they took for the $^{27}\text{Al}(n, \alpha)^{24}\text{Na}$ and $^{56}\text{Fe}(n, p)^{56}\text{Mn}$ reference reaction cross-sections or by the slight difference in neutron energy. Lack of more precise information about their experiments prevents further detailed discussion of possible causes and the only conclusion which can be reached is that they have made some systematic error in the assessment of their results. It was in view of these large discrepancies that the decision was taken to test the validity of the present methods of measuring the (n, α) cross-sections. The chemical exchange of active bromine with the carrier was investigated and shown to be satisfactory. The possibility that substantial quantities of bromine were being lost from the rubidium

nitrate and reacting with the iron granules was eliminated. Finally, a comparison of the $^{87}\text{Rb}(n,2n)^{86}\text{Rb}$ and $^{85}\text{Rb}(n,\alpha)^{82}\text{Br}$ cross-sections was made by counting irradiated rubidium nitrate directly and the ratio found to be of the expected order.

Sometime after this work was completed, König⁶⁹⁾ published his result for the total (n,α) cross-section in natural rubidium, measured by secondary particle methods. He obtained a value of 9.4 ± 1.4 mb at 14.8 MeV which is in much closer agreement with the present work than the results of Strohal et al⁶²⁾ and Poularikas and Gardner⁶⁸⁾.

The chemical exchange of the bromine activities.

^{82}Br was conveniently available in a "carrier-free" form and was used to test the exchange of bromine in the chemical procedure previously described. A sample of ^{82}Br was initially counted and then subjected to the chemical separation procedure. It was then recounted in the same form as before and the yield of bromine calculated. This result was compared with that subsequently determined by weighing.

5 ml of "Analar" ethyl bromide was irradiated with thermal neutrons near a 1 curie Ra/Be source for approximately 17 hours. The resulting (n,γ) bromine activities

^{80m}Br (4.5 hour), ^{80g}Br (18 min.) and ^{82}Br (36 hour), were extracted into 4 ml of 1 N NaHSO_3 solution. 1 ml of 6 N HNO_3 was added to the aqueous extract and the mixture heated to boiling to expel SO_2 and EtBr . The volume of the solution was adjusted to approximately 4 ml and two 2 ml aliquots were taken and counted in the 2" x 1 $\frac{3}{4}$ " NaI(Tl) well crystal. In view of the low specific activity obtained, time could not be afforded for the shorter lived activities to decay and by suitably adjusting the discriminator bias setting on the single channel analyser unit, only ^{82}Br , which decays almost entirely via a 0.77 MeV gamma transition, was counted. After initial measurements, one of the samples was added to 10 ml of the bromate carrier solution and the chemical procedure carried through until the back-extraction step for bromine had been completed. The volume of the bromide solution was adjusted to 2 ml and it was again counted in the well crystal. The untreated aliquot of ^{82}Br was counted at intervals to check the half-life and to provide a reference. Decay curves for the two aliquots were plotted and the chemical yield calculated from the decrease in activity of the treated aliquot. After counting, the volume of the treated solution was adjusted to 10 ml, Ag Br precipitated according to the chemical procedure and the yield of bromine determined by weighing.

The results were as follows:-

<u>Yield of bromine by counting</u>	<u>Yield of bromine by weighing</u>
-------------------------------------	-------------------------------------

62.8 ± 5.0%

66.5 ± 0.6%

The errors given are the estimated experimental errors and the large value in the case of the counting result was mainly due to the rather low specific activity obtained. (Approximately 100 cpm/ml of ^{82}Br solution initially). From the results it was assumed that within the limits of experimental error the exchange between bromide and bromate ions was complete. Based on this evidence it was concluded that it was not unreasonable to assume the exchange between the bromine activities in rubidium nitrate and the bromate carrier also to be complete.

The reaction of product bromine activities with the iron reference material.

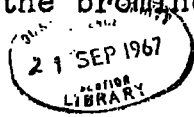
To ascertain whether or not bromine escaping from the rubidium nitrate was reacting with the iron granules making up the sample, the following experiment was carried out. Essentially, bromide carrier was added to the solution used to dissolve the iron and silver bromide precipitated and counted in the end-window counter. Although in previous irradiations no residual activity attributable to ^{82}Br had been noticed in the iron solutions, this procedure provided

a more sensitive test.

A sample consisting of 2 gm of RbNO_3 and 0.5 gm of iron granules was irradiated for one hour. After separation, the iron was dissolved in 20 ml of 5 M H_2SO_4 containing 0.042 gm $\text{MnSO}_4 \cdot 4\text{H}_2\text{O}$ and approximately 0.012 gm KBr. The strongly oxidising mixture which was normally used to dissolve the iron was avoided in this particular experiment to reduce the possibility of losing bromine by volatilisation. AgBr was precipitated from the solution by the addition of 2 ml of 0.1N AgNO_3 followed by 5 ml of 6N HNO_3 and the gentle application of heat. After filtration and thorough washing a source was prepared and counted in the end-window counter. Within the limits of experimental error, no activity was observed, indicating that the reaction between the bromine activities and the iron in the sample was negligibly small.

The measurement of the $^{87}\text{Rb}(n,2n)^{86}\text{Rb}$ and $^{85}\text{Rb}(n,\alpha)^{82}\text{Br}$ cross-sections without chemical separation.

An experiment was carried out to compare the $^{87}\text{Rb}(n,2n)^{86}\text{Rb}$ and $^{85}\text{Rb}(n,\alpha)^{82}\text{Br}$ cross sections without chemical separation of the product activities. The point of the experiment was to demonstrate that no serious systematic errors were present in the methods previously used to determine the bromine production cross-sections.



Strohal et al⁶²) had included a value of 838 ± 136 mb for the $(n, 2n)$ cross-section in their study of rubidium and it was of interest to see if the relative magnitudes of this, and the (n, α) cross-section given by them could be reproduced.

A sample of powdered RbNO_3 and iron granules was irradiated for one hour and, after separation, approximately 100 mg of the salt was taken and a source prepared for end-window counting. The decay of the source was followed for some 36 days and after the shorter lived activities had decayed completely a residual activity with a half-life of 19 days was observed. The good correspondence of this half-life with the accepted value for ^{86}Rb was somewhat unexpected since it was thought that there would have been a noticeable contribution to the residual component by the 33 day ^{84}Rb which decays to the extent of about 20% by positron emission. A 36 hour activity due to ^{82}Br could not be resolved but an initial maximum value, found to be 10% of the initial ^{86}Rb activity, was estimated by inspection of the decay curve. The absolute activities of ^{86}Rb and ^{82}Br were calculated by correcting for absorption, backscattering and geometry using the methods of Burt³⁸) and Gleason et al³⁷). In the case of ^{86}Rb the β^- -decay was taken to be 91% via 1.77 MeV and 9% via 0.696 MeV, transitions.

The results are given in the following table together with the estimated experimental error for the (n,2n) cross-section.

TABLE Comparison of the $^{87}\text{Rb}(n,2n)^{86}\text{Rb}$ and $^{85}\text{Rb}(n,\alpha)^{82}\text{Br}$ cross-sections.

Reaction	$^{87}\text{Rb}(n,2n)^{86}\text{Rb}$	$^{85}\text{Rb}(n,\alpha)^{82}\text{Br}$	$^{56}\text{Fe}(np)^{56}\text{Mn}$ (reference)
No. of target nuclei	1.138×10^{20}	2.959×10^{20}	3.920×10^{21}
A_{obs} cpm	1.04×10^3	1.04×10^2 (max.)	7.10×10^4
Calculated efficiency	0.275	0.092	0.0813
A_{abs} dpm	3.78×10^3	1.14×10^3	1.05×10^6
$(X \times \lambda_p)$	2.097	25.91	321.4
σ mb	1860 ± 372	17.4	97.7 (reference)

Despite the inaccuracies in the experimental method, the relative values of the two cross-sections are of the order expected in view of the previous determinations. Certainly the upper limit for the (n, α) reaction of some 17 mb would indicate that the value of 142 mb given by Strohal et al⁶²⁾ is erroneous, and add weight to the more accurate determination made in this work. Also the $(n, 2n)$ cross-section of 1860 ± 372 mb would suggest that their value (838 ± 136 mb) is, for some reason, too low.

3b. The measurement of the Krypton activities.

From the result obtained for the upper limit of the $^{87}\text{Rb}((n, \alpha n) + (n, n \alpha))^{83}\text{Br}$ cross-section using the silver bromide separation, it was calculated that it should be possible to observe the $^{83\text{m}}\text{Kr}$ daughter of ^{83}Br , provided that the cross-section was not much less than half this value. The isolation and detection of $^{83\text{m}}\text{Kr}$ would also provide definite evidence for the presence of the $(n, \alpha n) + (n, n \alpha)$ product. The 0.0093 and 0.03 MeV gamma transitions of $^{83\text{m}}\text{Kr}$ are strongly converted and the nuclide could conveniently be counted in a Geiger tube where it formed part of the gas filling.

Accordingly, a method was developed whereby the krypton products were swept from a solution of irradiated rubidium

nitrate by a stream of hydrogen gas. After purification from oxygen and water vapour, the krypton activities were introduced into a Geiger tube for counting. As a result of the work it was possible to determine values for the $Rb(n,p)$ cross-sections and demonstrate the absence of ^{83m}Kr in detectable quantities.

The apparatus used for the isolation of krypton

A diagram of the vacuum line used to separate and purify the krypton is shown in fig.26. The vacuum was maintained by a three stage mercury diffusion pump backed by an Edward's mechanical pump type 2S20B. Pressures of better than 10^{-3} mm Hg could be obtained and were monitored with a Mcleod gauge (Vacustat 2G) connected to the main line. Hydrogen gas was admitted to the solution vessel through a tube terminated at its external end with a porosity four glass sintered disc, and at its internal end with a similar disc of porosity three to act as a bubbler. The external end of the tube dipped into a mercury reservoir, the gas being bubbled into the immersed end through a capillary tube. It was essential that this whole assembly was cleaned using dilute nitric acid and water, and thoroughly dried after each run, to prevent mercury passing through the external sintered disc, while under vacuum.

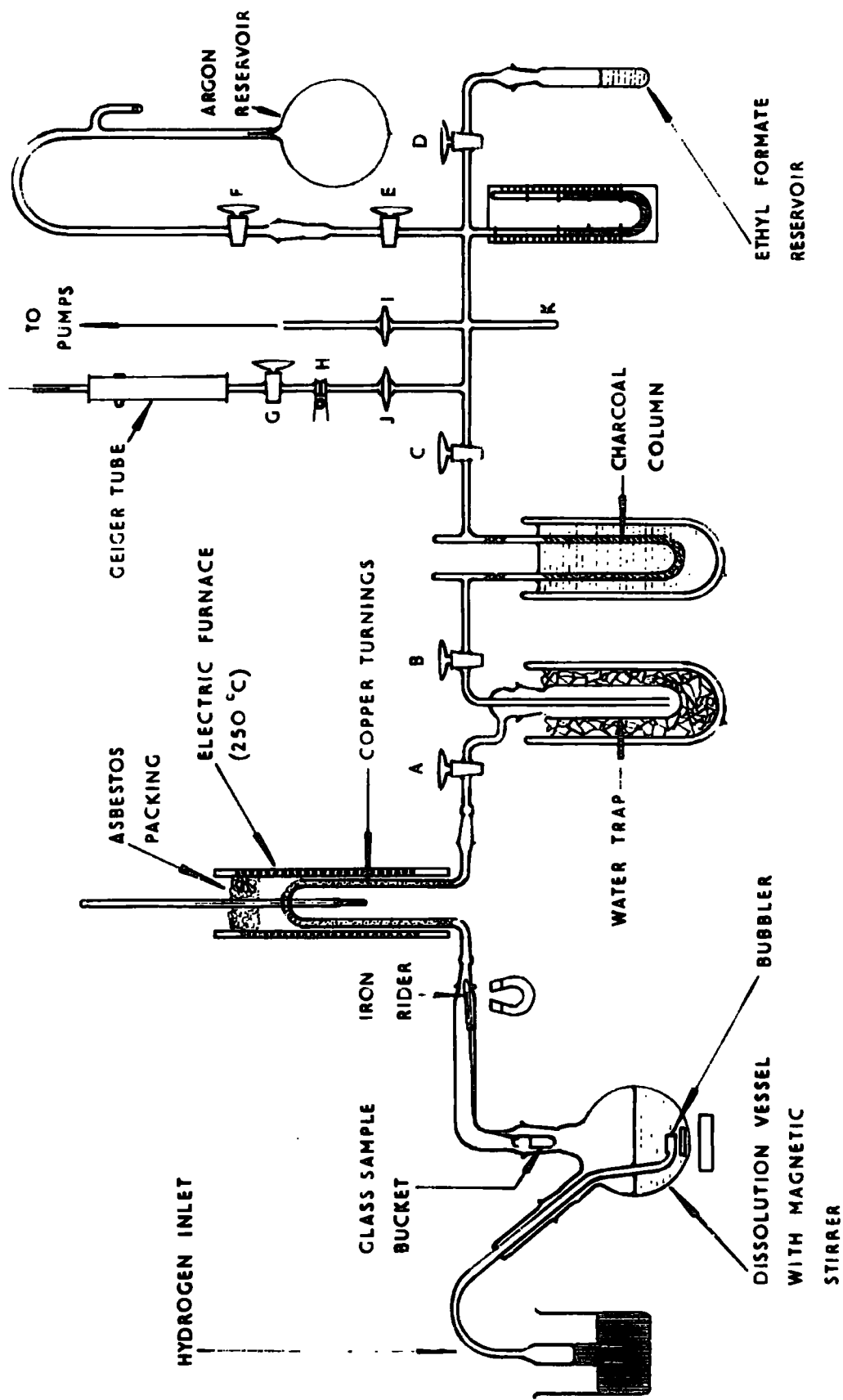


FIG. 24. DIAGRAM OF THE VACUUM APPARATUS USED FOR THE ISOLATION OF KRYPTON.

Initially, a suitable sintered disc, which contained no large holes, had to be selected by trial and error.

The weighed sample of rubidium nitrate was placed in a perforated glass bucket which could be lowered into the solution by means of an iron rider and a magnet. A glass-fibre string was used to attach the bucket to the rider.

To remove traces of oxygen, the mixture of gases swept from the solution was passed over fine copper turnings heated to 250°C in an electric furnace. By oxidation and subsequent reduction in a stream ^{of} hydrogen a fresh surface was prepared on the copper turnings prior to their introduction into the apparatus. Water vapour was condensed in the solid CO_2 trap and the remaining krypton and a substantial part of the hydrogen carrier gas were then adsorbed onto active charcoal cooled to -196°C in liquid nitrogen. After removal of the hydrogen, the krypton was desorbed by gentle warming and allowed to mix with the counter gas-filling.

A mixture of argon and ethyl formate vapour was used to fill the counter. Dissolved gases were removed from the ethyl formate before use by opening the reservoir to the pumps and allowing the liquid to boil off until its volume had been reduced by approximately one third. When filling

the counter the pressure of each gas was read off on a mercury manometer.

In initial tests, the counters were filled with various mixtures at slightly different pressures (in the region of a total pressure of 10 cm Hg) to ascertain which proportions resulted in the largest plateau. Each counter was attached to the line by a hemispherical joint (H) and evacuated by pumping for several hours until a hard vacuum was obtained. Leaks were tested for by closing the tap to the pumps and leaving the counter connected to the manometer for a period of several hours. To facilitate mixing of the ethyl formate and argon when filling the counters, a cold finger (K) was alternately cooled and allowed to warm up four times using liquid nitrogen. The optimum mixture was found to be 9 cm Hg of argon and 1 cm Hg of ethyl formate which gave a plateau some 120 volts in length, at an EHT voltage in the region of 1000v. Normally, the counters when not in use, were kept either evacuated or filled with the gas mixture.

The procedure for the isolation of krypton.

Samples consisting of 2 gm RbNO_3 and 0.5 gm iron granules were irradiated for periods of 40 to 90 minutes,

depending upon the age of the tritium target. After separation from the iron, the rubidium nitrate was weighed and placed in the glass bucket. The dissolving solution, which consisted of 10 ml of potassium bromide holdback carrier (~ 1 mg Br/ml) and 1 gm hydroxylamine sulphate in 100 ml H_2O , was then degassed by passing a steady stream of hydrogen through it with the pumps connected. Hydroxylamine sulphate was introduced into the solution to maintain reducing conditions and decrease the chance of free bromine being swept into the counter. After five minutes the flow of hydrogen was stopped and when all the gas remaining in the inlet had been exhausted, the connection to the pumps was closed. The tap C, isolating the counter-filling section of the line from the gas-purification section, was also closed. With the furnace and the cold traps at their working temperatures, the sample was dissolved with the aid of the magnetic stirrer. A steady stream of hydrogen was then admitted for four minutes until the pressure in the line approached that of the atmosphere as indicated by the decrease in the rate at which the gas was taken up. After allowing approximately a minute for adsorption, the tap B was closed and the charcoal column connected to the pumps by opening taps C and I to remove excess hydrogen. The pumps were then disconnected and tap B again opened to

admit more of the gas mixture to the charcoal trap. A minute was again allowed for adsorption and the excess hydrogen then pumped away as before. This cycle of operations was repeated from six to eight times until the pressure in the dissolving vessel had been considerably reduced. Two further sweeps of the solution were performed and the tap B was finally closed, the relative time of this last operation being noted.

The next step was to remove the excess hydrogen adsorbed on the charcoal. With a CO_2 /acetone eutectic mixture replacing the liquid nitrogen, the charcoal column was allowed to warm up to approximately -70°C . The desorbed hydrogen was pumped away until a good vacuum had again been obtained as indicated by the manometer. At this stage the counter was connected to the line and also evacuated. After pumping had been stopped, the charcoal column was finally allowed to warm up to room temperature to desorb the krypton. A small pressure of hydrogen, in the region of a few mm of Hg was released from the charcoal but was insufficient to interfere with the working of the counter. The desorption of krypton was encouraged by cooling the cold finger K in liquid nitrogen. After time had been allowed for desorption, 1 cm of ethyl formate vapour and 9 cm argon were admitted to the line. For a period of approximately twenty minutes

the gases were mixed by intermittently cooling the cold finger K in liquid nitrogen. After allowing equilibrium pressure to finally be attained at room temperature the counter was removed and the decay of the krypton (n,p) reaction products followed. Counting was started approximately 80 minutes after the end of each irradiation.

The residual gases in the counter-filling section were removed by pumping until a hard vacuum had been obtained. The second counter was then attached and evacuated. A period of four hours was allowed to elapse for ^{83m}Kr , the daughter of ^{83}Br , to grow into the rubidium nitrate solution which was again swept three times with hydrogen in the same way as before. A note was made of the times when the first sweep was started and when the tap B was closed, isolating the gases on the charcoal column. In this case, Geiger counting was started approximately five hours after the end of each irradiation.

Observations.

The decay of the activities isolated in the first counter was followed for a period of approximately two days until the background level had been reached. Two activities were resolved, with half-lives of 78 minutes and 4.5 hours,

corresponding respectively to ^{87}Kr and $^{85\text{m}}\text{Kr}$. A long lived residual activity due to $^{85\text{g}}\text{Kr}$ (10.6 years) was not observed. There was no evidence of the presence of $^{83\text{m}}\text{Kr}$ which would have grown into the sample during irradiation and been removed together with the (n,p) products.

No activity was observed in the second counter which it was thought might possibly contain a detectable quantity of $^{83\text{m}}\text{Kr}$. This precluded a definitive measurement of the ((n, α n) + (n,n α)) cross-section but did provide support for the value of the upper limit determined previously by the separation of bromine. Although an estimation of an upper limit from the result was thought to be of little value in view of the large uncertainties of the method, it was concluded that the procedure used to isolate the krypton (n,p) products was essentially valid, since any krypton remaining in the solution after the first sweeps would have been detected in the second counter.

Discussion.

As no results for the $^{87}\text{Rb}(n,p)^{87}\text{K}$ and $^{85}\text{Rb}(n,p)^{85\text{m}}\text{K}$ cross-sections were available in the literature, it was decided that an estimate of the values from the data obtained should be made. It was realised that the accuracy would be poor due to the large uncertainty in the chemical yield

of the products. This quantity was determined by finding the ratio of the active counter volume to the total volume of the counter and vacuum line in which the gases were finally equilibrated after mixing. The error in this estimation was calculated to be $\pm 30\%$. Other sources of error were considered to be negligibly small in relation to this value. Several assumptions were also made in evaluating the results. All the krypton was assumed to be removed from the solution and completely adsorbed onto the charcoal. Similarly, all the krypton was subsequently desorbed and mixed homogeneously with the counter gas-filling. The end and wall effects in the counter were taken to be negligible and the counting efficiency was assumed to be 100% for β^- -events occurring within the measured active volume.

^{87}Kr decays completely by β^- -transitions and its counting efficiency was taken as 100%. The efficiency of $^{85\text{m}}\text{Kr}$ was calculated by taking into account the conversion coefficient of the 0.305 MeV γ -transition (19%) as well as the 81% abundant 0.824 MeV β^- -transition. The overall efficiency was calculated to be 89% on the assumption that no gammas were recorded.

Tables 27 to 29 show the results together with the estimated experimental errors. The tolerable agreement of

TABLE 27

The $^{56}\text{Fe}(n,p)^{56}\text{Mn}$ reference reaction

Expt. No.	No. of ^{56}Fe nuclei	A_{obs} cpm	A_{obs} dpm	$(X_T \times \lambda_{\text{pr}})$
17	4.527×10^{21}	7.60×10^4	1.15×10^6	485.2
18	4.457×10^{21}	4.75×10^3	7.17×10^4	919.9
19	4.888×10^{21}	1.54×10^5	2.32×10^6	869.3

^{56}Mn $t_{1/2} = 2.58$ hours.

σ $^{56}\text{Mn} = 0.0795$

$E_n = 14.7$ MeV

σ $^{56}\text{Fe}(n,p)^{56}\text{Mn} = 97.7$ mb.

TABLE 28

The $^{85}\text{Rb}(n,p)^{85\text{m}}\text{Kr}$ cross section

Expt. No.	No. of ^{85}Rb nuclei	A_{obs} cpm	A_{obs} dpm	$(Xx \lambda p)$	σ mb
17	6.069×10^{21}	1.42×10^4	2.79×10^4	296.2	2.90
18	5.894×10^{21}	6.10×10^2	1.20×10^3	585.9	1.94
19	5.996×10^{21}	2.10×10^4	4.13×10^4	518.0	2.38

$t_{1/2}^{85\text{m}}\text{Kr} = 4.5$ hours

$C^{85\text{m}}\text{Kr} = 0.89$

Chem. yield = 0.572

Mean value $\sigma = 2.41 + 0.72$ mb.

TABLE 29

The $^{87}\text{Rb}(n,p)^{87}\text{Kr}$ cross section.

Expt. No.	No. of ^{87}Rb nuclei	A_{obs} cpm	A_{obs} dpm	$(Xx \lambda p)$	σ mb
17	2.342×10^{21}	9.10×10^4	1.59×10^5	832.9	15.2
18	2.275×10^{21}	3.75×10^3	6.56×10^3	1439	11.2
19	2.314×10^{21}	1.52×10^5	2.66×10^5	1574	13.1

$t_{1/2}^{87}\text{Kr} = 78$ minutes

C $^{87}\text{Kr} = 1$

Chem. Yield = 0.572

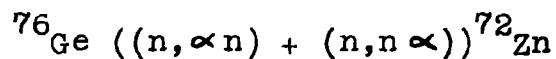
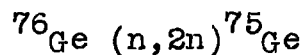
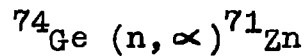
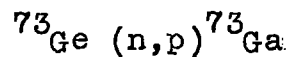
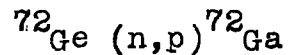
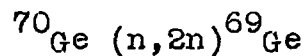
Mean value $\sigma = 13.2 \pm 4.0$ mb

the values for different determinations would indicate that the reproducibility of the method was not altogether unreasonable. For the $^{85}\text{Rb}(n,p)^{85m}\text{K}$ cross-section, the value of 2.4 ± 0.72 mb is a lower limit since only the meta-stable isomer was observed.

A more detailed discussion of the results in relation to the trends observed for (n,p) values is to be found in the final chapter.

4. The reactions of germanium.

The cross-sections of the following reactions occurring in germanium were measured at 14.8 MeV :-



Samples consisting of 99.999% pure germanium powder, mixed with iron granules, were irradiated for periods of one hour, the relative neutron flux being monitored at five minute intervals. The germanium was dissolved in an oxidising, alkaline, solution containing zinc and gallium carriers. After separation of the elements, solid sources of germanium sulphide, gallium 8 - hydroxyquinolate and zinc mercuri-thiocyanate were respectively prepared for counting.

The preparation and determination of the zinc carrier solution.

Approximately 2 gms. of "Analar" $\text{ZnSO}_4 \cdot 7\text{H}_2\text{O}$ were dissolved to give a solution with a concentration of about 1 mg Zn/ml. The solution was determined gravimetrically by precipitating Zn ($\text{Hg}(\text{SCN})_4$), using the following procedure⁷⁰:-

A 50 ml aliquot of the carrier solution was treated with 1 drop of 5N HNO_3 and diluted to 100 ml. While stirring vigorously the mercuric chloride - potassium thiocyanate reagent (27.1 gm HgCl_2 + 42.6 gm KSCN/litre) was added dropwise until a precipitate began to form. With continued stirring a further 10 ml of the reagent was slowly added and the mixture was then left to stand overnight to ensure complete precipitation. The precipitate was then

filtered by decantation at the pump, using a sintered glass crucible of porosity 4 and washed twice by decantation with a dilute solution of the precipitating agent (20 ml reagent diluted to 1 litre). After finally transferring all the precipitate to the crucible, it was further washed with a few mls. of the diluted precipitating agent and sucked as dry as possible. Drying was carried out at 110°C to constant weight, the precipitate being weighed as $\text{Zn}((\text{Hg}(\text{SCN})_4)$.

The washing solution was used to avoid loss of the precipitate, due to its slight solubility in the usual washing agents, H_2O , EtOH and Et_2O . Since some 380 mg of precipitate was being weighed the error introduced by the reagent remaining after washing (approximately 2.5 mg) was within the required tolerance. The results of three determinations were found to agree to within 1% and a blank experiment confirmed that no precipitation occurred in the absence of zinc.

The preparation and determination of the gallium carrier solution.

0.5 gm of 99.99% pure gallium metal was dissolved in 10 ml of aqua regia by boiling. The solution was evaporated to near dryness over a water bath, a further 10 ml of concentrated HCl added and the evaporation repeated. The

residue was then dissolved in H_2O to give a solution containing approximately 1 mg Ga/ml.

The concentration of gallium was determined gravimetrically by precipitation of the 8-hydroxyquinoline derivative ⁷¹.

25 ml aliquots of the carrier were taken and 2 gm of solid sodium acetate, 2 ml of 5N NH_4OH and 175 ml of H_2O added. With the solution at 70 - 80°C, 20 ml of a 1% solution of 8-hydroxyquinoline in absolute ethanol was added and the solution made acidic by the addition of 4 ml of 5N HCl. The yellow precipitate was digested on a water bath for one hour and the solution finally cooled. After filtration using a sintered glass crucible and washing with cold H_2O , the precipitate was dried at 120°C and weighed as $Ga(C_9H_6NO)_3$. Three determinations gave results in agreement to within 1.1% and a blank determination in the absence of gallium showed no sign of precipitation.

The chemical separation procedure.

Difficulty was experienced in selecting a suitable medium in which to dissolve the germanium reliably and rapidly. Initially, boiling with concentrated HCl was tried, this method seeming attractive as there was the

possibility of removing the bulk of the germanium as the volatile tetrachloride. It was found however, that a considerable quantity of germanium dioxide was precipitated during this process due to the hydrolysis of the tetrachloride, presumably by the water present in the concentrated acid, and the method was considered to be unsuitable.

Attempts to dissolve the metal in a 3% solution of hydrogen peroxide also met with little success. Clear solutions could be obtained, but only after the mixture had been boiled for several hours and allowed to stand overnight. The reagent finally adopted was a strongly alkaline solution of hydrogen peroxide, in which the metal could be dissolved after boiling for about twenty minutes. It was found that the concentration of the peroxide was critical and this reagent was added dropwise as the dissolution proceeded, to avoid an excess, which was liable to cause a slight turbidity due to the precipitation of germanium dioxide. Clear solutions could be obtained providing that care was exercised in the addition of the peroxide. An excess of this reagent was also undesirable with regard to the following step in the chemical procedure involving the passage of H_2S .

Other germanium compounds were considered for irradiation. The aged dioxide was found to be extremely insoluble.

able in the solution mentioned. Only when the compound had been freshly precipitated and was still damp, could it be dissolved, and it was therefore regarded as an unsuitable sample material.

Another possibility was sodium metagermanate, $\text{Na}_2 \text{Ge O}_3 \cdot 7\text{H}_2\text{O}$, which could be obtained commercially. This was soluble in water but was undesirable as its chemical composition was ill-defined and it was not available in a high state of purity.

The chemical separation procedure used was based upon information available in the Nuclear Science Series of volumes^{72,49,50}. The bulk of the germanium was initially removed by precipitation, the zinc and gallium being subsequently separated by precipitation and solvent extraction respectively. Chemical yields were determined by weighing, all the source materials being of gravimetric quality.

Step 1 After weighing, the germanium was dissolved in a boiling solution containing 10 ml each of the zinc and gallium carriers, 15 ml of 6M NaOH and 2 drops of 100 volume hydrogen peroxide. Further additions of 20 volume peroxide solution were made dropwise during the boiling, until all the metal had dissolved. 25 ml of 6N HCl was then added to the solution and the mixture boiled for a further ten

minutes to destroy as much of the excess peroxide as possible. H_2S was passed through the hot solution to precipitate GeS_2 which was filtered at the pump. (2 x Whatman 44) The filtrate was tested for complete precipitation and more H_2S passed if necessary. The last traces of GeS_2 in the filtrate were removed by boiling the suspension with a Whatman tablet and filtering through a porosity 4 sintered glass disc. The filtrate was retained. To prepare a solid germanium source for counting, a slurry of the appropriate quantity of GeS_2 in 40 ml H_2O was taken and filtered. The mounted precipitate was washed with a further 10 ml H_2O followed by 10 ml methyl alcohol. After sucking dry the source was finally dried at 110°C and counted.

Step 2. The filtrate from step 1 was boiled to remove H_2S and made 6N with respect to HCl. After cooling, the gallium was extracted into 60 ml diethyl ether in three equal portions and both phases were retained. The ether phase was washed with 20 ml of 6N HCl and the gallium was back-extracted into 40 ml H_2O in two equal portions. The ether was removed from the aqueous extract by boiling and the remaining solution was diluted to 100 ml with H_2O . 10 ml of a 5% solution of

8-hydroxyquinoline in 2M CH_3COOH was added, followed by the dropwise addition of 6M sodium acetate to precipitate

gallium 8-hydroxyquinolate. A solid source was prepared from the organic derivative and washed with 10 ml 2M acetic acid followed by 10 ml of hot H_2O . The source was dried at $110^{\circ}C$ and counted after approximately 180 minutes.

Step 3. 40 ml of diethyl ether was used to wash ^{the} aqueous phase from step 2 and after removing the residual ether, the solution was made alkaline with concentrated NH_4OH . H_2S was then passed to precipitate zinc sulphide and this was filtered off under gravity. (Whatman 44). The precipitate was washed with 20 ml H_2O and dissolved in 1 ml of 5N HCl. After adjusting the solution volume to 20 ml with H_2O , traces of H_2S were removed by boiling. The solution was cooled to approximately $0^{\circ}C$ and $Zn(Hg(SCN)_4)$ precipitated by the addition of 10 ml of $HgCl_2/KSCN$ reagent*. Several minutes were allowed for the white, granular precipitate to form and it was then filtered and washed with a dilute solution of the precipitating agent*, followed by 20 ml of ice cold water. The precipitate was dried at $80^{\circ}C$ and counted after approximately 200 minutes.

* See zinc determination p.114.

Observations.

The β -decay of the zinc sources was followed in the end-window counter until the background level had been

reached. Two activities with half-lives of 3.9 hours and 13.7 hours were resolved, corresponding respectively to ^{71m}Zn and ^{69m}Zn . The observed half-life of ^{71m}Zn agrees closely with the value obtained by Lavè⁷³) (4.1 hours) but throws some doubt on the value of LeBlanc et al⁷⁴) (3 hours), which would seem to be too short. ^{69m}Zn decays by internal transition to the β^- -emitter, ^{69g}Zn (55minute). The high β counting efficiency for the former nuclide was assumed to be due to the presence of ^{69g}Zn which had come to equilibrium.

The γ -spectra of the sources were observed in the 3" x 3" flat NaI(Tl) crystal, using 100 - channel analysis of the pulse height distribution. (fig. 27). Photopeaks corresponding to γ -transitions of 0.38, 0.49 and 0.61 MeV, due to ^{71m}Zn , which decays to a highly excited state in ^{71}Ga , were initially discerned. These decayed with a half-life of 3.9 hours leaving a residual peak at 0.435 MeV due to ^{69m}Zn . No 49 hour activity attributable to ^{72}Zn was observed, either in the end-window counter or the crystal. An upper limit for the $^{76}\text{Ge}((n,\alpha n) + (n,n\alpha))^{72}\text{Zn}$ cross-section was calculated by estimating the maximum detectable activity of this nuclide from the β -decay curves.

5% of the β -decay of ^{72}Zn leads to the β -active

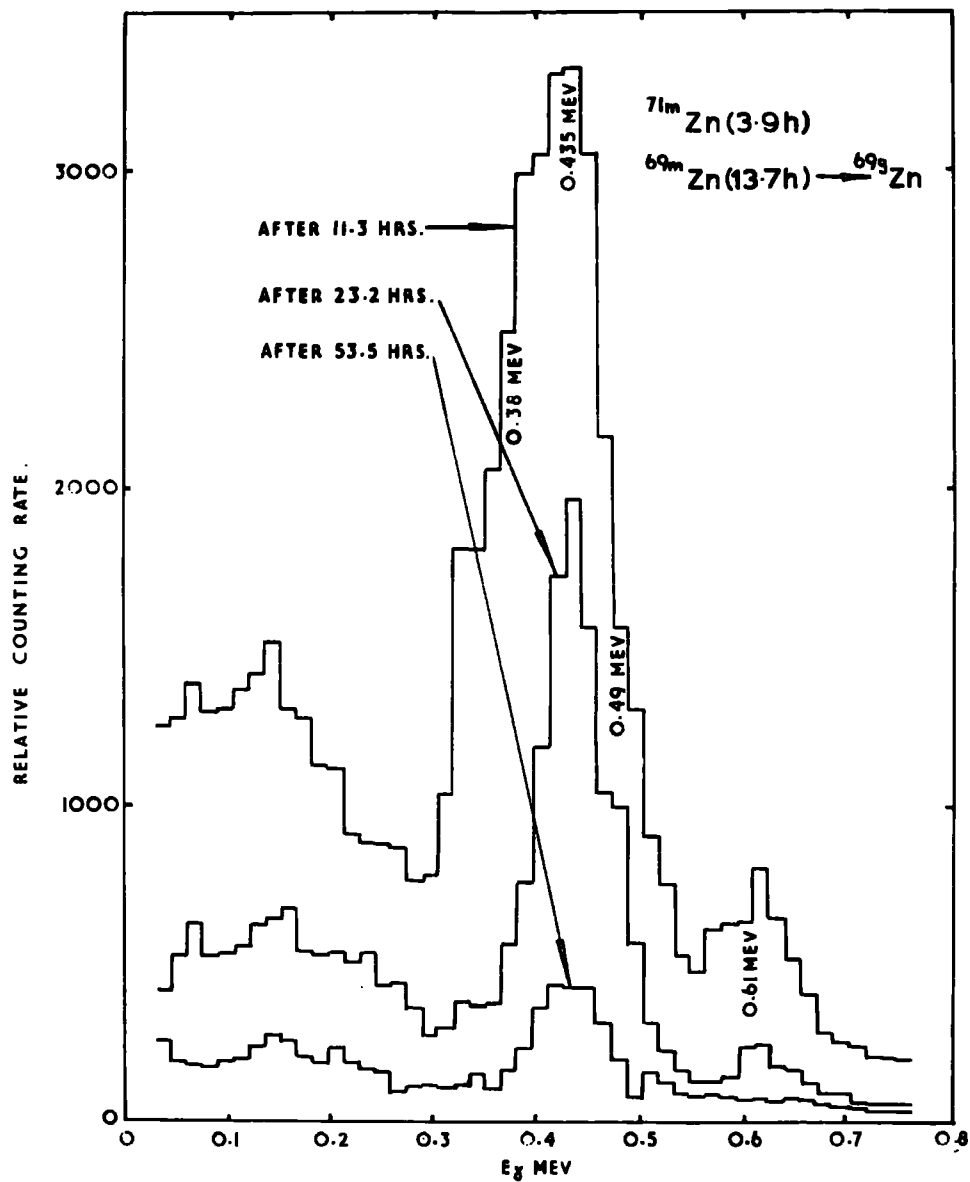


FIG 27 EXAMPLES OF THE OBSERVED γ -SPECTRA OF A ZINC SOURCE.

daughter, ^{72}Ga , and attempts were made to detect this by milking the zinc sources. After approximately six days the $\text{Zn}(\text{Hg}(\text{SCN})_4)$ was dissolved in a mixture of 5 ml of gallium carrier solution and 5 ml of concentrated HCl. Gallium 8-hydroxyquinolate was precipitated and solid sources prepared for counting. No activity was detectable in these gallium sources.

Two activities with half-lives of 5.0 and 13.8 hours, due to ^{73}Ga and ^{72}Ga respectively, contributed to the gallium decay curves. The value for ^{73}Ga agrees with the previous determination by Siegel and Glendenin⁷⁵⁾ whereas the ^{72}Ga value is somewhat higher than the accepted half-life of 13.4 hours for ^{72}Ga given by Levkovskii⁷⁶⁾ and is more nearly in agreement with earlier determinations in the region of 14 hours.^{94,95)} The time taken to separate the element did not allow accurate measurement of the 20 minute ^{70}Ga , but evidence of its presence was seen in some cases at the beginning of the decay curves. Further identification of the gallium activities was achieved by observing the decay of the sources in the 3" x 3" flat NaI(Tl) crystal. A photopeak of 0.30 MeV due to ^{73}Ga was superimposed on the more complex spectrum of ^{72}Ga . Fig. 28 shows the decay of a typical gallium source. As well as the photopeaks of 0.64 and 0.85 MeV from ^{72}Ga , the higher energy gammas of 1.05,

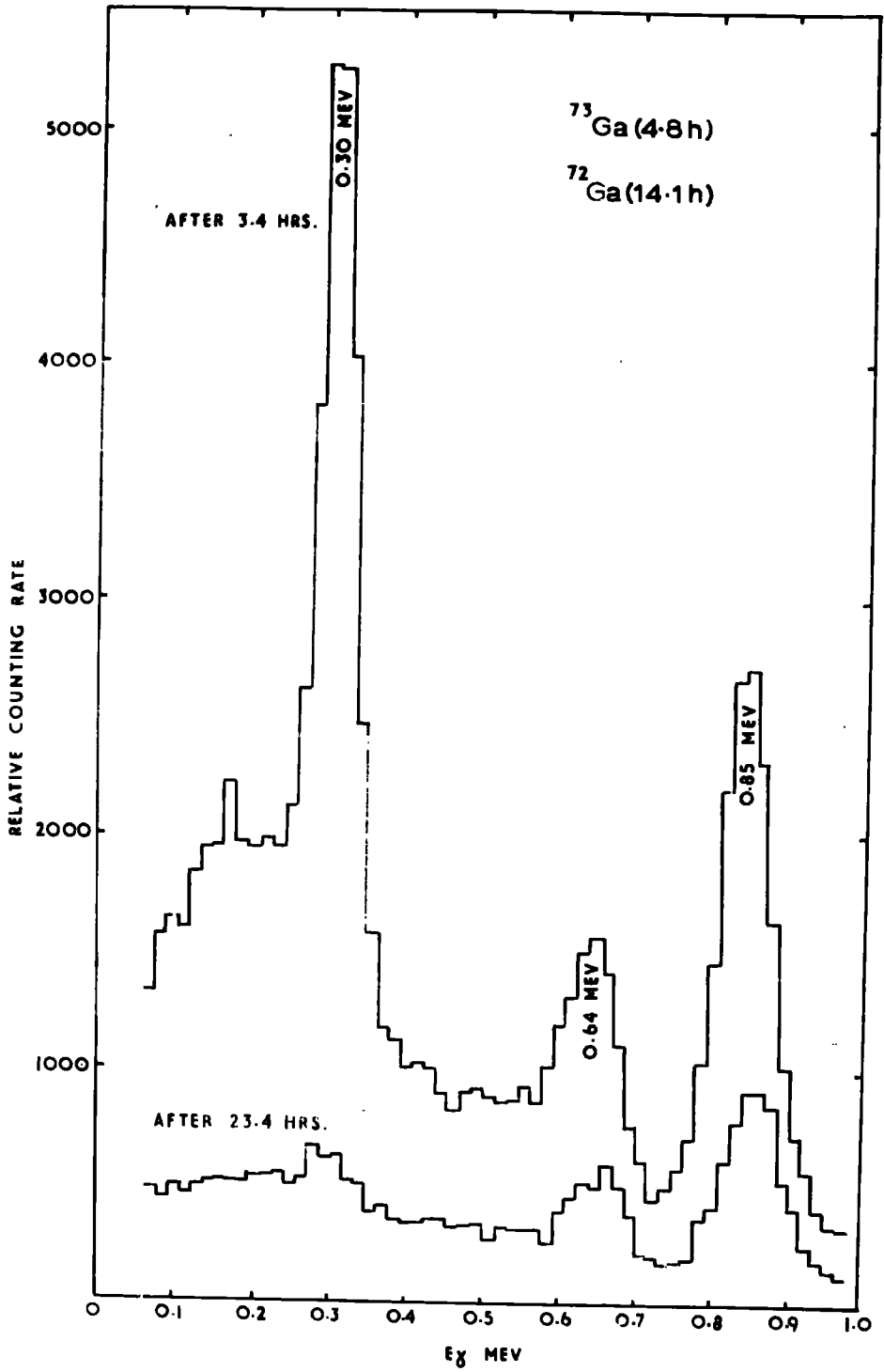


FIG 28 EXAMPLES OF THE OBSERVED γ -SPECTRA OF A GALLIUM SOURCE.

1.28, 1.48, 2.17 and 2.49 MeV were also seen. From the β -decay curves of the germanium sources, an activity due to the 83 minute β^- -emitter, ^{75g}Ge , was easily resolved. The calculated cross-section of the $^{76}\text{Ge}(n,2n)^{75}\text{Ge}$ reaction is essentially a total value including the contribution by the 49 second isomer, ^{75m}Ge , which decays by internal transition. A 41 hour activity corresponding to ^{69}Ge was also observed, this nuclide decaying approximately 36% by positron emission. Somewhat longer than several previous values, this half-life agrees most closely with those of Nussbaum et al⁷⁷) (40.4 hours) and Hopkins et al⁷⁸) (40 hours). There was also evidence of the 11 day ^{71}Ge as residual activity. This nuclide however decays 100% by electron capture, thus offering little possibility of accurately estimating the $^{72}\text{Ge}(n,2n)^{71}\text{Ge}$ cross-section, by this method of counting.

The germanium sources were also counted using the 3" x 3" flat NaI(Tl) crystal in conjunction with a thick aluminium absorber of approximately 1 gm/cm^2 . A rapidly decaying photopeak of 0.27 MeV was observed corresponding to the 11% decay of ^{75}Ge via a gamma of this energy. The positron annihilation photopeak at 0.51 MeV due to the decay of ^{69}Ge and ^{71}Ge was also resolved together with the gammas at 0.87 and 1.12 MeV from ^{69}Ge . (fig. 29).

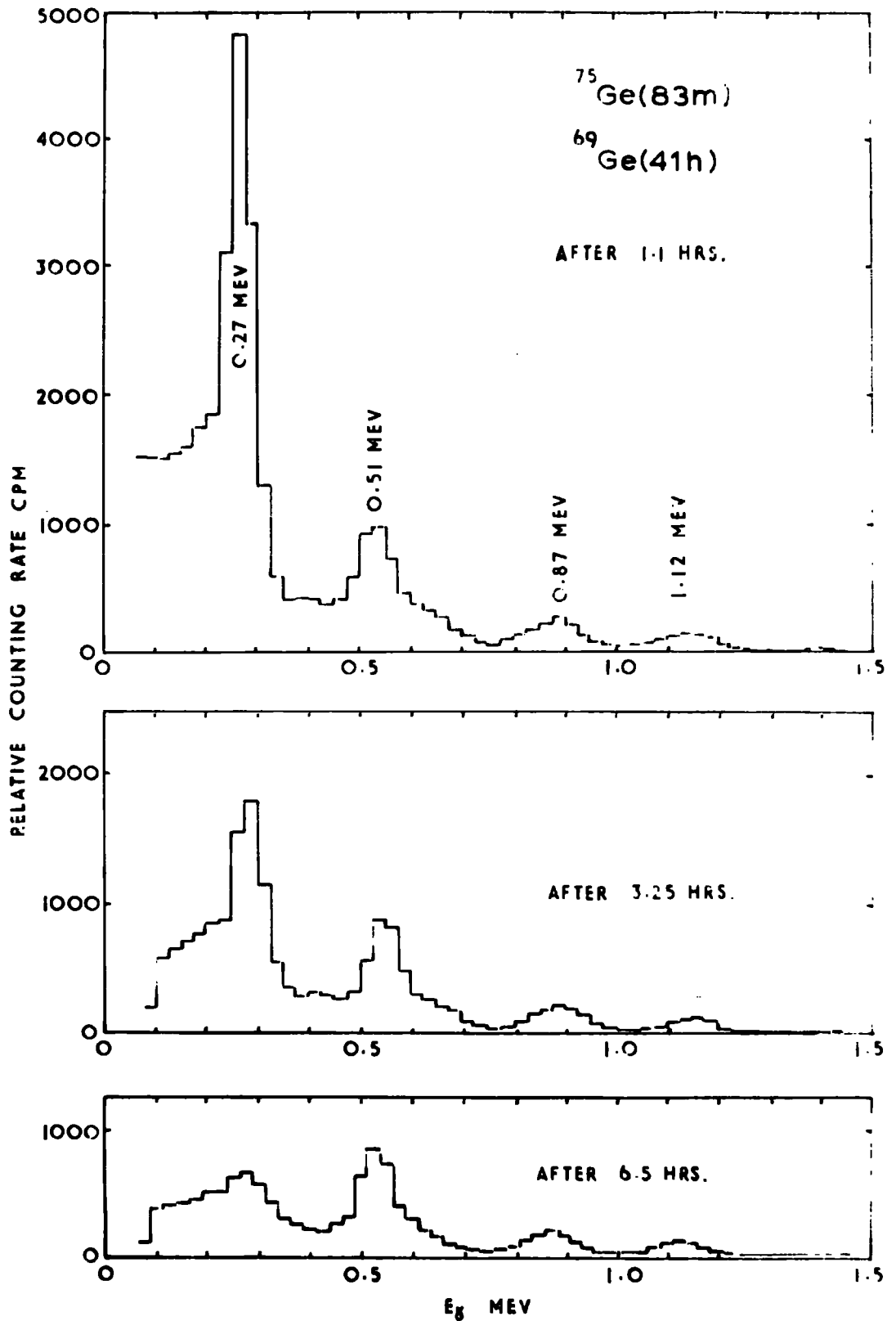


FIG 29 EXAMPLES OF THE OBSERVED γ -SPECTRA OF A GERMANIUM SOURCE.

Discussion.

The results are reported in the tables 30 to 36 which follow, the errors quoted being the standard deviations.

In the case of the $^{76}\text{Ge}((n, \alpha n) + (n, n \alpha))^{72}\text{Zn}$ cross-section the estimated upper limit of 0.59 mb is a considerable improvement on the value of < 2 mb set recently by Bramlitt⁴⁷) and represents a substantial increase in sensitivity over his measurements. Unfortunately, the $^{73}\text{Ge}((n, \alpha n) + (n, n \alpha))^{69}\text{Zn}$ cross-section could not be measured by the present method due to interference from the $^{72}\text{Ge}(n, \alpha)^{69}\text{Zn}$ reaction.

The cross-section of the $^{74}\text{Ge}(n, \alpha)^{71}\text{Zn}$ reaction is a lower limit, since only the metastable isomer of the zinc isotope, which decays 100% by β^- -emission to the 1.48 MeV level in ^{71}Ga , was observed. This probably accounts for the fact that the value of 3.43 ± 0.11 mb obtained is somewhat lower than the general trend of (n, α) cross-section values in the neighbouring elements. Khurana⁷⁹) and Paul and Clarke⁵⁸) have measured the $^{74}\text{Ge}(n, \alpha)^{71g}\text{Zn}$ (2.2m) cross-section and obtained values respectively of 40 ± 8 (at 14 MeV) and 14.9 ± 6 mb (at 14.5 MeV). Time has not permitted the measurement of the ^{71g}Zn production cross-section in the present work, but the relatively high values observed by these workers for the production cross-section of this isomer

TABLE 30

The $^{56}\text{Fe}(n,p)^{56}\text{Mn}$ reference reaction

Expt. No.	No. of ^{56}Fe nuclei	A_{obs} cpm	Counting Eff	A_{obs} dpm	$(X_r \times \lambda_{pr})$
20	4.779×10^{21}	2.84×10^4	0.0828	8.57×10^6	1702
21	4.782×10^{21}	1.87×10^4	0.0831	2.25×10^7	7394
22	4.851×10^{21}	4.40×10^4	0.0828	1.33×10^7	2362

$t_{1/2}^{56}\text{Mn} = 2.58$ hours.

$\sigma^{56}\text{Fe}(n,p)^{56}\text{Mn} = 96.7\text{mb.}$

$E_n = 14.8$ MeV.

TABLE 31

The upper limit of the $^{76}\text{Ge}((n,\alpha n) + (np\alpha))$ ^{72}Zn

Expt. No.	No. of ^{76}Ge nuclei	A_{Omax} cpm	<u>cross-section</u>			A_{Oabs} dpm	$(Xx\lambda_p)$	σ mb
			Counting Eff	Chem. Yield				
20	5.858×10^{20}	32	0.050	0.591	1.08×10^3	108.7	1.56	
21	4.179×10^{20}	32	0.140	0.314	7.28×10^2	447.9	0.59	
22	3.719×10^{20}	32	0.060	0.552	9.66×10^2	141.9	1.52	

^{72}Zn $t_{1/2} = 49$ hours.

$\sigma < 0.59$ mb

TABLE 32

The $^{74}\text{Ge}(n,\alpha)^{71\text{m}}\text{Zn}$ cross section

Expt. No.	No. of ^{74}Ge nuclei	A_{obs} cpm	Chem Yield	A_{obs} dpm	$(X \times \lambda_p)$	σ mb
20	2.759×10^{21}	2.56×10^4	0.591	1.21×10^5	1154	3.49
21	1.968×10^{21}	2.35×10^4	0.314	2.09×10^5	4915	3.28
22	1.751×10^{21}	2.30×10^4	0.552	1.16×10^5	1565	3.53

$^{71\text{m}}\text{Zn}$ $t_{1/2} = 3.9$ hours

C $^{71\text{m}}\text{Zn} = 0.358$

Mean value $\sigma = 3.43 \pm 0.14$ mb

TABLE 33

The $^{72}\text{Ge}(n,p)^{72}\text{Ga}$ cross section

Expt. No.	No. of ^{72}Ge nuclei	A cpm o_{obs}	Counting Eff	Chem Yield	A dpm o_{abs}	($\Sigma x \lambda \bar{p}$)	σ mb
20	2.077×10^{21}	4.00×10^4	0.305	0.428	3.06×10^5	367.7	36.8
21	1.477×10^{21}	5.00×10^4	0.335	0.305	4.89×10^5	1534	32.8
22	1.315×10^{21}	2.42×10^4	0.330	0.271	2.71×10^5	484.1	35.5

^{72}Ga $t_{\frac{1}{2}} = 13.8$ hours

Mean value $\sigma = 35.0 \pm 1.7$ mb

TABLE 34

The $^{73}\text{Ge}(n,p)^{73}\text{Ga}$ cross section

Expt. No.	No. of ^{73}Ge nuclei	A_{obs} cpm	Counting Eff.	Chem Yield	A_{obs} dpm	($X\lambda p$)	σ mb
20	5.858×10^{20}	3.15×10^4	0.330	0.428	2.23×10^5	995.1	35.1
21	4.179×10^{20}	4.05×10^4	0.346	0.305	3.84×10^5	4215	33.1
22	3.719×10^{20}	1.95×10^4	0.346	0.271	2.08×10^5	1341	34.7

^{73}Ga $t_{1/2} = 5.0$ hours

Mean value $\sigma = 34.3 \pm 0.9$ mb

TABLE 35
The $^{76}\text{Ge}(n,2n)^{75}\text{Ge}$ Cross Section

Expt. No.	No. of ^{76}Ge Nuclei	A_0 obs cpm	Counting Eff.	Chem. Yield	A_0 abs dpm	($X \times \lambda p$)	σ mb
20	5.858×10^{20}	6.82×10^4	0.358	0.0091	2.09×10^7	2813	1164
21	4.179×10^{20}	3.75×10^5	0.342	0.0292	3.76×10^7	12830	1066
22	3.719×10^{20}	1.80×10^5	0.355	0.0254	2.00×10^7	4126	1086

$t_{1/2}^{75}\text{Ge} = 83$ minutes

Mean value $\sigma = 1105 \pm 41$ mb.

TABLE 36.

The $^{70}\text{Ge}(n,2n)^{69}\text{Ge}$ cross section.

Expt. No.	No. of ^{70}Ge nuclei	$A_{\text{obs}}^{\text{cpm}}$	Counting Eff	Chem. Yield	$A_{\text{abs}}^{\text{dpm}}$	$(Xx \lambda p)$	σ mb
20	1.549×10^{21}	1.48×10^3	0.128	0.0091	1.27×10^6	129.6	581
21	1.105×10^{21}	9.45×10^3	0.127	0.0292	2.55×10^6	534.3	656
22	9.853×10^{20}	4.28×10^3	0.128	0.0254	1.32×10^6	162.2	688

$t_{1/2}^{69}\text{Ge} = 41$ hours.

Mean value $\sigma = 642 \pm 45$ mb

in comparison with the low value obtained here for the metastable isomer, would suggest a substantial contribution by direct processes to the overall reaction mechanism.

For the $^{72}\text{Ge}(n,p)^{72}\text{Ga}$ (13.8 hour) cross-section, the observed value of 35.0 ± 1.7 mb agrees well with the ≈ 32 mb obtained by Zabel⁸⁰⁾ at 14.0 MeV. Paul and Clarke obtained the higher value of 65.2 ± 26 mb for this reaction and it is probable that they confused the product activity with that of 13.7 hour ^{69m}Zn , since no chemical separation was made. As already mentioned, the latter nuclide has a high β -counting efficiency due to its 55 minute daughter, ^{69g}Zn .

Contrary to the trend observed by Levkovskii⁸¹⁾ that the (n,p) cross-section for the (Z, A + 1) target nuclide is approximately half the magnitude of that for its (Z,A) neighbour, the $^{73}\text{Ge}(n,p)^{73}\text{Ga}$ (5 hour) value of 34.3 ± 0.9 mb is almost identical with that of the $^{72}\text{Ge}(n,p)^{72}\text{Ga}$ cross-section. This value also disagrees by approximately a factor of four with the 137 ± 70 mb determined by Paul and Clarke⁵⁸⁾. Here again, confusion on their part with the 3.9 hour ^{71m}Zn from the $^{74}\text{Ge}(n,\alpha)$ reaction might account for the discrepancy, in view of the fact that they did not perform a chemical separation.

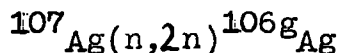
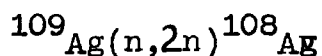
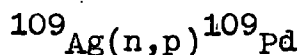
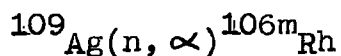
Khurana⁶¹⁾ has previously measured the $^{76}\text{Ge}(n,2n)^{75}\text{Ge}$

cross-section and found it to be 920 ± 184 mb* at 14.8 Mev. The present work supports this result, a value of 1105 ± 41 mb being obtained. His value for the $^{70}\text{Ge}(n,2n)^{69}\text{Ge}$ reaction of 1228 ± 184 mb* is however inexplicably high in comparison with the 642 ± 45 mb observed. This latter value adds further weight to the determinations by Paul and Clarke (666 ± 230 mb) and Rayburn⁶⁰) (598 ± 45 mb).

*Adjusted using a value of 96.7 mb for the $^{56}\text{Fe}(n,p)^{56}\text{Mn}$ reference reaction. (Original value taken by Khurana = 126 mb).

5. The reactions of silver.

The following neutron-induced reactions of silver were examined:-



In initial experiments, samples consisting of approximately 2 gms. of powdered silver nitrate mixed with iron

granules were irradiated. The recrystallised silver nitrate contained no impurities in sufficient quantities to give rise to interfering activities. To prevent reaction between the salt and the iron, each was dried for several days in a dessicator before mixing. The silver nitrate was kept in darkness as far as possible to prevent photo-decomposition. Each sample was mixed just before irradiation and sealed into a thin polythene bag. No noticeable reaction took place when these precautions had been taken and there were no signs of adverse effects when the various products were separated and counted.

Attempts were made to observe the 2.3 minute ^{108}Ag in some of the experiments using silver nitrate. Despite the speed with which sources of silver chloride could be prepared, it was found that they took too long to dry satisfactorily before counting. Sources which were counted within about six minutes of the end of irradiations were found to give erratic counting rates and this was attributed to the sources still being damp. In order to observe ^{108}Ag therefore, silver foil was irradiated and counted without chemical separation.

The pure silver foil (0.52 mm thick) was cut into discs 1.6 cm in diameter. In each experiment a single disc weighing approximately 1 gm and covered with a thin layer of

polythene, was irradiated for two minutes. During this short period the neutron flux was assumed to be constant for the purposes of calculation. Approximately one minute after the end of the irradiation the disc was placed in the centre of an aluminium planchet and the decay followed in the end-window counter. The diameter of the disc was chosen to be identical with that of the solid sources normally prepared by precipitation in order to achieve a similar counting geometry. Using this technique, the 23 minute activity was easily observed, together with the 24.4 minute ^{106}gAg . The cross-section of the $^{109}\text{Ag}(n,2n)^{108}\text{Ag}$ reaction was calculated relative to the $^{107}\text{Ag}(n,2n)^{106}\text{gAg}$ cross-section, this being known from the other irradiations using silver nitrate as the sample material. The possible interference of the short-lived rhodium activities, together with the difficulties of assessing the β -efficiency for these thick sources are discussed later.

Similar foils of silver were also irradiated for one hour and subjected to the chemical procedure used for silver nitrate to test the general validity of the method and the reproducibility of the cross-section measurements. In these experiments, pure iron foil was used as the monitor. The silver foil was sandwiched between two discs of iron approximately 1.7 cm in diameter and 0.16 mm thick. To facilitate

the rapid dissolution of the silver, the chemical procedure was slightly modified by increasing the concentration of nitric acid in the dissolving solution.

In the separation procedure the silver and silver nitrate samples were dissolved in a solution of Pd(II) and Rh(II) carriers. The silver was initially removed by precipitation, and the rhodium and palladium then isolated. Solid sources of silver chloride, rhodium metal and palladium dimethylglyoximate were respectively prepared for end-window β -counting. All these precipitates were of gravimetric quality and the chemical yields were determined by weighing. Precautions were taken to avoid the photo-decomposition of the silver sources by storing them in subdued lighting conditions. Radiochemically, the decomposition of the chloride was not a serious drawback as the loss of silver could safely be assumed to be negligible. A complication in the initial step of the chemical procedure, was that the dissolving solution had to be free of chloride, bromide and iodide ions. The carrier solutions were specially prepared to achieve this.

The preparation of rhodium carrier solution.

The presence of interfering ions in an aqueous solution of ammonium chlororhodite was confirmed by testing with

silver nitrate and nitric acid. Attempts were initially made to prepare a solution of Rh(II) nitrate by precipitating $\text{Rh}_2\text{O}_3 \cdot 5\text{H}_2\text{O}$ from the chlororhodite solution under alkaline conditions and dissolving this in nitric acid. It was found however, that the yellow precipitate was only partially soluble and the following method, involving the evaporation of fuming HNO_3 solutions, was subsequently adopted for the preparation of the carrier.

Step 1. 1 ml of concentrated HCl and 10 ml of concentrated HNO_3 were added to approximately 0.5 gm of $(\text{NH}_4)_3\text{RhCl}_6$ in a large evaporating basin. The mixture was gently heated until the evolution of nitrous fumes had ceased and the red chlororhodite complex had been decomposed to give a yellow solution. Strong heating was then applied to remove the bulk of HCl and HNO_3 .

Step 2. As dryness approached, the basin was transferred to a water bath and 3 ml of fuming HNO_3 added. Finally, the solution was evaporated to dryness. It was essential that this step was carried out under mild heating conditions to avoid the decomposition of the residue to rhodium metal, which, it was discovered, was unavoidable when using a flame directly.

Step 3. The yellow-brown residue from step 2 was treated with 20 ml of concentrated HNO_3 and again evaporated to near dryness over a flame. 3 ml of fuming HNO_3 was added and the solution taken to dryness on the water bath.

Step 4. Step 3 was repeated, the residue taken up in 30 ml H_2O and then filtered (Whatman 44). A reddish-brown precipitate of Rh_2O_3 was removed at this stage leaving a clear yellow solution of rhodium nitrate. A portion of the filtrate was tested with silver nitrate to confirm the absence of halide ions and the solution was diluted to give a concentration of approximately 1 mg Rh/ml. If halide ions were still present after the completion of the last step, the solution was evaporated to 5 ml, 20 ml of concentrated HNO_3 added, and the step repeated. Generally it was found that three evaporations were sufficient to remove the interfering ions.

The slightly acidic carrier solution was stored in a glass vessel to avoid reductive decomposition which was often troublesome with plastic containers, and was found to be stable to hydrolysis over a period of several months.

The determination of the rhodium carrier solution.

After unsuccessful attempts to obtain reproducible

results using 2 - mercaptobenzo-thiazole⁸²) as the precipitating agent, the following method⁸³) was adopted and gave satisfactory results.

Step 1. 25 ml of the rhodium carrier was taken and evaporated to 20 ml in a conical flask. 10 ml of concentrated HCl was added and the mixture heated to boiling for approximately two minutes to form the rose-red chlororhodite complex. Hillebrand et al⁸³) in their account of the method suggested that the boiling should be continued for about fifteen minutes. However, when this was tried a yellow precipitate of rhodium oxide was obtained after approximately five minutes. This proved to be extremely difficult to redissolve and determinations in which this precipitate was produced, had to be discarded.

Step 2. The chlororhodite solution was diluted to 400 ml, heated to boiling, and H₂S passed rapidly for thirty minutes to precipitate black rhodium sulphide. While maintaining the flow of H₂S, the solution was allowed to cool.

Step 3. After filtration, (Whatman 44) the rhodium sulphide was washed with dilute H₂SO₄ (2.5 ml H₂SO₄ + 97.5 ml H₂O), dilute HCl (1 ml HCl + 99 ml H₂O) and the damp precipitate and paper transferred to a weighed porcelain-crucible. The

dried precipitate was ignited in air and the residue of rhodium oxide finally ignited in a stream of dry hydrogen to a constant weight of rhodium.

The determination was carried out in triplicate and results agreeing to within 3% were obtained.

The preparation of the palladium carrier solution.

Attempts were made to prepare a solution of palladium (II) nitrate from available palladium metal, using a method similar to that described for rhodium. Approximately 0.25 gm of palladium wire was dissolved in 10 ml of concentrated HNO_3 , 1 ml of concentrated HCl and the solution subjected to successive evaporation processes with fuming nitric acid. Yields of palladium nitrate were, however, found to be poor due to the low solubility of the residues. A red-black deposit of palladium oxide was obtained when the solutions were taken to dryness on the water bath and only a small fraction of this would redissolve in concentrated HNO_3 . The method was therefore abandoned.

Commercial palladium (II) nitrate was eventually used to prepare the carrier solution. 0.54 gm of this salt was dissolved in 250 ml of 0.5 N HNO_3 . A brown residue was obtained at this stage and was filtered off leaving a clear

yellow solution. Silver nitrate was used to test a portion of the carrier and it was found to be free from interfering halides. The solution was stored in a glass vessel to avoid reductive decomposition.

The determination of the palladium carrier.

A standard method⁸⁴) using an alcoholic solution of dimethylglyoxime as the precipitating agent, was employed to determine the palladium gravimetrically.

Step 1. A 20 ml aliquot of the carrier solution was placed in a 600 ml beaker, 1 ml of concentrated HCl added and the mixture diluted to 300 ml with H₂O. 10 ml of the reagent solution (1% dimethylglyoxime in 100% EtOH) was added and after stirring, the mixture was allowed to digest for at least two hours.

Step 2. The yellow precipitate of palladium dimethylglyoxime complex was collected on a weighed sintered glass crucible of porosity 4 by filtration, washed with 100 ml of dilute HCl (1 ml concentrated HCl + 99 ml H₂O) and 100 ml of H₂O. After drying to constant weight, initially at 80°C and then in a desiccator, the precipitate was weighed as Pd(C₄H₇O₂N₂)₂.

The determination was repeated in triplicate and the

results' agreed to within 0.5%. A blank determination in the absence of palladium confirmed that no precipitation of the reagent took place.

The chemical separation procedure.

The procedure was largely developed from information available in the National Research Council volumes on the radiochemistry of the appropriate elements^{85,86,87}).

Step 1. After separation from the iron, the silver nitrate was dissolved in a hot solution consisting of 10 mls each of the palladium and rhodium carriers, 5 ml of concentrated HNO_3 and 25 ml of H_2O .

Step 1a. The weighed silver foil was dissolved in a mixture of 10 ml of each of the carriers, 10 ml of concentrated HNO_3 and 20 ml of H_2O , by heating to near boiling.

Step 2. 10 ml of 2N HCl was added to the silver solution to precipitate the chloride. Before complete coagulation of the precipitate had taken place, approximately 20 ml of the suspension was filtered to prepare a solid source for end-window counting.

The source was washed with 10 ml of 5N HNO_3 , 50 ml of

H₂O, 10 ml of diethyl ether and dried in the oven at 120°C. Counting was started after ten to fifteen minutes.

Step 3. The suspension from step 2 was filtered at the pump (2 x Whatman 44) to remove the silver chloride. 50 ml of H₂O was used to wash the precipitate and the filtrate and washings were retained. After neutralising excess acid in the filtrate, by the addition of approximately 16 ml of 6M NaOH, K₃Rh(NO₂)₆ was precipitated by adding 2 gm of solid KNO₂ and heating the mixture to boiling. When the solution had been allowed to cool, the K₃Rh(NO₂)₆ was filtered off using a sintered glass disc of porosity 4 and the filtrate containing palladium retained. The rhodium salt was washed twice with 10 ml portions of cold H₂O, sucked dry, and dissolved in 8 ml of boiling concentrated HCl. The resulting rose-red solution was diluted to 50 ml. Excess powdered magnesium was then added to precipitate rhodium metal and the solution boiled for several minutes to promote coagulation. The rhodium was filtered using a glass fibre disc and washed with approximately 10 ml of 5N HCl to remove any undissolved magnesium. After final washing with 10 ml of H₂O, followed by 10 ml diethyl ether, the source was dried at 80°C and counted after about forty minutes.

Step 4. The filtrate from step 3 containing palladium, was

allowed to stand for several hours to ensure the complete precipitation of $K_3Rh(NO_2)_6$, and then filtered under gravity. (Whatman 44). To the filtrate was added 10 ml of 5M HCl and the whole heated to boiling to destroy excess KNO_2 . 10 ml of dimethylglyoxime reagent (1% DMG in 95% EtOH) was added to the cooled solution and the mixture set aside for the precipitate of palladium dimethylglyoximate to form. This was then filtered using a glass fibre disc, washed with 20 ml 50% EtOH, 20 ml H_2O and dried at $80^\circ C$. Counting of the resulting source was commenced after approximately eight hours.

Observations.

The β -decay of each rhodium source was followed for a period of several days until the background level had been reached. In some sources a residual activity was observed, but as this was always less than 0.01% of the initial ^{105}Rh activity it was considered to be negligible for the purposes of calculation. However, it did represent evidence of contamination of the source which would otherwise have been expected to decay down to the background level with a half-life of thirty six hours, characteristic of ^{105}Rh . Identification of the residual activity was difficult in view of the very low counting rates. The most likely contaminant was thought to be ^{106}Ag (8.3 day), although it was expected that

appreciable quantities of silver would have been eliminated from the rhodium source during the chemical separation. Cases where contamination did occur could not be related to any unusual observations during the separation procedure.

Activities corresponding to ^{106m}Rh and ^{105}Rh were resolved from the β -decay curves, a typical example of which is shown in fig. 30. The observed half-lives of 2.2 hours and 36 hours respectively, were in good agreement with the accepted values. No other activities were seen, although it was thought that there might have been some sign of the 57 minute ^{103m}Rh isomer from the $^{107}\text{Ag}(n,\alpha n)$ reaction. Since counting was not started until some forty minutes had elapsed after the end of each irradiation, there was little possibility of observing the 4.4 minute ^{104m}Rh isomer resulting from the $^{109}\text{Ag}(n,\alpha)$ reaction. No indication of the presence of 54m ^{103m}Rh from the $^{107}\text{Ag}((n,\alpha n) + (n,n\alpha))$ reaction was observed.

Certain ambiguities arise with regard to the modes of production of the two nuclides observed. ^{105}Rh can be produced both from the $^{109}\text{Ag}((n,\alpha n) + (n,n\alpha))$ and $^{107}\text{Ag}(n^3,\text{He})$ reactions. No distinction could be made between these two reactions and the cross-section was calculated specifically for the $^{109}\text{Ag}((n,\alpha n) + (n,n\alpha))$ reaction.

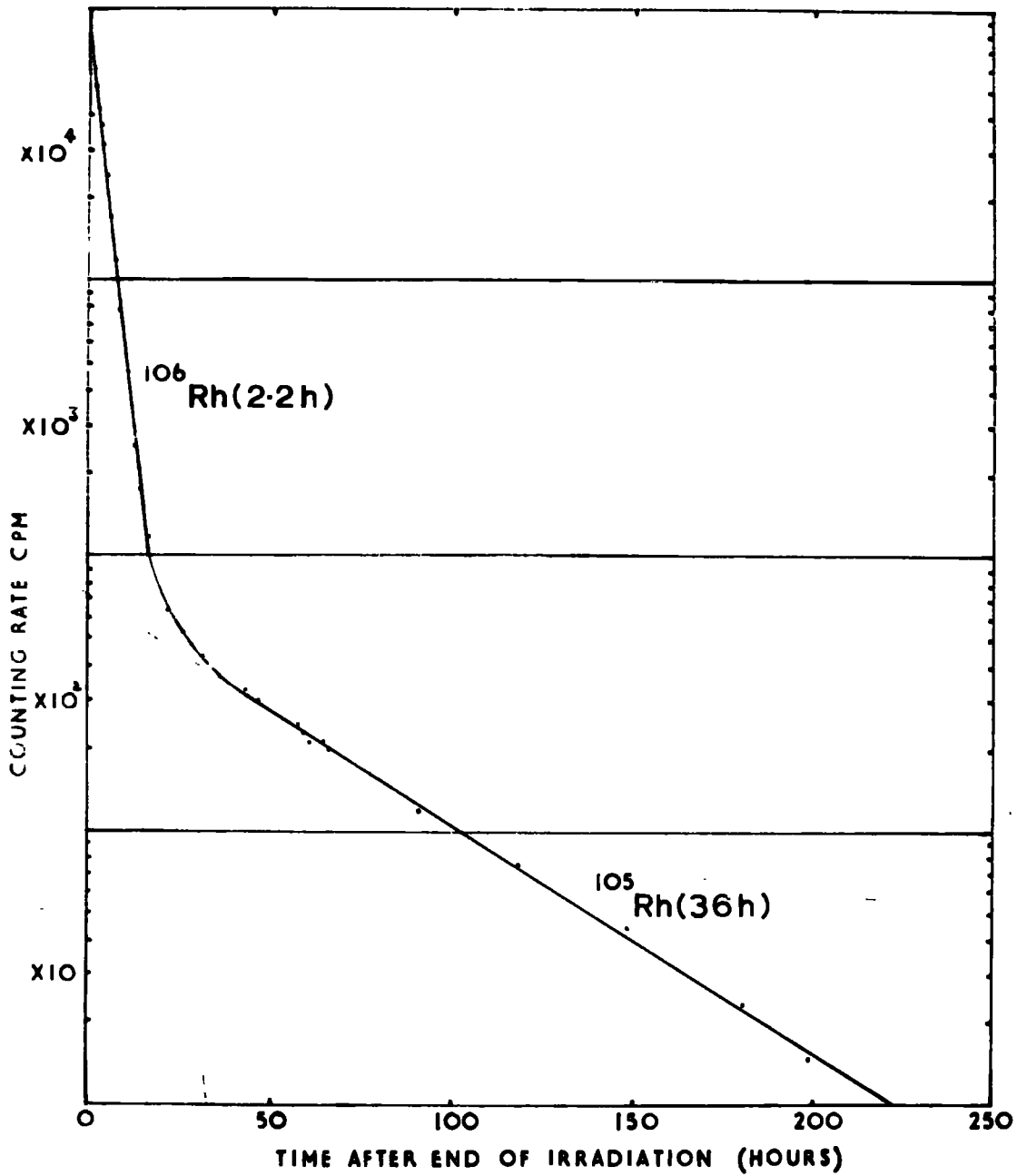


FIG 30 AN EXAMPLE OF THE β -DECAY OF A RHODIUM SOURCE.

Since the cross-section of the $(n, {}^3\text{He})$ reaction was expected to be relatively small⁴⁷), this procedure was assumed to be valid.

In the case of ${}^{106}\text{Rh}$, the two reactions ${}^{109}\text{Ag}(n, \alpha)$ and ${}^{107}\text{Ag}(n, 2p)$ are possible production routes. The cross-section for the latter reaction was again expected to be extremely small and the (n, α) reaction was considered to be the sole source of ${}^{106}\text{Rh}$.

In some cases the decay of the rhodium sources was also followed in the 3" x 3" flat NaI(Tl) crystal. The sources were counted at a distance of approximately 0.5 cm from the crystal with a 1 gm/cm² aluminum absorber interposed to stop the β -particles. Initially, the complex spectrum of ${}^{106m}\text{Rh}$ was observed and the occurrence of photopeaks found to be in good agreement with the γ -decay scheme of ${}^{106}\text{Pd}$. At variance with the accepted scheme however, a photopeak corresponding to a transition of 0.32 MeV was also observed. (fig 31). This was initially assumed to be contributed by ${}^{105}\text{Rh}$ which has a 10% decay via a gamma of this energy. However spectra of the ${}^{106}\text{Pd}$ γ -decay to the ground state were also observed in the silver sources, the ${}^{106g}\text{Ag}(8.3d)$ isomer decaying by electron capture to a highly excited state of ${}^{106}\text{Pd}$. In these sources there was no expected contribution from ${}^{105}\text{Rh}$ and yet a similar photopeak was observed.

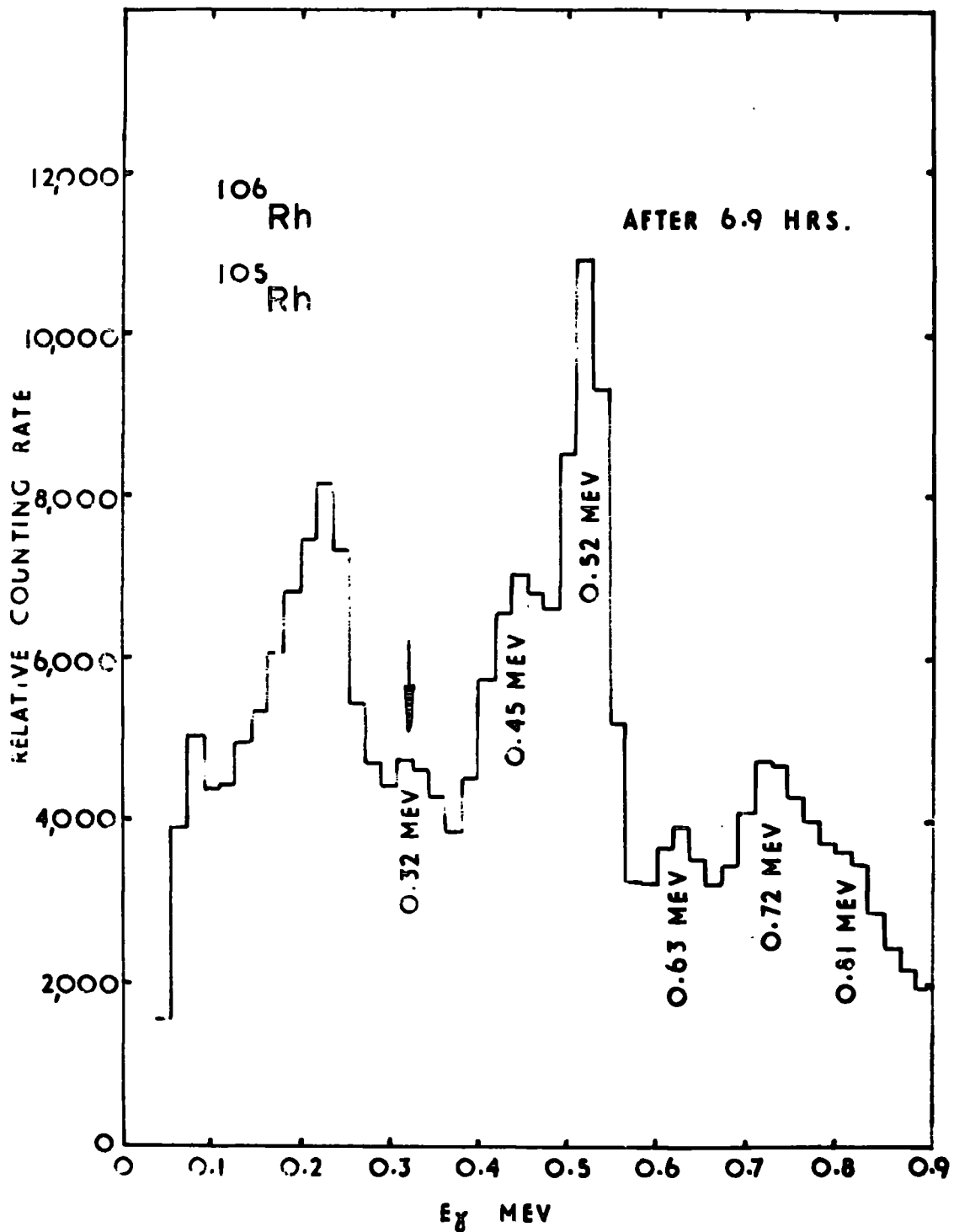


FIG 31 AN EXAMPLE OF THE OBSERVED γ -SPECTRUM OF A RHODIUM SOURCE.

O. J. Segaert and J. Demnynck⁸⁸), in their elucidation of the ^{106m}Rh spectrum had obtained the nuclide by irradiating palladium with 25 MeV deuterons. After separation of the other elements (Pd and Ag) by chemical means their rhodium sources were still contaminated with ^{105}Rh . They subtracted the contribution by this nuclide in order to obtain the γ -spectrum of ^{106m}Rh , so that it is possible that the existence of a gamma of 0.32 MeV was overlooked. The present evidence would suggest the possible presence of a γ -transition of this energy in the decay of ^{106}Pd .

When the 2.2 hour ^{106m}Rh had been allowed to decay a photopeak corresponding to 0.32 MeV remained. (fig.32). This was found to decay with a half-life of approximately forty hours which was somewhat longer than expected. The counting rates involved were, however, rather lower than was desirable for accurate γ -counting and the errors inherent in the quantitative estimation of the activity were thought to account for this discrepancy. In view of this, the evidence obtained by γ -counting was considered to provide good support for the presence of ^{105}Rh .

In the case of palladium, a purely exponential decay was observed in the β -counter, having a half-life of 13.5 hours. (fig. 33). This value agreed closely with that of J. W. Starner⁸⁹) (13.45 hours). Other values available in

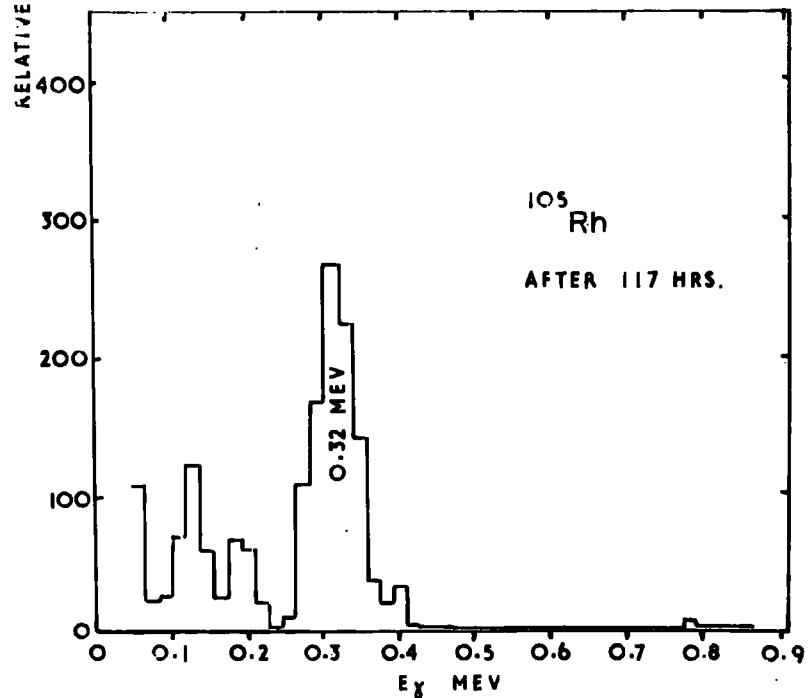
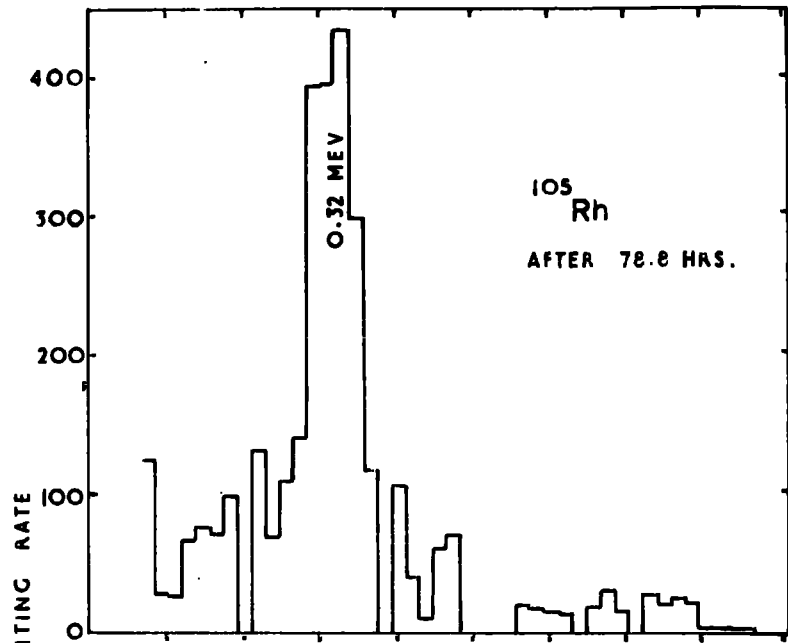


FIG 32 EXAMPLES OF THE OBSERVED γ -SPECTRA OF A RHODIUM SOURCE.

from

the literature were at some variance, extending λ 13.6 to 14.1 hours. Since the lower value was consistently reproduced in several experiments in the present work it was justifiably adopted for the purposes of calculation in preference to the higher literature values. The palladium sources were also counted in the flat 3" x 3" NaI(Tl) crystal using multichannel analysis. A photopeak corresponding to the 100% decay of ^{109}Pd via a 0.09 MeV γ -ray was well defined. (fig. 34).

In the silver chloride sources, two components were resolved from the decay curves: a 24 minute activity corresponding to ^{106g}Ag and a 8.3 day activity due to ^{106m}Ag . The half-life of the long-lived component was established by following its decay for approximately sixteen days in each case. The metastable isomer decayed almost entirely by electron capture giving the complex γ -spectrum of ^{106}pd . Due to the large uncertainties in estimating the efficiency of the proportional counter for this nuclide, no attempt was made to calculate the value of the $^{107}\text{Ag}(n,2n)^{106m}\text{Ag}$ cross-section. The γ -spectrum was however observed in the 3" x 3" flat NaI(Tl) crystal, and found to have the expected half-life. A comparison was made between this spectrum and that obtained with ^{106m}Rh (2.2 hours), as mentioned previously, the geometrical arrangement for γ -counting being identical in each case.

When the silver foil from the short irradiations was

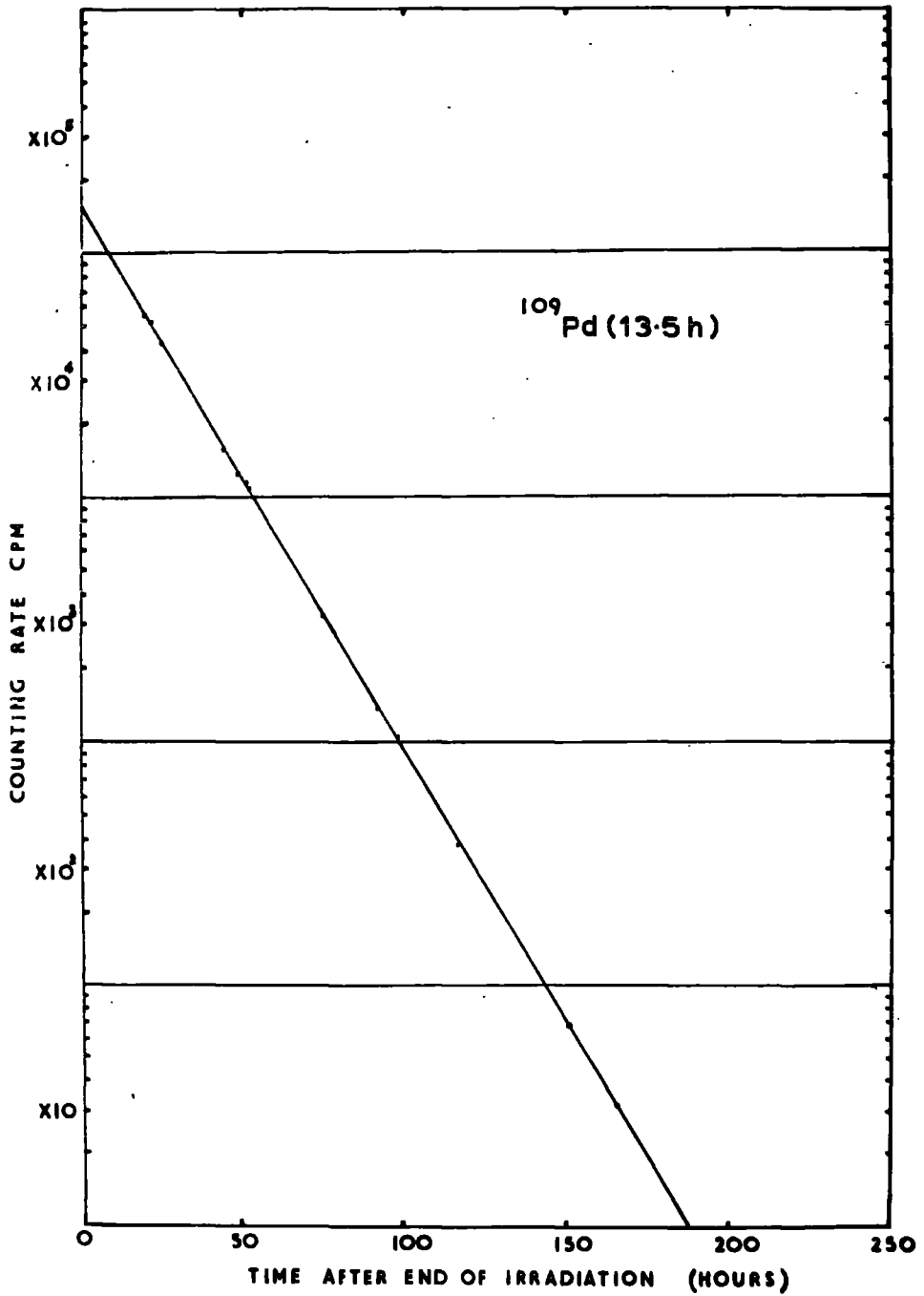


FIG 33 AN EXAMPLE OF THE OBSERVED β -DECAY OF A PALLADIUM SOURCE.

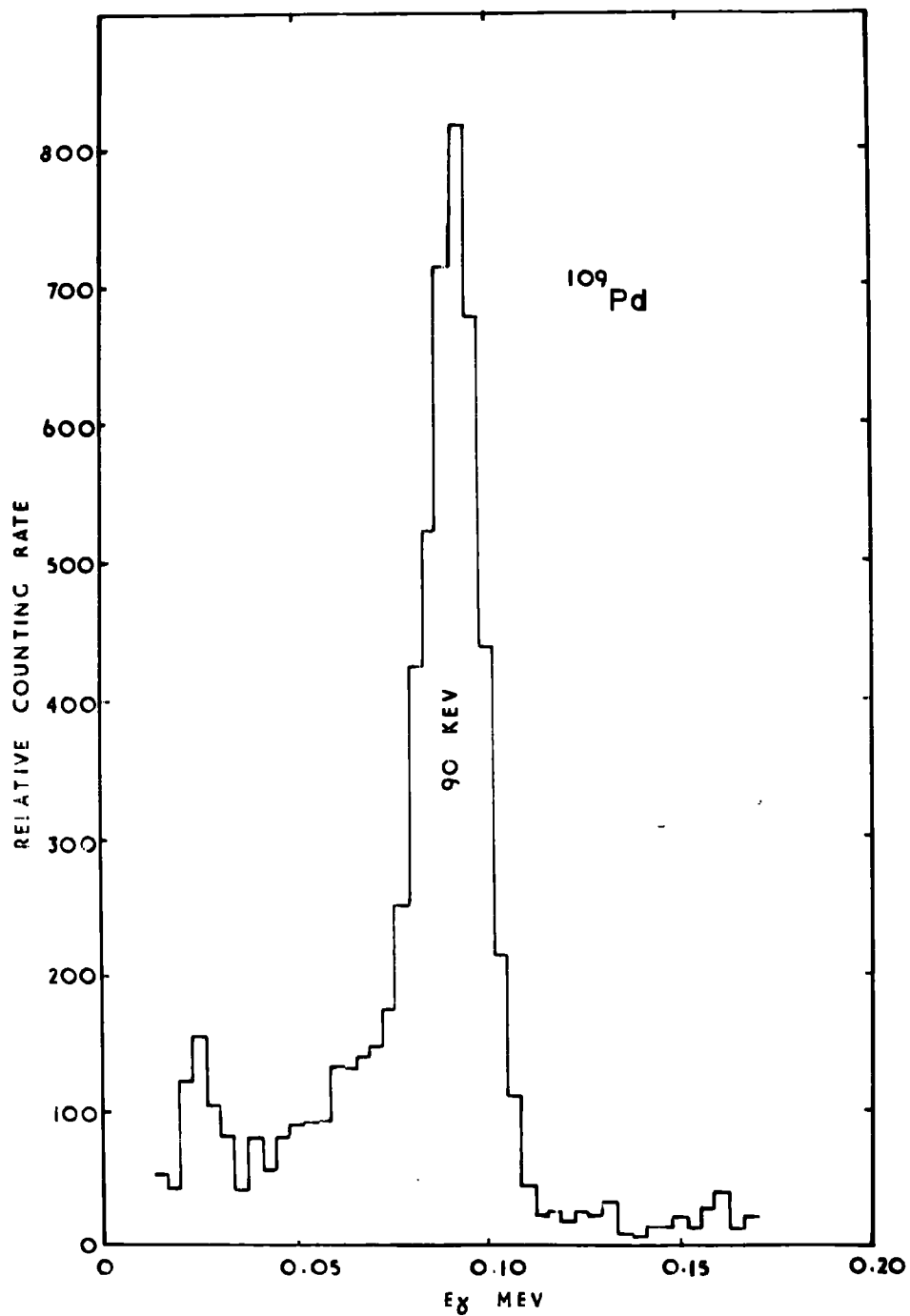


FIG 34 AN EXAMPLE OF THE OBSERVED γ -SPECTRUM OF A PALLADIUM SOURCE.

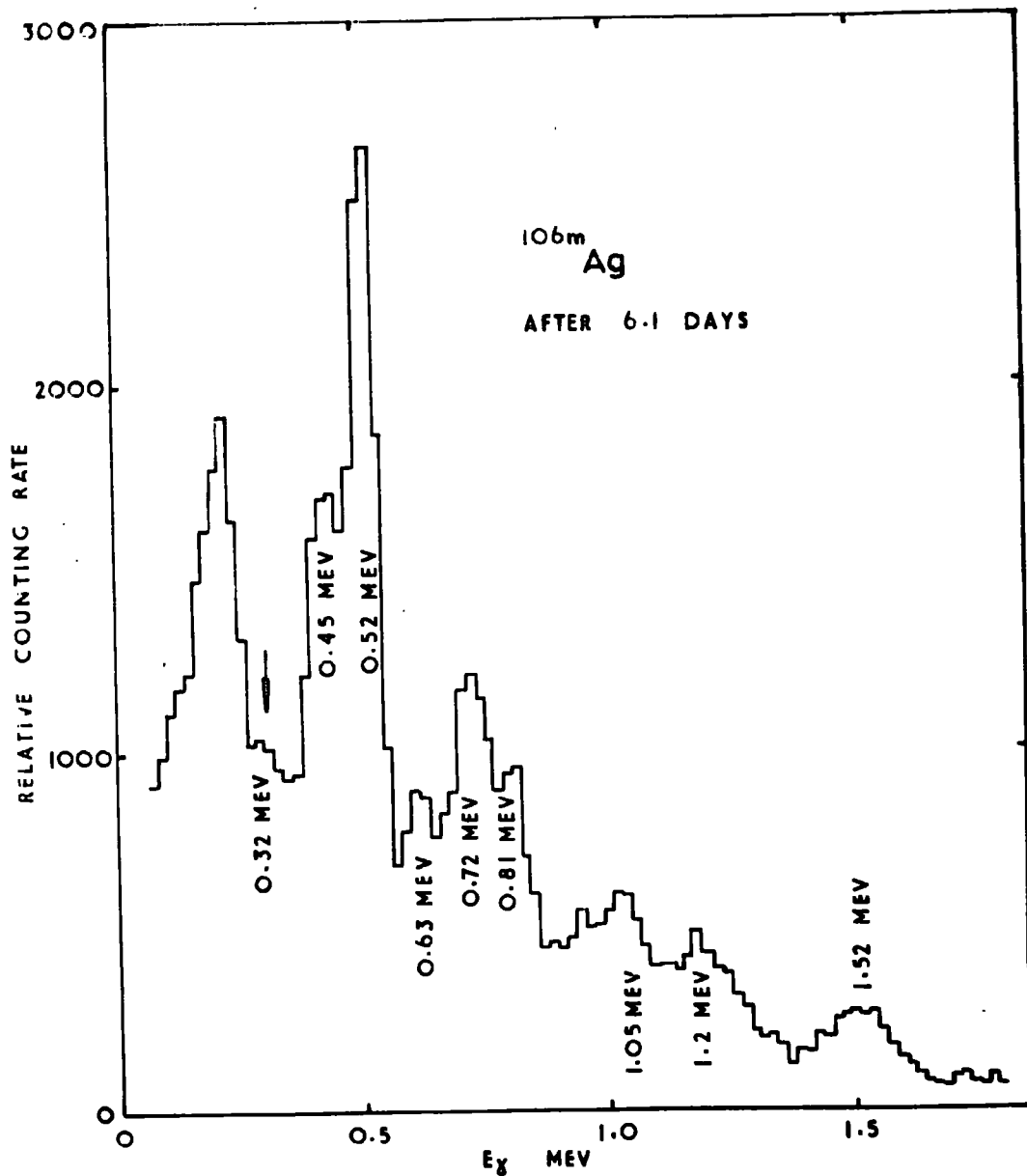


FIG 35 AN EXAMPLE OF THE OBSERVED γ -SPECTRUM OF A SILVER SOURCE.

counted without chemical separation, the initial counting rate was found to be considerable (approximately 3×10^5 cpm). Two scalers were connected in series to accommodate this and the dead-time adjusted to $5 \mu\text{sec}$ to keep counting errors to a minimum. The sources were counted until a negligible residual level of activity had been reached and two components were resolved from the decay curves. Activities corresponding to the 2.4 m $^{108}\text{g}_{\text{Ag}}$ and the 24 minute $^{106}\text{g}_{\text{Ag}}$ were seen and there was no sign of other interfering activities. Counting was started approximately two to three minutes after each irradiation. The most serious possibilities of interference which could not be distinguished from the decay curve were from the $^{107}\text{Ag}(n, \gamma)^{108}\text{Ag}$ and $^{109}\text{Ag}(n, ^3\text{He})^{107}\text{Rh}(23')$ reactions. However, in each case the cross-sections were assumed to be negligible compared with those of the two $(n, 2n)$ reactions under consideration. The short irradiation time of two minutes also differentiated strongly against the production of the comparatively long-lived activities and indeed, the level of the residual activity was always less than 0.0001% of the observed initial activity of $^{106}\text{g}_{\text{Ag}}(24\text{m})$.

The largest error in the determination of the $^{109}\text{Ag}(n, 2n)^{108}\text{Ag} / ^{107}\text{Ag}(n, 2n)^{106}\text{g}_{\text{Ag}}$ cross-section ratio lay in the estimation of the counter efficiencies for these two nuclides, since the sources were extremely thick (half-

thickness = approximately 240 mg/cm^2). Total absorption factors were determined by summing the individual factors found for each β -particle weighted by the percentage abundance of the transition, using information available in the paper by Gleason et al³⁷). Backscattering and geometrical corrections were also applied as explained previously.

(p. 39). For such thick sources the error in the estimation of the absorption corrections predominates and it is doubtful whether an accuracy of much better than $\pm 20\%$ can be claimed for the value of the $^{109}\text{Ag}(n,2n)^{108}\text{Ag}$ cross-section.

Discussion

The results of the five cross-sections measured are presented in tables 37 to 42 . All the determinations were made relative to the $^{56}\text{Fe}(n,p)^{56}\text{Mn}$ cross-section except in the case of the $^{109}\text{Ag}(n,2n)^{108}\text{Ag}$ cross-section, which was determined relative to the $^{107}\text{Ag}(n,2n)^{106}\text{gAg}$ value. Calculated errors are the standard deviations from the mean, and the error of the $^{109}\text{Ag}(n,2n)^{108}\text{Ag}$ reaction includes the error in the internal reference reaction.

The observed value of $0.242 \pm 0.032 \text{ mb}$ for the $^{109}\text{Ag}((n,\alpha n) + (n,n\alpha))$ reaction is well within the limit of $< 0.60 \text{ mb}$ quoted recently by Bramlitt et al⁴⁷) and would seem to be plausible enough. There is marked disagreement between the

TABLE 37

The reference reaction $^{56}\text{Fe}(n,p)^{56}\text{Mn}$

Expt. No.	Sample	No. of ^{56}Fe nuclei	A_0 cpm obs	Counter Eff	A_0 dpm abs	(Xr x λ pr)
23	Fe granules	6.060×10^{21}	1.28×10^4	0.0828	3.86×10^6	1173
24	"	5.825×10^{21}	3.76×10^4	0.0832	2.26×10^7	4386
25	"	5.086×10^{21}	2.20×10^4	0.0832	1.32×10^7	3087
26	Fe foils	4.344×10^{21}	1.10×10^5	0.0828	3.32×10^7	4134
27	"	4.749×10^{21}	7.45×10^4	0.0828	2.25×10^7	2978

$t_{1/2}^{56}\text{Mn} = 2.58$ hours.

$E_n = 14.8$ MeV

$\sigma^{56}\text{Fe}(n,p)^{56}\text{Mn} = 96.7$ mb.

TABLE 38
The $^{109}\text{Ag}(n, xn) + (n, n\alpha)$ ^{105}Rh cross-section

Expt. No.	Sample	No. of ^{109}Ag nuclei	A_o cpm _{obs}	Chem. Yield	A_o dpm _{abs}	$(Xx \lambda p)$	σ mb
23	AgNO_3	3.063×10^{21}	1.02×10^2	0.703	4.80×10^2	96.20	0.290
24	"	3.114×10^{21}	5.80×10^2	0.821	2.34×10^3	357.6	0.230
25	"	3.068×10^{21}	4.60×10^2	0.913	1.67×10^3	249.3	0.251
26	Ag foil	2.754×10^{21}	7.10×10^2	0.531	4.43×10^3	340.4	0.247
27	"	2.722×10^{21}	5.30×10^2	0.841	2.09×10^3	242.8	0.192

$t_{\frac{1}{2}}^{105}\text{Rh} = 36$ hours.

$C^{105}\text{Rh} = 0.302$

Mean value $\sigma = 0.242 \pm 0.032$ mb

TABLE 39.

The $^{109}\text{Ag}(n, \alpha)^{106\text{m}}\text{Rh}$ cross section.

Expt. No.	No. of ^{109}Ag nuclei	A_{obs} cpm	Chem. Yield	A_{obs} dpm	$(X \times \lambda p)$	σ mb
23	3.063×10^{21}	1.01×10^4	0.703	4.07×10^4	1285	1.84
24	3.114×10^{21}	7.55×10^4	0.821	2.61×10^5	4810	1.90
25	3.068×10^{21}	5.70×10^4	0.913	1.77×10^5	3388	1.96
26	2.754×10^{21}	9.30×10^4	0.531	4.96×10^5	4530	2.08
27	2.722×10^{21}	7.00×10^4	0.841	2.35×10^5	3264	1.61

$t_{1/2}^{106\text{m}}\text{Rh} = 2.2$ hours.

$C^{106\text{m}}\text{Rh} = 0.353$

Mean value $\sigma = 1.88 \pm 0.16$

TABLE 40.

The $^{109}\text{Ag}(n,p)^{109}\text{Pd}$ cross section.

Expt. No.	No. of ^{109}Ag Nuclei	A_0 cpm obs	Chem. Yield	A_0 dpm abs	$(Xx \lambda p)$	σ mb
23	3.063×10^{21}	1.39×10^4	0.504	7.79×10^4	249.7	18.1
24	3.114×10^{21}	9.90×10^4	0.524	5.34×10^5	928.0	20.2
25	3.068×10^{21}	7.30×10^4	0.706	2.92×10^5	647.7	16.9
26	2.754×10^{21}	1.56×10^5	0.652	6.76×10^5	883.1	14.5
27	2.722×10^{21}	4.25×10^4	0.224	5.30×10^5	630.1	18.8

$t_{1/2}^{109}\text{Pd} = 13.5$ hours

$C_{109}\text{Pd} = 0.354$

$C_{109}\text{Pd} = 0.358$

Mean value $\sigma = 17.7 \pm 1.9$ mb

TABLE 41

The $^{107}\text{Ag}(n, 2n)^{106}\text{gAg}$ cross section

Expt. No.	No. of ^{107}Ag nuclei	A_0 cpm obs	Chem. Yield	A_0 dpm abs	$(Xx \lambda p)$	σ mb
23	3.239×10^{21}	4.45×10^4	3.74×10^{-3}	5.41×10^7	3872	767
24	3.294×10^{21}	4.05×10^5	4.91×10^{-3}	3.75×10^8	14980	831
25	3.244×10^{21}	2.90×10^5	5.17×10^{-3}	2.55×10^8	11010	821
26	2.875×10^{21}	4.05×10^5	3.65×10^{-3}	5.04×10^8	13120	699
27	2.879×10^{21}	6.50×10^5	9.20×10^{-3}	3.24×10^8 *	10100	677

$t_{1/2}^{106}\text{gAg} = 24.4$ minutes

$C^{106}\text{gAg} = 0.220$

* $C^{106}\text{gAg} = 0.218$

Mean value $\sigma = 759 \pm 62$ mb

TABLE 42

The cross section ratio: $\frac{c^{109}_{Ag(n,2n)} c^{108}_{Ag}}{c^{107}_{Ag(n,2n)} c^{106}_{Ag}}$ $\frac{108_{Ag}}{106_{Ag}}$

<u>The $^{109}_{Ag}(n,2n)^{108}_{Ag}$ reaction</u>		<u>The $^{107}_{Ag}(n,2n)^{106}_{Ag}$ reaction</u>		$\frac{c^{108}_{Ag}}{c^{106}_{Ag}}$	
Expt. No.	No. of $^{109}_{Ag}$ nuclei	A_0 dpm obs	No. of $^{107}_{Ag}$ nuclei	A_0 dpm abs	
28	2.630×10^{21}	1.17×10^6	2.781×10^{21}	1.40×10^5	0.824
29	2.730×10^{21}	8.30×10^5	2.880×10^{21}	9.80×10^4	0.833
30	2.635×10^{21}	8.90×10^5	2.787×10^{21}	1.06×10^5	0.828

$t_{\frac{1}{2}}^{108}_{Ag} = 2.4$ minutes
 $t_{\frac{1}{2}}^{106}_{Ag} = 24.4$ minutes
 Cald. $c^{108}_{Ag} = 0.055$
 Cald. $c^{106}_{Ag} = 0.040$
 $(1 - e^{-\lambda^{108}_{Ag} T}) = 0.4387$
 $(1 - e^{-\lambda^{106}_{Ag} T}) = 0.0562$

Mean value of the cross section ratio

$= 0.828 \pm 0.004$

Cross section of the $^{109}_{Ag}(n,2n)^{108}_{Ag}$

reaction = 628 ± 51 mb.

$^{109}\text{Ag}(n, \alpha)^{106}\text{Rh}$ cross-section of 1.88 ± 0.16 mb and the values given by Mukherjee et al⁹⁰⁾ (12 ± 3 mb) and Khurana et al⁷⁹⁾ (38 ± 6). To obtain their result, Mukherjee et al resolved a gross decay curve with five components and also calculated the counter efficiency. Errors in both these operations might account for the large discrepancy.

Weight is added to the results of Coleman et al⁹¹⁾ (12.5 ± 2 mb) and Prestwood et al⁹²⁾ (14.9 ± 1.8 mb) by the present observed value of 17.7 ± 1.9 mb for the $^{109}\text{Ag}(n, p)^{109}\text{Pd}$ cross-section. The two literature values were measured at neutron energies of 14.5 and 14.68 MeV respectively so that it would seem the excitation function increases steadily over the energy range 14.5 to 14.8 MeV. Mukherjee et al obtained a value of 2.7 ± 0.5 mb at 14.8 MeV using the techniques just mentioned, which does not fit this trend at all well.

The value of 759 ± 62 mb for the $^{107}\text{Ag}(n, 2n)^{106}\text{gAg}$ cross-section is in agreement with that previously obtained by Mukherjee et al⁹⁰⁾ (662 ± 66 mb) when the errors in each result are taken into consideration, but is appreciably higher than that observed by Khurana et al⁶¹⁾ (540 ± 82 mb)* at the same neutron energy. Rayburn⁶⁰⁾ has also measured the cross-section at 14.4 MeV (889 ± 65 mb) relative to the $^{63}\text{Cu}(n, 2n)^{62}\text{Cu}$ reaction for which a cross-section of 503 ± 37 mb was assumed. This higher value might be due to uncertainty in the cross-

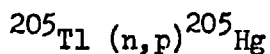
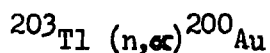
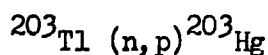
section of the reference reaction, or might represent a genuine increase of the $^{107}\text{Ag}(n,2n)^{106}\text{gAg}$ cross-section with decreasing neutron energy.

The observed cross-section of 628 ± 126 mb for the $^{109}\text{Ag}(n,2n)^{108}\text{Ag}(2.4\text{m})$ reaction agrees most closely with the 583 ± 88 * mb obtained by Khurana et al. Other values in the literature are somewhat higher, (Mukherjee et al - 883 ± 88 mb and Vonach⁹³) - 840 ± 150 mb) suggesting the possible under-estimation of counting efficiency for ^{108}Ag , by these workers.

* Recalculated relative to a value of 96.7 mb. for the $^{56}\text{Fe}(n,p)^{56}\text{Mn}$ cross-section.

6. The reactions of thallium.

The following reactions of thallium were studied:-



Samples consisting of approximately 1 gm of "Analar" grade thalious sulphate mixed with 0.5 gm of pure iron granules were irradiated for periods of 30 or 60 minutes, depending.

upon the age of the tritium target. After separation from the iron the salt was weighed and dissolved in a solution containing Au(III) and Hg(II) carriers. To facilitate rapid separation, the thallium and gold were extracted into diethyl ether, leaving mercury in the aqueous phase. Mercuric sulphide was then precipitated and used to prepare sources for end-window counting, the chemical yield of mercury being subsequently determined by titration. Other more desirable source materials, such as mercuric iodide and mercuric thiocyanate were tried, but it was found that such sources could not be prepared rapidly enough to observe the 6 minute ^{205}Hg . Gold sources consisted of the finely divided metal, precipitated under controlled conditions. The chemical yield of gold was determined by weighing, the precipitate being of gravimetric quality.

The reproducibility of the method was tested by irradiating thallic carbonate and subjecting this to the same chemical procedure. Agreement between results using this salt and those using the sulphate provided good support for the method.

The preparation of the mercury carrier solution.

A solution of mercurous nitrate was prepared by dissolving 0.5 gm of "Analar" grade mercury metal in 10 ml of 5N HNO_3 with

gentle heating. The solution was diluted with H_2O to give a concentration of approximately 1 mg Hg/ml.

The determination of the chemical yield of mercury.

The carrier solution was titrated against ammonium thiocyanate using Volhard's method⁹⁶). This provided a standardisation of the thiocyanate solution which was then used to determine the mercury in the solid sources after their dissolution. Errors in the preparation of the solutions were eliminated since the chemical yield was obtained as the ratio of two titres. Standardisation of the thiocyanate solution against the carrier was carried out at the same time as the determination of the mercury sources, to avoid systematic errors.

The mercuric sulphide sources were dissolved in the following manner⁹⁷). Each source was placed in a 100 ml Erlenmeyer flask with 5 ml of concentrated H_2SO_4 . 0.5 gm of $KMnO_4$ was then added cautiously in small portions and the walls of the flask rinsed with a further 5 ml of concentrated H_2SO_4 . The mixture was heated to boiling over a period of thirty minutes and allowed to cool. 0.5 gm of oxalic acid was added to dissolve the MnO_2 formed and the solution was evaporated to white fumes. After dissolving the residue and making the solution up to 25 ml with H_2O , aliquots were taken

for titration. During this treatment the glass filter disc was broken down to give a fine suspension which did not obviously interfere with the determination.

For the standardisation, 10 ml of the carrier solution was diluted to 50 ml to achieve a similar concentration of mercury to that obtained in the final source solutions. Both solutions were then subjected to the same titration procedure.

To 5 ml aliquots of the mercury solution were added:- 0.5 ml of 5N HNO_3 , 1 drop of 0.5% KMnO_4 solution, 1 drop of 2 volume H_2O_2 and 4 drops of ferric alum indicator. The mixture was titrated against 0.01 M NH_4SCN solution, the end-point being indicated by the first pinkish tint to persist for five minutes, after frequent agitation. Results, reproducible to within 1.5%, were obtained and the chemical yield of mercury calculated from the ratio of the titres.

The preparation of the gold carrier solution.

0.5 gm of fine gold wire (99.97% pure) was dissolved in a mixture of 8 ml of concentrated HCl , 2 ml of concentrated HNO_3 and 10 ml of H_2O , by boiling. The Au(III) solution was evaporated to near dryness on a water bath and the wet crystals dissolved in 5 ml 5N HCl . Dilution with H_2O gave

a slightly acidic solution with a known concentration in the region of 1 mg Au/ml.

The chemical separation procedure.

The chemical separation procedure was developed from information available in the literature^{98,99}) and was as follows:-

Step 1. The dissolving solution was prepared by initially adding the mercury carrier to prevent the redox reaction between Hg(I) and Au(III). 10 ml of the mercury carrier was mixed with 6 ml of concentrated HNO₃ and 8 ml of concentrated HCl, followed by the addition of 10 ml of gold carrier. The solution was then evaporated to approximately 10 ml in a 150 ml Erlenmeyer flask.

Step 2. The irradiated thallium salt was dissolved in the mixture by heating to boiling. After cooling, the solution was diluted to 20 ml and the thallium and gold extracted into 60 ml diethyl ether, saturated with 6 M HCl, in three equal portions. Both layers were retained.

Step 3. To the aqueous layer, containing the mercury, was added 1 gm Na₂CO₃ powder to neutralise excess acid. H₂S was then passed to precipitate black mercuric sulphide. After boiling to facilitate coagulation, the precipitate was

filtered, using a glass disc, washed with 5 ml 5N HCl, 5 ml H₂O, 5 ml diethyl ether and sucked as dry as possible. Final drying was carried out in the oven at 110°C and the source was counted approximately twenty minutes after the end of the irradiation.

Step 4. The combined ether phase from step 2 was washed with two 40 ml portions of 6M HCl and the washings were rejected. The thallium and gold were stripped from the ether by evaporating the organic layer over 50 ml H₂O on a water bath and by boiling the resulting aqueous solution. After transferring the hot solution to a clean beaker its volume was adjusted to 100 ml and 10 ml of 1% hydrazine hydrate solution was added. A brown precipitate of finely divided gold was obtained by boiling the mixture for approximately five minutes. The gold was filtered, washed with 20 ml H₂O, 10 ml acetone, 5 ml ether and dried in the oven at 110°C. Counting of the resulting source was commenced after about 100 minutes.

Observations.

The decay of the gold sources was followed in the end-window counter until the background level had been reached. Purely exponential curves were obtained with a half-life corresponding to the 48.4 minute ²⁰⁰Au from the ²⁰³Tl(n, α) reaction. There was no indication of the presence of the shorter lived

nuclide, ^{201}Au (26m), which would have resulted from the $^{205}\text{Tl}((n, \alpha n) + (n, n \alpha))$ or $^{203}\text{Tl}(n, ^3\text{He})$ reactions. In two cases a low residual activity of a few counts per minute was seen but this could not be identified with any certainty. The expected long-lived component was the 3.15 day ^{199}Au , from the $^{203}\text{Tl}((n, \alpha n) + (n, n \alpha))$ reaction.

Attempts were made to observe the γ -spectra of the gold sources using a NaI(Tl) crystal. The activities proved to be too low and no definite conclusions could be drawn from the ill-defined spectra obtained. It was established however, that no contaminating activities were present and in particular that there was no tendency for thallium to coprecipitate with metallic gold during the separation procedure.

Confirmation of the presence of 47 day ^{203}Hg was obtained by counting the mercury sources for periods of up to 90 days. Despite the low levels of activity a decay corresponding to this nuclide was observed on each occasion. Almost 100% of ^{203}Hg decays to the 0.279 Mev level in ^{203}Tl and attempts were made to observe the γ -transition to the ground state. These proved to be unsuccessful however, due to the low activity of the sources.

The short-lived ^{205}Hg was also easily resolved and in the three irradiations the observed half-life was found to vary by

only approximately 4%, having a mean value of 5.4 minutes. This was in closest agreement with the result of Poularikas et al¹⁰⁰) (5.45m).

In order to fix the upper limits of the $^{205}\text{Tl}((n, \alpha n) + (n, n \alpha))$, ^{201}Au and $^{203}\text{Tl}((n, \alpha n) + (n, n \alpha))$, ^{199}Au cross-sections, the maximum observable activities of the product nuclides were found by inspection of the decay curves. For the first case, increasing contributions by a hypothetical 26 minute activity were added to the observed decay until a change in the shape of the curve was just noticeable. It was found that a contribution with an initial activity equivalent to 5% of that of the ^{200}Au was the minimum value which produced a significant change. This was taken as the maximum possible activity of ^{201}Au and used to calculate the upper limit of the $^{205}\text{Tl}((n, \alpha n) + (n, n \alpha))$, ^{201}Au cross-section.

The maximum activity of ^{199}Au was estimated by assuming the limit of certain detection in the end-window counter to be 40% above the background level. A curve with the correct half-life was then fitted to the observed decay to give the initial maximum activity of ^{199}Au , and the upper limit for the cross-section was then calculated in the usual way. Since the activity of the residual component was fixed by the detection limit of the counter, the result for the upper limit of the cross-section depended upon the neutron yield in any given

experiment. Thus for higher neutron yields a lower value could be set.

Discussion.

The results are given in the following tables 43 to 48 , the errors being the standard deviations from the mean.

The observed value of 0.372 ± 0.020 mb for the $^{203}\text{Tl}(n, \alpha)^{200}\text{Au}$ cross-section agrees well with the 0.37 ± 0.4 mb obtained previously by Coleman et al⁹¹) at 14.5 MeV. Bramlitt et al⁴⁷) have also suggested an upper limit for the $^{203}\text{Tl}((n, \alpha n) + (n, n\alpha))^{199}\text{Au}$ reaction of < 0.012 mb which is of the same order as that observed (< 0.014 mb).

There is however some disagreement as regards both the (n,p) cross-sections measured. The value of 1.67 ± 0.08 mb for the $^{205}\text{Tl}(n, p)^{205}\text{Hg}$ reaction, throws little light on the discrepancy between the results of Coleman et al⁹¹) (6.8 ± 0.7 mb) and Poularikas et al¹⁰⁰) (3.0 ± 0.3 mb). The latter workers however quote a neutron energy of 14.8 MeV which is the same as that used, whereas Coleman et al again give 14.5 MeV. The two lower results in comparison with the higher value might indicate a fairly rapid variation of the excitation function of this reaction in the region of 14 MeV.

For the $^{203}\text{Tl}(n,p)^{203}\text{Hg}$ cross-section the value of 30 ± 10 mb put forward by Poularikas et al is in disagreement with the 4.23 ± 0.29 mb observed. The latter value is comparable with other (n,p) cross-sections in this mass region and would thus seem to be more reasonable.

TABLE 43

Results for the reference reaction $^{56}\text{Fe}(n,p)^{56}\text{Mn}$.

Expt. No.	No. of ^{56}Fe nuclei	A_0 cpm obs	Liquid counter efficiency	A_0 dpm A_0 obs	$(X_p \times \lambda_{pr})$
31	5.125×10^{21}	1.75×10^4	0.0832	1.05×10^7	136.1
32	4.967×10^{21}	6.50×10^3	0.0831	7.82×10^6	947.7
33	4.815×10^{21}	3.05×10^3	0.0831	3.67×10^6	1678
34	4.978×10^{21}	2.59×10^4	0.0831	3.12×10^7	5672

$t_{\frac{1}{2}}^{56}\text{Mn} = 2.58$ hours.

$E_n = 14.8$ MeV.

$\sigma^{56}\text{Fe}(n,p)^{56}\text{Mn} = 96.7$ mb.

TABLE 44

The $^{203}\text{Tl}(n, \alpha)^{200}\text{Au}$ cross section results.

Expt. No.	Sample Material	No. of ^{203}Tl nuclei	A_0 cpm obs	Chem. Yield	A_0 dpm abs	$(Xx \lambda p)$	Cross section σ mb
31	Tl_2SO_4	7.254×10^{20}	4.38×10^3	0.766	1.61×10^4	3750	0.380
32	Tl_2SO_4	7.425×10^{20}	3.05×10^3	0.752	1.14×10^4	2235	0.400
33	Tl_2SO_4	7.006×10^{20}	1.20×10^3	0.687	4.92×10^3	4166	0.359
34	Tl_2CO_3	7.823×10^{20}	1.14×10^4	0.713	4.50×10^4	14460	0.348

$t_{1/2}^{200}\text{Au} = 48.4$ minutes

$C^{200}\text{Au} = 0.355$

Mean value $\sigma = 0.372 \pm 0.020$ mb

TABLE 45

Results for the upper limit of the $^{203}\text{Tl}(n,\alpha) + (n,n\alpha)$ ^{199}Au cross-section

Expt. No.	No. of ^{203}Tl nuclei	Max A_0 obs	Chem Yield	A_0 dpm abs	$(\bar{x} \times \lambda p)$	σ mb
31	7.254×10^{20}	4	0.766	2.51×10	49.06	0.045
32	7.425×10^{20}	4	0.752	2.56×10	36.63	0.055
33	7.006×10^{20}	4	0.687	2.80×10	63.99	0.130
34	7.823×10^{20}	4	0.713	2.70×10	220.5	0.014

$t_{1/2}^{199}\text{Au} = 3.15$ days

$C^{199}\text{Au} = 0.208$

Mean value $\sigma < 0.014$ mb.

TABLE 46

Results for the upper limit of the $^{205}\text{Tl}((n,\alpha) + (n,n\alpha))^{201}\text{Au}$ cross-section

Expt. No.	No. of ^{205}Tl nuclei	A_0 cpm obs	Chem. Yield	A_0 dpm abs	$(X \times \lambda \times p) \dagger$	σ mb
31	1.734×10^{21}	2.19×10^2	0.766	7.90×10^2	5911	0.0050
32	1.884×10^{21}	1.53×10^2	0.752	5.62×10^2	3109	0.0056
33	1.674×10^{21}	6.00×10	0.687	2.41×10^2	5721	0.0054
34	1.873×10^{21}	5.70×10^2	0.713	2.21×10^3	18060	0.0057

$t_{1/2}^{201}\text{Au} = 26$ minutes

$C^{201}\text{Au} = 0.362$

Mean value $\sigma < 0.0050$ mb.

TABLE 47

The $^{203}\text{Tl}(n,p)^{203}\text{Hg}$ cross-section results.

Expt. No.	No. of ^{203}Tl nuclei	A_0 cpm obs	Chem Yield	$C^{203}\text{Hg}$	A_0 dpm abs	$(\bar{X} \times \lambda p)$	σ mb
31	7.254×10^{20}	2.14×10	0.822	0.154	1.69×10^2	3.296	4.54
32	7.425×10^{20}	1.69×10	0.790	0.160	1.34×10^2	2.467	4.26
33	7.006×10^{20}	7.00	0.680	0.170	6.06×10	4.306	4.28
34	7.823×10^{20}	5.28×10	0.569	0.182	5.10×10^2	14.85	3.84

$t_{1/2}^{203}\text{Hg} = 47$ days

Mean value $\sigma = 4.23 \pm 0.29$ mb

TABLE 48

The $^{205}\text{Tl}(n,p)^{205}\text{Hg}$ cross-section results.

Expt. No.	No. of ^{205}Tl nuclei	A_0 cpm obs	Chem. Yield	A_0 dpm abs	$(X \times \lambda p)$	σ mb
31	1.734×10^{21}	1.42×10^5	0.822	4.77×10^5	10200	1.73
32	1.884×10^{21}	5.03×10^4	0.790	1.76×10^5	3494	1.56
33	1.674×10^{21}	1.92×10^4	0.680	7.80×10^4	5772	1.72

$t_{1/2} \text{ } ^{205}\text{Hg} = 5.4$ minutes

$C \text{ } ^{205}\text{Hg} = 0.362$

Mean value $\sigma = 1.67 \pm 0.08$ mb.

CHAPTER 4.The Discussion1. An assessment of the experimental techniques

All the cross-section measurements have been related to either one or the other of the two reference reactions, $^{56}\text{Fe}(n,p)^{56}\text{Mn}$ and $^{27}\text{Al}(n,\alpha)^{24}\text{Na}$, so providing a consistent set of results. The absolute values of the cross-sections of these reactions, used throughout this work, had previously been measured, together with the cross-section ratio, by the associated particle method described briefly in chapter 2 (p.31). Recently, support has also been given to the validity of these values by the work of Williams¹⁰²) in this laboratory, who has measured the absolute $^{56}\text{Fe}(n,p)^{56}\text{Mn}$ cross-section by an independent method involving the detection of the recoiling α -particles from the $\text{T}(d,n)^4\text{He}$ reaction by means of a silicon solid-state counter. His result of 98.3 ± 5.4 mb for the cross-section is in agreement with the value of Hemingway et al³⁰ when the errors in each measurement are taken into account. The problem of introducing the reference materials into the samples has been overcome by using homogeneous-mixture and sandwiched-foil techniques, the success of which is reflected by the reproducibility of the results. While such techniques have been widely used by other workers:

the values taken for the cross-sections of the reference reactions have frequently not had such a reliable basis as those used in the present work. Also, many workers have employed the more ideal procedure of relating individual measurements to convenient internal reference reactions, that is, reactions other than those of immediate interest also occurring in the sample element, with an appreciable cross-section. However, the advantages gained by this method, which ensures a perfectly homogeneous mixture, have often been lost by then placing reliance upon cross-section values for the chosen reactions, determined in other laboratories in a variety of ways, to calculate the results, with little attempt at interrelation. In two cases in this work, (the reactions of gallium and silver) use has been made of convenient internal references but ultimately these have been related directly to one or other of the secondary standards mentioned above.

With regard to the identification of the product nuclides, the use of gamma spectroscopy has proved to be invaluable. In conjunction with half-life determinations and radiochemical separations, it has provided good confirmatory evidence and is thought to be a substantial improvement on much previous work, where, on occasions, the determination of half-lives only has been relied upon.

Although it has not been possible to make such measurements in the present studies, it is realised that the determination of β -spectra would have been extremely useful for the more definite identification of those nuclides for which gamma spectroscopy could not be used conveniently.

The calibration of the proportional counter in terms of the average β -energy, rather than the β end-point energy - the method which has been widely used in the past, is considered to be a step forward, since it is probable that this has enabled better interpolations to be made from the average energy versus efficiency curves. It is also of interest to compare the calibrated counting efficiencies with those which had, of necessity, to be calculated using the empirical data of Burt³⁸) and of Gleason et al³⁷), in the early work. Although the accuracy which can be claimed for the latter estimates is lower than that for the calibrations, the correspondence between the values is remarkably good, indicating the validity of the assumptions made in the calculations.

In the tables of collected results which follow, the errors given are the standard deviations from the mean, except in those cases where a lower accuracy is claimed and where an estimate has been made of the overall experimental error. No allowance has been made for

systematic errors or the errors in the cross-sections of the secondary standard reactions when calculating the standard deviations. The values which are obtained result from uncertainties in the determination of the chemical yields and the neutron flux, together with the statistical errors in the measurement of the product activities.

For completeness, the number of observations made for each result is also recorded in the tables.

2. The collected results and the discussion.

As mentioned in the introduction, it is particularly in the case of the (n, charged particle) reactions which occur at an energy of 14 MeV, where large discrepancies have been found between the observed values and the theoretical values of the cross-sections calculated on the basis of an evaporation from a compound nucleus. Generally, the observed cross-sections of these reactions become larger than those calculated as the atomic number of the target element increases. This is because the compound nucleus theory favours the production of low energy secondary particles and when these are charged, their emission is more effectively suppressed by the Coulomb barrier at high atomic numbers. The direct interaction theory, which allows for the increased probability that more energetic secondary particles, with a better chance of

negotiating the Coulomb barrier, are produced, has been introduced to explain these deviations. It has been suggested that over the mass range both types of mechanism contribute to the overall reaction, the relative contribution by each being determined principally by the height of the Coulomb barrier.

There can be little doubt that to consider the direct mechanism as being entirely separate from the evaporative process is an oversimplification of the problem. In the general sense, the mechanisms are perhaps considered to be examples of the two extremes of the actual situation. In practice, the overall mechanism in most nuclear reactions is probably, somewhere between the two extremes. Cindro¹⁰³) in a recent survey of the trends in the study of fast neutron-induced reactions, refers to the intermediate mechanism put forward by Izumo¹⁰⁴). Izumo visualises the attainment of a partial equilibrium in which the interacting nucleons are not necessarily localised but can be distributed throughout the nuclear volume. It is assumed that the reaction then takes place after partial equilibrium has been reached in a time several orders of magnitude shorter than for the compound nucleus process but much longer than the nuclear transit time. The order of time suggested for such an intermediate process is

10^{-20} sec. Further, the nucleons in the target nucleus are assumed to be divided into two groups - those in an inert core and those in outer regions. Izumo suggests that only the outer nucleons interact while the inert core remains in the ground state.

It is difficult, as yet, to make predictions of cross-sections using such a relatively complicated model and in the present discussion the extreme cases of the compound nucleus and direct mechanisms have been resorted to as a basis for comment.

Looking first at the results of the $(n,2n)$ cross-sections, these are consistent with the accepted view that the compound nucleus model accounts well for the values over most of the mass range. The collected results appear in table 49. They are also plotted versus the mass number of the target nucleus in fig 36, together with a compilation of the results of many other workers. It can be seen from the figure that the present results fit the overall trend well. Over the mass range, the $(n,2n)$ cross-sections show an initial steep rise from values of a few millibarns for the light nuclei, up to a value of about 1500 mb, in the region of $A \approx 70$. From then on, the cross-sections lie on a plateau, remaining fairly constant over the rest of the mass-range. The initial rise can be explained

TABLE 49

The (n, 2n) cross-sections

Reaction	E _n MeV	σ _{obomb}	No. of observations	σ _{calc} ^{mb} ‡	$\frac{\sigma(n, 2n)_{obs}}{\sigma(n, 2n)_{calc}}$
⁶⁹ Ga(n, 2n) ⁶⁸ Ga	14.7	621 ± 124	3	970	0.64
⁷⁰ Ge(n, 2n) ⁶⁹ Ge	14.8	642 ± 45	3	840	0.76
⁷⁶ Ge(n, 2n) ⁷⁵ Ge	14.8	1105 ± 41	3	1500	0.74
¹⁰⁷ Ag(n, 2n) ^{106g} Ag	14.8	759 ± 62	5	1880	0.40
¹⁰⁹ Ag(n, 2n) ^{108g} Ag	14.8	628 ± 126	3	1850	0.34

‡ Calculated by Khurana and Hans⁶¹)

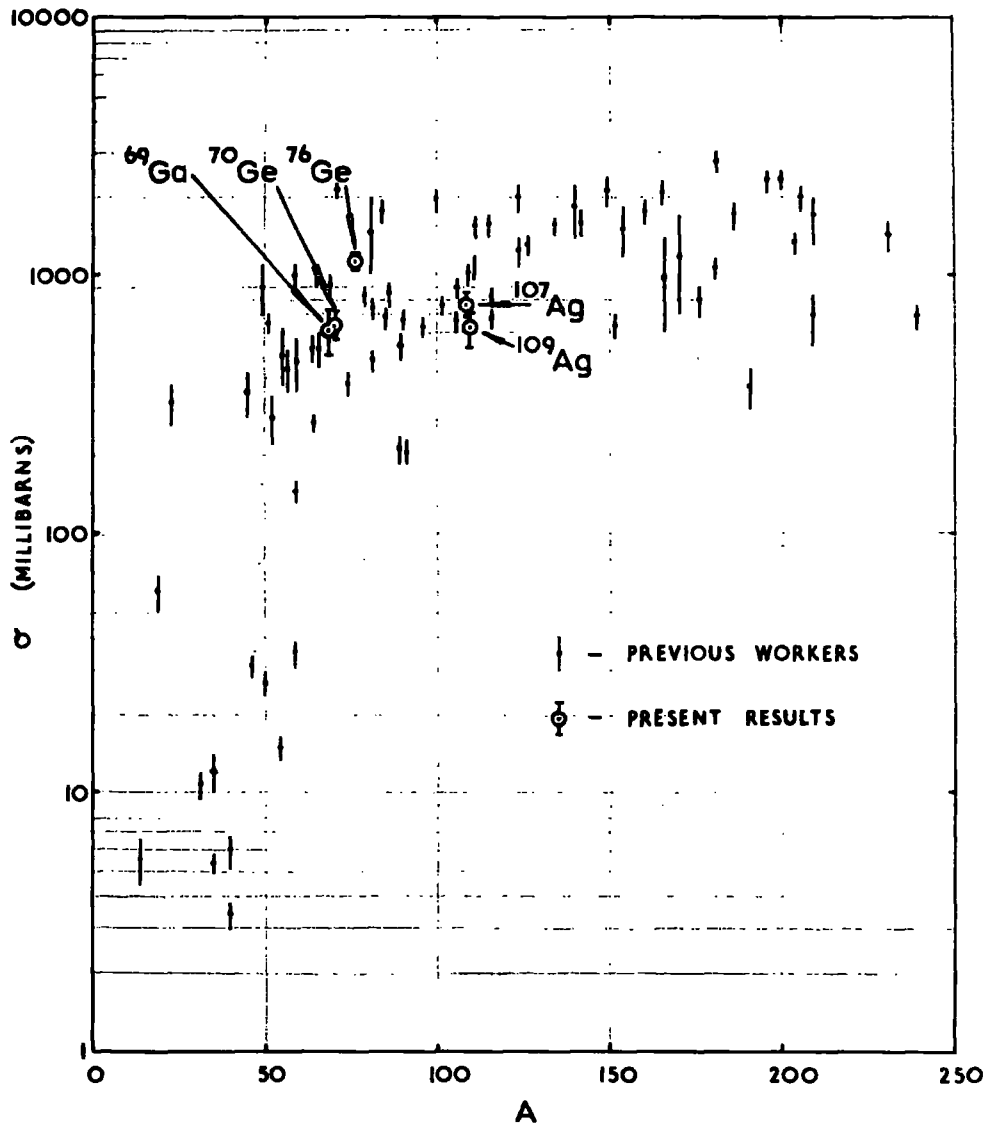


FIG 36 OBSERVED (n,2n) CROSS-SECTIONS AS A FUNCTION OF A, THE MASS NUMBER.

by competition from the (n, α) and (n, p) reactions which are favoured in the case of the light elements, by the relatively low Coulomb barrier.

In order to examine the present values in greater detail, they are compared with the theoretical values given by Khurana and Hans⁶¹), which are also included in table 49. The calculations made by these workers were based on the statistical model and the level density formula of Newton was used to take into account shell effects. It can be seen that in all cases, the ratio $\frac{\sigma(n, 2n)_{\text{obs}}}{\sigma(n, 2n)_{\text{calc}}}$ is less than unity. A contributory factor in the cases of ^{107}Ag and ^{109}Ag , where the ratios are noticeably low, is that only one of two possible isomeric products was observed. In the other cases, which represent the total cross-sections, there seems to be a fairly constant relationship between the observed and theoretical values, the former always being slightly lower. An explanation for such low observed values, which has been put forward by Weisskopf¹⁰⁵), is that the compound nucleus might decay before all the incoming excitation energy has been distributed evenly throughout the nucleus. Thus, the initially emitted neutron might be more energetic than expected from the compound nucleus model, leaving the residual nucleus in a low state of excitation, so

reducing the probability of the second neutron being emitted.

Taking into account the simplicity of the theoretical picture and the accuracy with which measurements can be made, it can be concluded that the compound nucleus model is a good representation of the mechanism involved in most $(n,2n)$ reactions. The deviations, which have been pointed out however, would indicate that further refinement of the theory is required to take account of the non-statistical distribution of energy in the excited nucleus, although it is not clear how such a complex problem might be resolved.

The observed cross-sections of the (n,p) reactions are collected in table 50. Together with many previous values, they are also plotted as a function of the mass number of the target nucleus in fig. 37. From the graph, it can be seen that all the present values, excepting that for ^{85}Rb , fit the accepted trend well. Since only the one isomer, ^{85m}Kr was observed from the $^{85}\text{Rb}(n,p)^{85}\text{Kr}$ reaction, the cross-section value must be regarded as a lower limit. This is a feasible explanation for the low value in this case. The deviation is, however, quite marked and this would suggest that the reaction proceeds predominantly to the ground state, ^{85}Kr . König⁶⁹)

TABLE 50

The (np) cross-sections

Reaction	E_n MeV	σ_{obs} mb	No. of observations
$^{69}\text{Ga}(n, p)^{69m}\text{Zn}$	14.7	18.2 ± 3.6	3
$^{72}\text{Ge}(n, p)^{72}\text{Ga}$	14.8	35.0 ± 1.7	3
$^{73}\text{Ge}(n, p)^{73}\text{Ga}$	14.8	34.3 ± 0.9	3
$^{85}\text{Rb}(n, p)^{85m}\text{Kr}$	14.7	2.41 ± 0.72	4
$^{87}\text{Rb}(n, p)^{87}\text{Kr}$	14.7	13.2 ± 4.0	4
$^{109}\text{Ag}(n, p)^{109}\text{Pd}$	14.8	17.7 ± 1.9	5
$^{203}\text{Tl}(n, p)^{203}\text{Hg}$	14.8	4.23 ± 0.29	4
$^{205}\text{Tl}(n, p)^{205}\text{Hg}$	14.8	1.67 ± 0.08	3

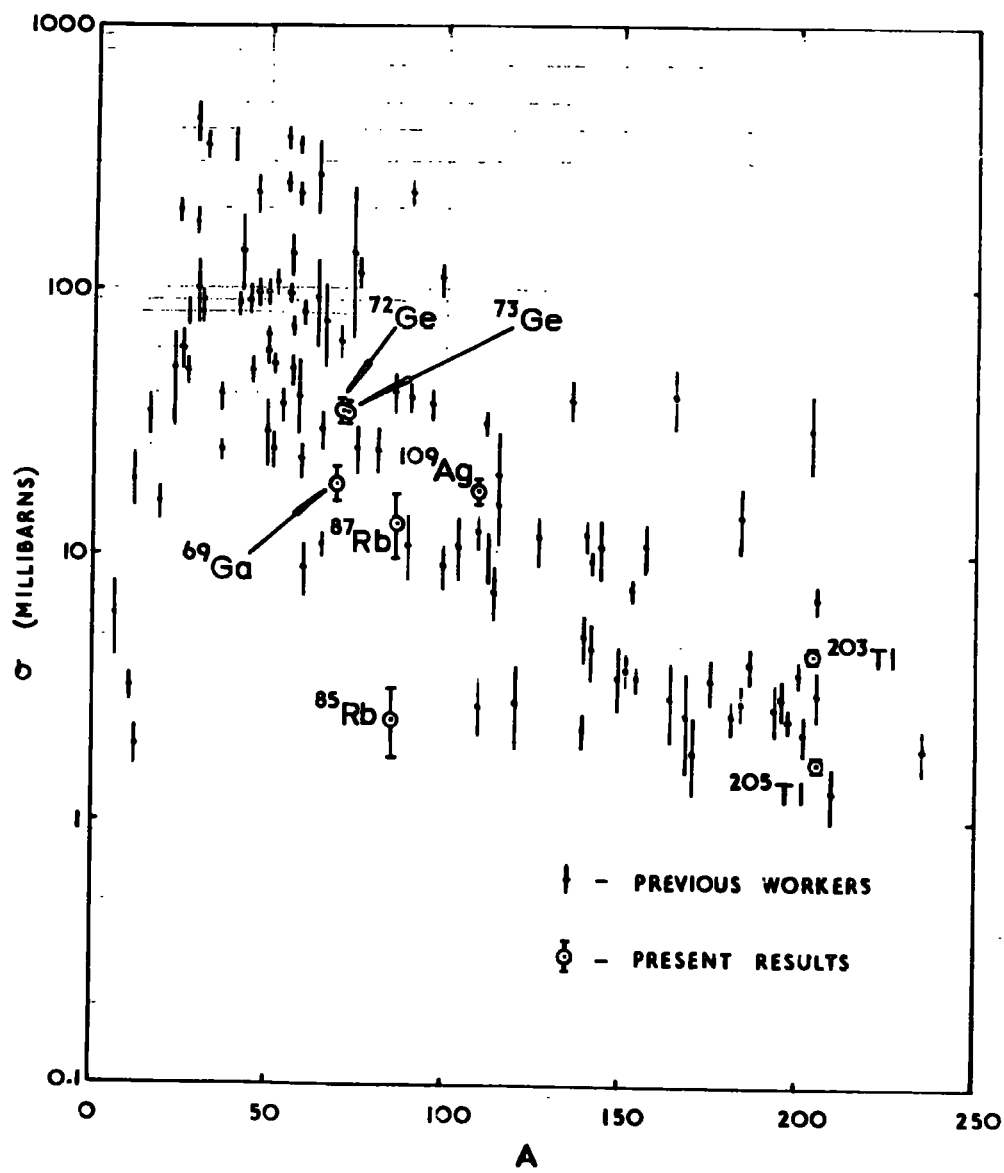


FIG 37 OBSERVED (n,p) CROSS-SECTIONS AS A FUNCTION OF A, THE MASS NUMBER.

has recently examined the total (n,p) cross-section in natural rubidium by a secondary particle method and has obtained a value of ≈ 42 mb at 14.7 MeV. In conjunction with the present results this gives a value of approximately 50 mb for the $^{85}\text{Rb}(n,p)^{85}\text{gKr}$ cross-section after making allowance for the natural abundances of ^{85}Rb (72.2%) and ^{87}Rb (27.8%).

From the trend of the (n,p) cross-sections the effect of the Coulomb barrier is immediately apparent, manifesting itself as a steady decrease in magnitude of the cross-sections with increasing Z. For nuclides with mass numbers of $A \leq 100$, it is already well established that the observed cross-sections can be predicted quite well by the compound nucleus model, which takes into account the effect of the Coulomb barrier. For target nuclides above $A \approx 100$, the observed cross-sections become larger than those predicted by this model, as direct effects increase in importance.

In table 51 the (n,p) cross-sections are compared with the values predicted by the theory of Brown and Muirhead³) which accounts for a contribution by direct interactions to the overall reaction mechanism. Essentially, the theoretical cross-sections are made up of two independent components, one due to evaporative processes and one due to direct processes. Also the theory allows for direct

TABLE 51

A comparison of the (n,p) cross-sections with theoretical values

Reaction	Brown and Muirhead ³⁾		Gardner ²⁰⁾	
	$\sigma_{\text{calc}}(\text{mb})$	$\frac{\sigma(n,p)_{\text{obs}}}{\sigma(n,p)_{\text{calc}}}$	$\sigma_{\text{empirical}}(\text{mb})$	$\frac{\sigma(n,p)_{\text{obs}}}{\sigma(n,p)_{\text{empirical}}}$
$^{69}\text{Ga}(n,p)^{69\text{m}}\text{Zn}$	30	0.61	40	0.46
$^{72}\text{Ge}(n,p)^{72}\text{Ga}$	30	1.17	25	1.40
$^{73}\text{Ge}(n,p)^{73}\text{Ga}$	36	0.95	12	2.9
$^{85}\text{Rb}(n,p)^{85\text{m}}\text{Kr}$			32	0.08
$^{87}\text{Rb}(n,p)^{87}\text{Kr}$			8	1.65
$^{109}\text{Ag}(n,p)^{109\text{d}}\text{Pd}$	21.8*	0.81	10	1.77
$^{203}\text{Tl}(n,p)^{203}\text{Hg}$			4.5	0.94
$^{205}\text{Tl}(n,p)^{205}\text{Hg}$	2.6*	0.64	1.1	1.51

* Calculated by Coleman and Hawker⁹¹⁾ using the Brown and Muirhead model.

interactions with protons throughout the nuclear volume.

It can be seen in those cases where a comparison has been made, that the ratio $\frac{\sigma^{(n,p)}_{\text{obs}}}{\sigma^{(n,p)}_{\text{calc.}}}$ has a value in

the region of unity. The low value in the case of $^{69}\text{Ga}(n,p)^{69\text{m}}\text{Zn}$ cross-section is again somewhat misleading, since only one of two possible isomeric reaction products was observed. While there is some spread in the remaining values of the ratio, the agreement, considering the widely different masses of the target nuclei, is good.

In the same table the (n,p) cross-sections are also compared with the values predicted by Gardner²⁰). He has attempted to make a systematic assessment of all the available (n,p) cross-sections which have been measured and has derived empirical equations from collected results which relate the cross-sections for different elements over almost the whole mass range. Remembering the large discrepancies which have often occurred between measurements made in different laboratories, the difficulty of such an assessment can be realised. It would seem, however, from the variation of the ratio of $\frac{\sigma^{(n,p)}_{\text{obs}}}{\sigma^{(n,p)}_{\text{emp.}}}$ in the case of the present results, that the predictions made on this basis are not so satisfactory as those using the more rigorous approach. Neglecting the low values of

the $^{69}\text{Ga}(n,p)^{69\text{m}}\text{Zn}$ and $^{85}\text{Rb}(n,p)^{85\text{m}}\text{Kr}$ reactions, where a comparison is difficult, the variation in the ratio is certainly much more pronounced than that with Brown and Muirhead's model. It is interesting to note that whereas for the $^{73}\text{Ge}(n,p)^{73}\text{Ga}$ reaction there is a large discrepancy between the cross-section predicted by Gardner, who takes into account the Levkovskii trend, and the present result, Brown and Muirhead's model predicts the cross-section very closely.

It is concluded that the theory put forward by Brown and Muirhead is a good representation of the reaction mechanisms contributing to (n,p) reactions and still appears to be the more useful of the two approaches.

The results of the (n, α) cross-section measurements are given in table 52. They are also plotted in the same way as the (n,2n) and (n,p) cross-sections, as a function of the mass number of the target nucleus in fig. 38. Included for comparison in this figure are many previous values obtained by other workers. The effect of the Coulomb barrier is, as would be expected, more pronounced than for the (n,p) reactions.

It can be seen that the present results follow the general trend, but a notable feature is that they all lie on the lower side of the spread of previous values. A

TABLE 52

The (n, α) cross-sections

Reaction	E_n Mev	σ_{obs} (mb)	No. of observations	σ_{calc} (Mb)	$\frac{\sigma(n, \alpha)_{obs}}{\sigma(n, \alpha)_{calc}}$
$^{65}\text{Cu}(n, \alpha)$	14.7	8.54 ± 0.53	2	8.5^B	1.00
$^{74}\text{Ge}(n, \alpha)$	14.8	3.53 ± 0.11	3		
$^{85}\text{Rb}(n, \alpha)$	14.7	4.37 ± 0.25	4	4.12^S	1.06
$^{87}\text{Rb}(n, \alpha)$	14.7	1.07 ± 0.01	4	0.27^B	3.96
$^{109}\text{Ag}(n, \alpha)$	14.8	1.88 ± 0.16	5	1.3^B	1.45
$^{203}\text{Tl}(n, \alpha)$	14.8	0.372 ± 0.020	4	0.0005^B	744

B - calculated by Bramlitt et al⁴⁷S - calculated by Strohal et al⁶²

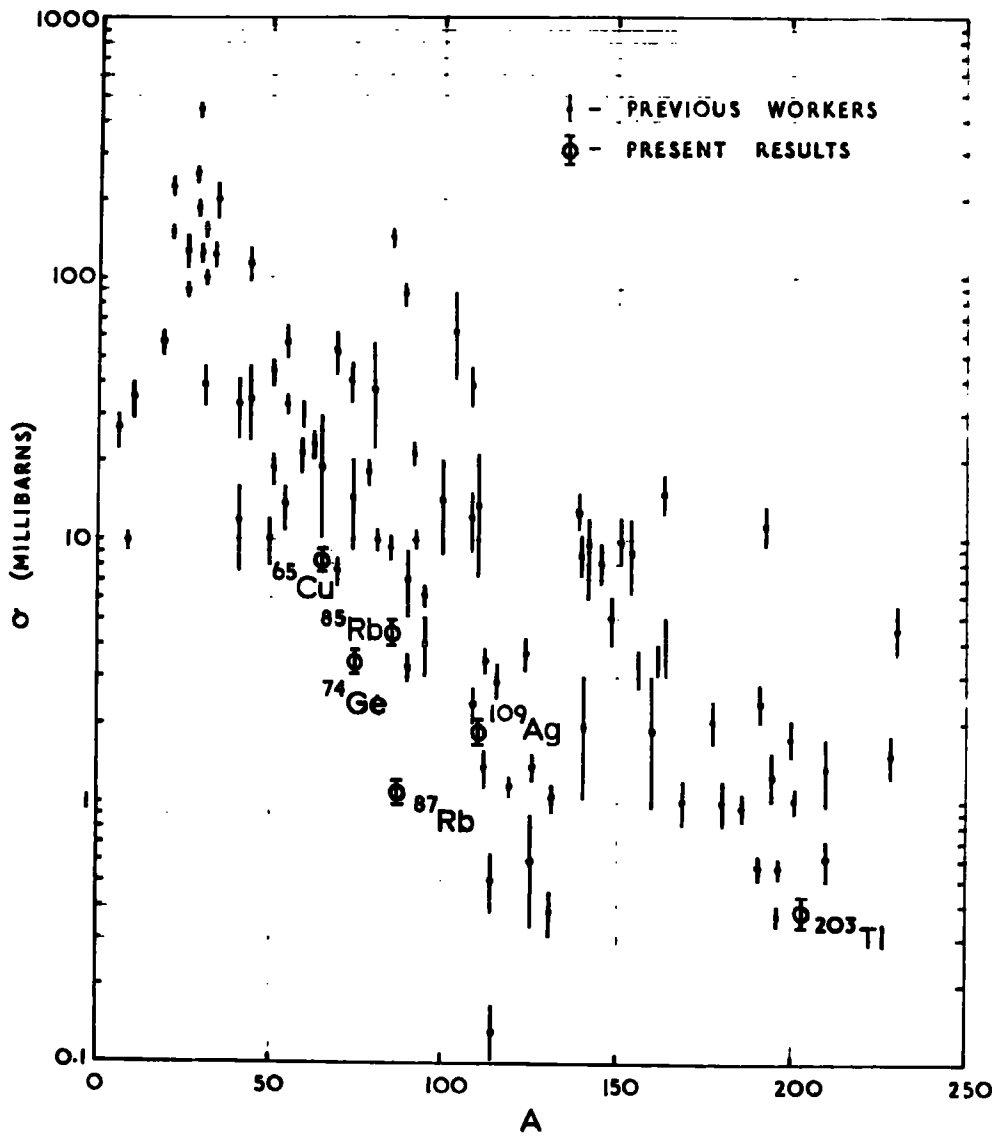


FIG 38 OBSERVED (n, α) CROSS-SECTIONS AS A FUNCTION OF A , THE MASS NUMBER.

contributory factor in the cases of ^{65}Cu , ^{74}Ge , ^{87}Rb and ^{108}Ag , is that only one of two possible isomeric reaction products, each decaying by β^- -emission was observed, so that these cross-sections are lower limits only.

It is now generally known that for target nuclides up to approximately $A=60$, the theoretical cross-sections calculated using the compound nucleus model agree well with the observed values. Also, at the closed neutron shells ($N=50, 82$ and 126) maxima are observed in the (n, α) values, since the effect of the (n, n') reaction, which predominantly competes, is reduced. These maxima are also predicted well by the compound nucleus model. In the remaining regions, the observed cross-sections become larger than the theoretical values, often by several orders of magnitude for the heaviest elements, indicating the inadequacy of the theoretical treatment. The present (n, α) cross-sections are compared with theoretical values of the total cross-sections calculated using the evaporation model in table 52. The only result where there is close agreement is that for $^{85}\text{Rb}(n, \alpha)^{82}\text{Br}$, for which the ratio, $\frac{\sigma(n, \alpha)_{\text{obs}}}{\sigma(n, \alpha)_{\text{calc}}}$, has a value near unity. This particular result contrasts with the much higher value obtained by Strohal et al⁶²) (p.97) and provides strong evidence that the maximum in the (n, α) cross-sections

observed in the region of the closed neutron shell ($N = 50$) is by no means as pronounced as they suggest. Although the results for the $^{65}\text{Cu}(n, \alpha)^{62g}\text{Co}$ and $^{109}\text{Ag}(n, \alpha)^{106}\text{Rh}$ reactions at first sight seem to be in good agreement with the theory, it must be remembered that they represent lower limits only, so that in practice the ratio is probably larger. The disagreement of the last result for $^{203}\text{Tl}(n, \alpha)^{200}\text{Au}$ is outstanding, and is indicative of the order of the discrepancies found for some of the heaviest elements. Generally, the results seem to show the well-established trend of increasing divergence from the predictions of the statistical theory with increasing Z .

Since the emission of low energy α -particles by evaporation is expected to be strongly inhibited in the regions of high Z , the enhancement of the observed cross-sections has, in analogy with the (n,p) reactions been attributed to direct interactions which can give rise to α -particles sufficiently energetic to negotiate the Coulomb barrier. The situation for these particles is however by no means as simple as for protons and this is perhaps borne out by the fact that no quantitative theoretical treatment has yet been developed for direct interactions involving them.

The rarer reaction $((n, \alpha n) + (n, n \alpha))$, is closely linked with the (n, α) reaction and its study allows some comments to be made about the likelihood of direct processes. Since there are no bound states of ^5He and knockout or pick-up processes are precluded, the reaction can be considered to involve two steps. The overall mechanism can thus be envisaged either as two evaporation steps, or as a direct interaction followed by an evaporation. If this is the case, the cross-section of the reaction, in relation to the (n, α) cross-section gives an indication of the excitation level of the residual nucleus after the emission of the first particle has taken place.

It is necessary to establish which of the possible routes, $(n, \alpha n)$ or $(n, n \alpha)$, the rare reaction takes. At first sight, the emission of the α -particle might be expected to follow an $(n, n \alpha)$ reaction, since the emission of a neutron is unaffected by the Coulomb barrier and therefore is much more likely to occur initially. For the α -particle to compete successfully with the emission of a proton or a neutron after the emission of the initial neutron however, the alpha separation energy must be much less than both the neutron and proton separation energies. This is invariably so for the neutron separation energy but not always for the proton separation energy. In the latter

case, the $(n, n\alpha)$ reaction cannot compete successfully with the (n, np) reaction and thus the $(n, \alpha n)$ process is probably the predominant route.

The results of the $((n, \alpha n) + (n, n\alpha))$ reactions are given in table 53. Generally, the results show the expected trend due to the effect of the rising Coulomb barrier, decreasing in magnitude as Z increases. In the cases of ^{65}Cu , ^{71}Ga and ^{109}Ag , the observation that the reaction has an appreciable cross-section points to a substantial contribution by an evaporation process to the (n, α) and $((n, \alpha n) + (n, n\alpha))$ reactions of these elements. It would seem that the initial (n, α) reaction involves a low energy α -particle (in comparison with a direct process) and leaves the residual nucleus with a sufficiently high excitation energy to make the emission of a further neutron fairly probable.

The difficulty of observing the reaction in the remaining cases of ^{76}Ge , ^{87}Rb , ^{203}Tl and ^{205}Tl and the low upper limits which have been established, are consistent with a marked contribution by direct interactions. According to Butler¹⁰⁶), direct processes can be expected to leave the residual nucleus in a low state of excitation, most of the incident energy being carried away by the outgoing particle. Direct (n, α) reactions in these nuclides

would thus leave the residual nucleus with insufficient energy to emit a further neutron and give an $(n, \alpha n)$ reaction.

TABLE 53

The $(n, \alpha n) + (n, n \alpha)$ cross sections

Reaction $\#$	E_n Mev	$\sigma_{\text{obs}}^{\text{mb}}$	No. of observations
$^{65}\text{Cu}(n, \alpha n) ^{61}\text{Co}$	14.7	1.01 ± 0.05	3
$^{71}\text{Ga}(n, \alpha n) ^{67}\text{Cu}$	14.7	1.23 ± 0.22	5
$^{76}\text{Ge}(n, \alpha n) ^{72}\text{Zn}$	14.8	< 0.59	3
$^{87}\text{Rb}(n, \alpha n) ^{83}\text{Br}$	14.7	< 0.052	3
$^{109}\text{Ag}(n, \alpha n) ^{105}\text{Rh}$	14.8	0.242 ± 0.32	3
$^{203}\text{Tl}(n, \alpha n) ^{199}\text{Au}$	14.8	< 0.014	4
$^{205}\text{Tl}(n, \alpha n) ^{201}\text{Au}$	14.8	< 0.0050	4

$\#$ The total reaction $((n, \alpha n) + (n, n \alpha))$ is written as $(n, \alpha n)$ for brevity.

BIBLIOGRAPHY

1. J.N. MASSOT et al AEC acc. no. 34769. Rept. No.
N.P. 14085 Available AEC 109 pp.
(1963)
2. J.N. MASSOT et al Nucl. Phys. 58(2) 273-82 (1964)
3. G. BROWN and H. MUIRHEAD Phil. Mag. 2, (16) 473 (1957)
4. W. TOBOCMAN Theory of direct nuclear reactions.
Oxf. Univ. Press. (1961)
5. M.D. GOLDBERG Progress in fast neutron physics.
Univ. Chicago Press (1963). p. 5.
Ed. G.C. Philips, J.B. Marion, J.R. Risser.
6. M.D. GOLDBERG. Ibid. p. 16.
7. J.L. PERKIN, L.P. O'CONNOR and R.F. COLEMAN. Proc.
Phys. Soc. 72, 505 (1958)
8. M. SAKISAKA J. Phys. Soc. Japan 14, 554-63
(1959)
9. W.PATZAK and H. VONACH Oesterr. Akad. Wiss. Math-
Naturw. 203-9 (1961)
10. J.C. ROBERTSON Nucl. Phys. 49(2) 306-14 (1963)
11. G. MARCAZZAN et al Nuovo Cimento 20, 903-13 (1961).
12. H. FARRAR, W.B. CLARKE, H.G. THODE and R.H. TOMLINSON.
Can. J. Phys. 42, 2063 (1964)
13. M. BORMANN Nucl. Phys. 65(2) 257-74. (1965).
14. S. PEARLSTEIN. U.S. At. En. Comm. BNL 897 (1964)
15. L.P. O'CONNOR et al J. Inorg and Nucl. Chem. 13,
5-12 (1960)

16. L.A. RAYBURN. Proc. Conf. Direct Interactions
Nuclear Reaction Mech. Int. Phys.
Univ. Padua (1962) 322-4.
17. J. PICARD and C.F. WILLIAMS. Nucl. Phys. 63(4)
673-84 (1965)
18. D.W. BARR et al Phys. Rev. 123, 859-64 (1961)
19. R.J. PRESTWOOD and B.P. BAYHURST Phys. Rev. 121,
1438-41 (1961)
20. D.G. GARDNER Nucl. Phys. 29, 373-99 (1962)
21. A. CHATERJEE Nucl. Phys. 60(2) 273-93 (1964)
22. L. COLLI Progress in fast neutron physics
Univ. Chicago Press (1963) p.9.
Ed. G.C. Philips, J.B. Marion, J.R. Risser.
23. E. SAETTA-MENICHELLA et al. Nucl. Phys. 51(3)
449-59 (1964)
24. U. FACCHINI et al Ibid. 460-9
25. G.S. MANI and I. IORI Nuovo Cim. (10) 32; 1092-1102 (1964)
26. A. CHATERJEE Nucl. Phys. 47(3) 511-20 (1963)
27. A. CHATERJEE Nucl. Phys. 49(4) 686-93 (1963)
28. D.G. GARDNER Nucl. Phys. 60(1) 49-64 (1964)
29. M. BORMANN et al Z. für Physik 166, 477-93 (1962)
30. J.D. HEMINGWAY, R.H. JAMES, E.B.M. MARTIN and G.R. MARTIN
Proc. Royal Society Series A. 1429,
vol. 292, 180. (1966).
31. E.B.M. MARTIN Londonderry Laboratory for
Radiochemistry Handbook. Durham
University.

32. J.H. DAVIES. Ph.D. Thesis Sept. 1960 Durham University
33. WILSON and EVANS Atomics 9, 238 (1958)
34. J.L. FOWLER and J.E. BROLLEY Jr. Revs. Mod. Phys. 28, (2) 103 (1956)
35. Interpolated data from UCRL-4266.
36. BLACKMAN See ref. 38
37. T.H. GLEASON, M.N. TAYLOR and P. TABERN Nucleonics 8, No. 5, 12 (1951)
38. B.P. BURTT Nucleonics 5, No. 2. 28 (1949)
39. B.P. BAYHURST and R.J. PRESTWOOD Nucleonics 17, No. 3, 82-85 (1959)
40. B.D. PATE and L. YAFFE Can. J. Chem. 33, (15) 610 and 1656 (1955). Ibid 34, 265 (1956)
41. Radiochemistry of copper NAS-NS 3027
42. Radiochemistry of nickel NAS-NS 3051
43. Radiochemistry of cobalt NAS-NS 3041
44. H. FLASCHKA Microchemie ver Mikrochim. Acta 39, 38-50 (1952) (C.A. 46. 4953 (1952))
45. E.T. BRAMLITT, R.W. FINK, D.G. GARDNER and A. POULARIKAS Phys. Rev. 125, 297 (1962)
46. J. KANTELE and D.G. GARDNER Annual Progress report 277 (1962) Contr. A.T. (40-1) Univ. of Arkansas.

47. E.T. BRAMLITT and R.W. FINK. Phys. Rev. 131 (6)
2649-63.
48. M. BORMANN et al. Z. für Physik 166, 477-93, (1962).
49. Radiochemistry of zinc. NAS-NS 3015.
50. Radiochemistry of aluminium and gallium NAS-NS 3023.
51. The analytical uses of EDTA. F.J. WELCHER. Wiley
(1957) p. 178.
52. Ibid. p. 150.
53. G. RUDSTAM. Thesis. Univ. Uppsala. (Nuclear data sheets.
National Academy of Sciences.
N.R.C.).
54. H.T. EASTERDAY, Phys., Rev. 91, 653. (1953).
55. H.H. HOPKINS Jr. Phys. Rev. 77, 717 (1950).
56. Priv. comm. E.B.M. MARTIN
57. G. FRIEDLANDER AND J.W. KENNEDY, Nuclear and radiochemistry
Wiley (1960).
58. E.B. PAUL and R.L. CLARKE, Can. J. Phys. 31, 267 (1953).
59. M. CEVOLANI, Nuovo Cim. 26, (6) 1328. (1962).
60. L.A. RAYBURN, Phys. Rev. 122, 168. (1961).
61. C.S. KHURANA and H.S. HANS, Nucl. Phys. 28, 560. (1961).
62. P. STROHAL, N. CINDRO and B. EMAN, Nucl. Phys. 30
49-67 (1960).
63. Radiochemistry of sodium, potassium and rubidium.
NAS-NS 3053.
64. Radiochemistry of fluorine, chlorine, bromine and
iodine, NAS-NS 3005.

65. FLASCHKA and HUDITZ. Z. Analyt. Chem. 137, 104-7
(1962). Am. Chem. Abs.
Vol. 47, 443 (1953).
66. Inorganic syntheses. Vol. II, p. 227 McGraw-Hill Book
Co. Inc. (1946). Ed. W.C. Fernelius.
67. V.N. LEVKOVSKII. Doklady Akademii Nauk SSSR 113, 1032
(1957).
68. A. POULARIKAS. See refs. 26 and 27.
69. V. KONIG. Nucl. Phys. 71, 497-510 (1965).
70. Methods of quant. inorg. analysis. Ed. K. KODAMA. p. 280
Interscience publishers. (1963).
71. Ibid. p. 316.
72. Radiochemistry of germanium. NAS-NS 3043.
73. W.J. LAVEN to H.J. van der BOLD. priv. comm. (see
Nuclear Data sheets, National
Academy of Science, NRC).
74. J.M. Le BLANC, J.M. CORK and S.B. BURSON, Phys. Rev.
97, 750 (1955); 94, 1436A
(1954).
75. J.M. SIEGEL and L.E. GLENDENIN. NNES 9, 549. (1950)
76. V.N. LEVKOVSKII, Atomnaya Energ. 4, 79. (1958).
77. R.H. NUSSBAUM and S.K. SURI, Phys. Rev. 105, 1272 (1958).
78. H.H. HOPKINS and A.B. SMITH, Phys. Rev. 84, 289, (1951).
79. C.S. KHURANA and H.S. HANS, Proc. Symp. Low Energy
Nucl. Phys. Waltair 297 (1960).

80. C.W. ZABEL, WASH 191 (1956).
81. V.N. LEVKOVSKII Soviet Phys. JETP 6, 1174 (1958) 4,
291 (1957).
82. R.L. HARRIS and D.E. RYAN, Can. J. Research. 27 (2)
72.
83. Applied inorg. analysis HILLEBRAND, LUNDELL, BRIGHT
and HOFFMAN, Wiley, 2nd Ed.
p. 380. (1959).
84. Ibid. p. 379.
85. Radiochemistry of rhodium NAS-NS 3008.
86. Radiochemistry of palladium. NAS-NS 3052.
87. Radiochemistry of silver. NAS-NS 3047.
88. O.J. SEGAERT and J. DEMNYNCK. Nucl. Phys. 16, 492 (1960).
89. J.W. STARNER Bull. Am. Phys. Soc. 4 No. 2, 99, (L2)
(1959).
90. S.K. MUKHERJEE, A.K. GANGULY and N.K. MAJUMDAR,
Proc. Phys. Soc. 77A, 508-14. (1961).
91. R.F. COLEMAN, B.E. HAWKER, L.P. O'CONNOR and J.L.
PERKIN, Proc. Phys. Soc. 73A,
215-20. (1959).
92. R.J. PRESTWOOD and B.P. BAYHURST, Los Almos Scientific
Lab. La-2493, TID-4500 (1961).
93. H. VONACH, M.I.R. 545a (1961).
94. G.R. BISHOP, R. WILSON and H. HALBAN, Phys. Rev. 77,
416. (1950).

95. R. SAGANE Phys. Rev. 55, 31. (1939).
96. Applied inorganic analysis HILLEBRAND, LUNDELL, BRIGHT,
and HOFFMAN, Wiley, 2nd Ed.
p. 216. (1959).
97. Methods of quant. inorg. analysis. K. KODAMA,
Interscience publishers (1963) p. 150
98. Radiochemistry of gold, NAS-NS 3036.
99. Radiochemistry of mercury. NAS-NS 3026.
100. A. POULARIKAS, R.W. FINK and D.G. GARDNER, Univ.
of Arkansas Nucl. Chem. Research
Ann. report 4 (1960).
101. A. POULARIKAS to D.G. GARDNER Priv. Comm. (1961)
(See D.G. Gardner N.P. 29,
373 (1962)).
102. C.G.B. WILLIAMS. Ph.D. Thesis 1966, Durham Univ.
103. N. CINDRO. Rev. Mod. Phys. 38, 391 (1966).
104. K. IZUMO Progr. Theoret. Phys. (Kyoto) 26, 807,
(1961), (See ref. 103).
105. J.M. BLATT and V.F. WEISSKOPF. Theoretical Nuclear
Physics. Wiley (1962), p. 484.
106. S.T. BUTLER, Phys. Rev. 106, 272 (1957): also
S.T. BUTLER and N. AUSTERN
ibid 92, 350 (1953).

